DESIGN AND ANALYSIS OF DIELECTRIC WAVEGUIDE ANTENNAS

Linghui KONG

Supervisor:
Prof. dr. ir. Guy A. E. Vandenbosch

Members of the Examination Committee:
Prof. dr. ir. Jan Van Humbeeck (Chair)
Prof. dr. ir. Sen Yan (Co-supervisor)
Prof. dr. ir. Dominique Schreurs
Prof. dr. ir. Dirk Van Troyen
(KU Leuven, De Nayer Campus)
Dr. Ulf Johannsen (TU Eindhoven)
Dr. Vladimir Volskiy

Dissertation presented in partial fulfilment of the requirements for the degree of PhD in Engineering

June. 2019

ABSTRACT

With the rapid development of telecommunication technology towards the higher frequencies, the need for low-loss and low-cost transmission media leads to a renewed interest for dielectric waveguides. The higher the frequency, the more conventional metallic transmission lines suffer from conductive losses. Various types of dielectric waveguides have been investigated for very low transmission loss, such as the dielectric rod line and strips, with successful applications in optical frequency bands as a result. Inspired by this success, we concentrate our effort on the design and analysis of dielectric waveguides at microwave frequencies, and employing them in antenna design to reach a better performance and more flexibility.

In the first part of the thesis, we focus on the investigation of the rectangular dielectric waveguide, more specifid on the mode analysis and coupling effect. Based on Marcatili's approximation method, the modal field distribution inside the rectangular dielectric waveguide is analyzed and verified with simulations. A printed dipole connected with microstrips is used to excite the mode inside the waveguide. The coupling effect between the travelling wave and the printed metal patch is also studied. With adequate design parameters, a high coupling and radiating efficiency is obtained, matching the measured results.

Then, we switch to the design of antennas based on the rectangular dielectric waveguide for different application purposes. A four-element non-uniform antenna array is proposed for in-house x band radar and localization use with a bi-directional radiation pattern. To further extend this antenna topology for WiFi applications, a metal ground is added at the bottom side in consideration of the mounting environment. The influence from the ground size and the distance between the ground and the antenna is researched, and a single beam radiation is obtained with significant improvement of the gain performance as well.

In the second part of the thesis, we propose a new type of dielectric transmission line combined with the dielectric image guide and EBG units. The surface wave propagation band is overlapping the forbidden band of the EBG units positioned aside the guiding channel. This can help to reduce the leakage of surface waves at the waveguide edges. The method on how to determine the bandgap of EBG structures is explained in detail with the eigenmode analysis method. A feeding structure is adopted for the modal excitation incorporating a transition from CPW to SIW. With a careful design, this structure achieves a high efficiency and a smooth mode conversion to the guiding channel.

Finally, the proposed waveguide is used in the design of a six-element periodic leaky wave antenna array working in Ku band. The realized design achieves a broadband working frequency range with a high radiation efficiency and gain performance, as well as a 30° beam scanning in the forward quadrant with increasing frequency.

SAMENVATTING

Met de snelle ontwikkeling van telecommunicatietechnologie naar hogere frequenties toe, leidt de behoefte aan verliesarme en goedkope transmissiemedia tot een hernieuwde belangstelling voor diëlektrische golfgeleiders. Hoe hoger de frequentie, hoe meer conventionele metalen transmissielijnen te kampen hebben met geleidingsverliezen. Er is veel onderzoek gedaan naar verschillende soorten diëlektrische golfgeleiders met het oog op een zeer laag transmissieverlies, zoals de diëlektrische “rod” en strips, met als resultaat succesvolle toepassingen in optische frequentiebanden. Geïnspireerd door dit succes, concentreren we onze inspanningen op het ontwerp en de analyse van diëlektrische golfgeleiders op microgolffrequenties, en gebruiken ze voor het ontwerpen van een antenne om betere prestaties en meer flexibiliteit te bereiken.

In het eerste deel van het proefschrift focussen we ons op het onderzoek van de rechthoekige diëlektrische golfgeleider, meer specifiek op een analyse van de modi en het koppelingseffect. Gebaseerd op de benaderingsmethode van Marcatili wordt de modale veldverdeling binnen de rechthoekige diëlektrische golfgeleider geanalyseerd en geverifieerd met simulaties. Een geprinte dipool verbonden met microstrips wordt gebruikt om de mode binnen de golfgeleider te activeren. Het koppelingseffect tussen de lopende golf en de geprinte metalen patch wordt ook bestudeerd. Met adequate ontwerpparameters wordt een hoge koppelings- en stralingsefficiëntie verkregen, die overeenkomen met de gemeten resultaten.

Vervolgens schakelen we over naar het ontwerp van antennes gebaseerd op de rechthoekige diëlektrische golfgeleider voor verschillende toepassingsdoeleinden. Een vier-elementen niet-uniforme antenne-array met een bi-directioneel stralingspatroon wordt voorgesteld voor binnenshuis x-bandradar en lokalisatie. Om deze antennetopologie te kunnen gebruiken voor WiFi-toepassingen wordt een metalen ondergrond aan de onderkant toegevoegd met het

oog op de montage. De invloed van de grond en de afstand tussen de grond en de antenne wordt onderzocht, en een enkele stralende bundel wordt verkregen.

In het tweede deel van het proefschrift stellen we een nieuw type diëlektrische transmissielijn voor, gecombineerd met de diëlektrische beeldgeleider en EBG-eenheden. De voortplantingsband van de oppervlaktegolf overlapt met de verboden band van de EBG-eenheden die naast het geleidingskanaal zijn gepositioneerd. Dit helpt om de lekkage van oppervlaktegolven aan de randen van de golfgeleider te verminderen. De methode om de bandgap van EBG-structuren te bepalen wordt in detail uitgelegd met de eigenmode-analysemethode. Er wordt een voedingsstructuur gebruikt voor de modale excitatie waarin een overgang van CPW naar SIW is opgenomen. Met een zorgvuldig ontwerp bereikt deze structuur een hoog rendement en een soepele modusomzetting in het geleidingskanaal.

Tenslotte wordt de voorgestelde golfgeleider gebruikt bij het ontwerpen van een uit zes elementen bestaande periodieke lekgolfantenne-array die in de Ku-band werkt. Het gerealiseerde ontwerp bereikt een breedband werkfrequentiebereik met een hoge stralingsefficiëntie en winst.

List of Acronyms

AMC	Artificial Magnetic Conductor
Aps	Access Points
AUT	Antenna Under Test
BW	Bandwidth
BZ	Brillouin Zone
CPW	Coplanar Waveguide
CST MWS	Computer Simulation Technology Microwave Studio
DIG	Dielectric Image Guide
DRA	Dielectric Resonant Antenna
DFW	Dielectric-filled waveguide
DW	Dielectric Waveguide
EBG	Electromagnetic Band Gap
FSS	Frequency Selective Surface
HIS	High Impedance Surface
ISM	Industrial, Scientific and Medical
LOS	Line of Sight
LTCC	Low Temperature Co-fired Ceramic
LWAs	Leaky Wave Antennas
ML	Microstrip Line
MMIC	Monolithic Microwave Integrated Circuit
NRD Guide	Non-radiative Dielectric Guide
PCB	Printed Circuit Board
PEC	Perfect Electrical Conductor
PMC	Perfect Magnetic Conductor
RDW	Rectangular Dielectric Waveguide
RF	Radio Frequency
RWG	Rectangular Waveguide

SIW	Substrate Integrated Waveguide
SIIG	Substrate Integrated Image Guide
SMT	Surface Mount Technology
UWB	Ultra-Wideband
VNA	Vector Network Analyzer
WiFi	Wireless Fidelity
WLAN	Wireless Local Area Network

CONTENTS

CHAPTER 1 INTRODUCTION

1.1 Background and Motivation

Antenna is an important element in a communication system, which enables transmitting and receiving of RF signals. They provide a transition from a guided wave on a transmission line to free space [1-1]. Therefore, information can be transferred between different locations without any intervening structures. Nowadays, a large variety of antennas have been developed, from simple structures like monopoles and dipoles to complex structures such as phased arrays. With different system requirements, different types of antennas are selected for certain applications. Currently, they are involved in almost all communication systems, radios, TVs, mobile phones, etc., and even in navigation and wireless charging (Fig. 1.1).

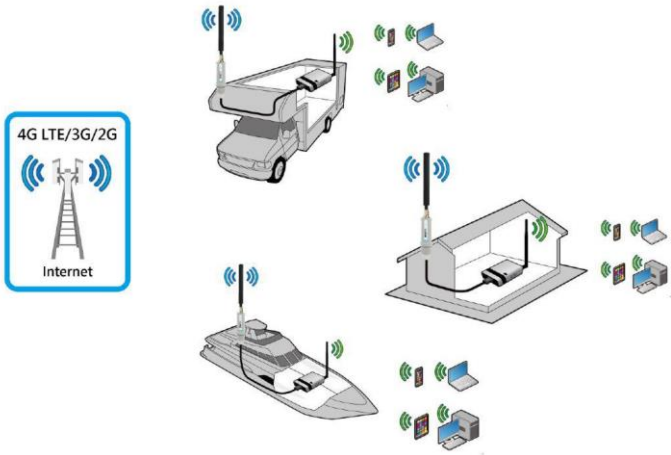

Fig. 1.1 Antenna applications

When discussing antenna design, several parameters will usually be used for evaluation. Consider an antenna which is located in a spherical coordinate system in Fig. 1.2.

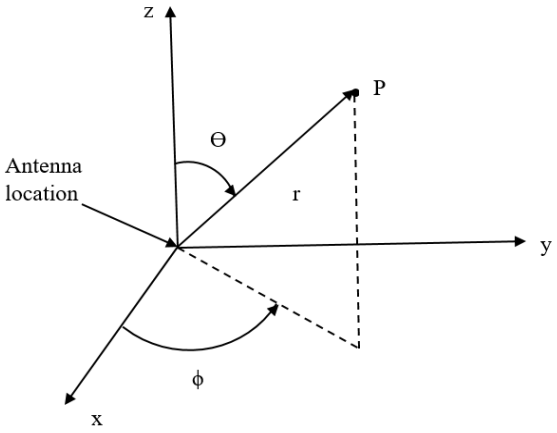

Fig. 1.2 An antenna in a spherical coordinate system

- **Radiation pattern** $\varphi(\theta,\varphi)$**:** Angular variation of radiation at a fixed distance from an antenna.
- **Directivity** ***D***: ratio of power density in the direction of the pattern maximum to the average power density at the same distance from the antenna.
- **Radiation efficiency** η**:** ratio of the radiated power to the accepted power of an antenna.
- **Gain** ***G*****:** Directivity reduced by the losses on the antenna
- **Polarization:** the figure traced out with time by the instaneous electric field vector associated with the radiation from an antenna when transmitting.
- **Impedance** ***Z*****:** input impedance at the antenna terminal.
- **Bandwidth:** range of frequencies over which important performance parameters are acceptable.

The first antenna experiment can be tracked back to 1888, when the German physicist Heinrich Hertz proved the existence of electromagnetic waves predicted by the theory of James Clerk Maxwell [1-2, 3]. Hertz discovered that electrical disturbances could be detected with a single loop of the proper dimensions for resonance that contains an air gap for sparks to occur. In 1901, Guglielmo Marconi built a transmitting antenna and achieved a transatlantic radio

communication for the first time. The antenna consisted of a 70 KHz spark transmitter connected between the ground and a system of 50 wires. It was also the first antenna put into practical applications [1-4].

Then, with a host of stable, coherent microwave sources available [1-5], the interest in using microwave and millimeter waves for communication systems grew steadily as its advantages became more apparent. When the frequency came into the Giga Hertz regime, small antenna apertures were capable of producing a high gain performance and a narrow bandwidth of the main lobe [1-6, 7]. In the late 1950s, more and more institutions became involved in this field. Lots of efforts were placed on planar antenna design and possibilities of new transmission lines [1-8].

In the 1970s and 1980s, integrated antenna systems gained a great popularity. As integrated circuit technology grew more sophisticated, many groups were investigating and experimenting with millimeter-wave communication links. A V-band dielectric rod antenna was reported by Shiau in 1976 [1-9]. In 1987, Wiltse and Black published their papers on Fresnel zone plates with emphasis on the performance of the antenna at millimeter wavelengths [1-10]. After the year 2000, communication devices became more and more compact and sophiscated. Antenna designs were also required to work with a wide bandwidth, miniaturized shape, high efficiency and performance. Recent developments of chip-to-chip communications and system-on-chip solutions rely heavily on the design of waveguides and antenna performance [1-11, 12].

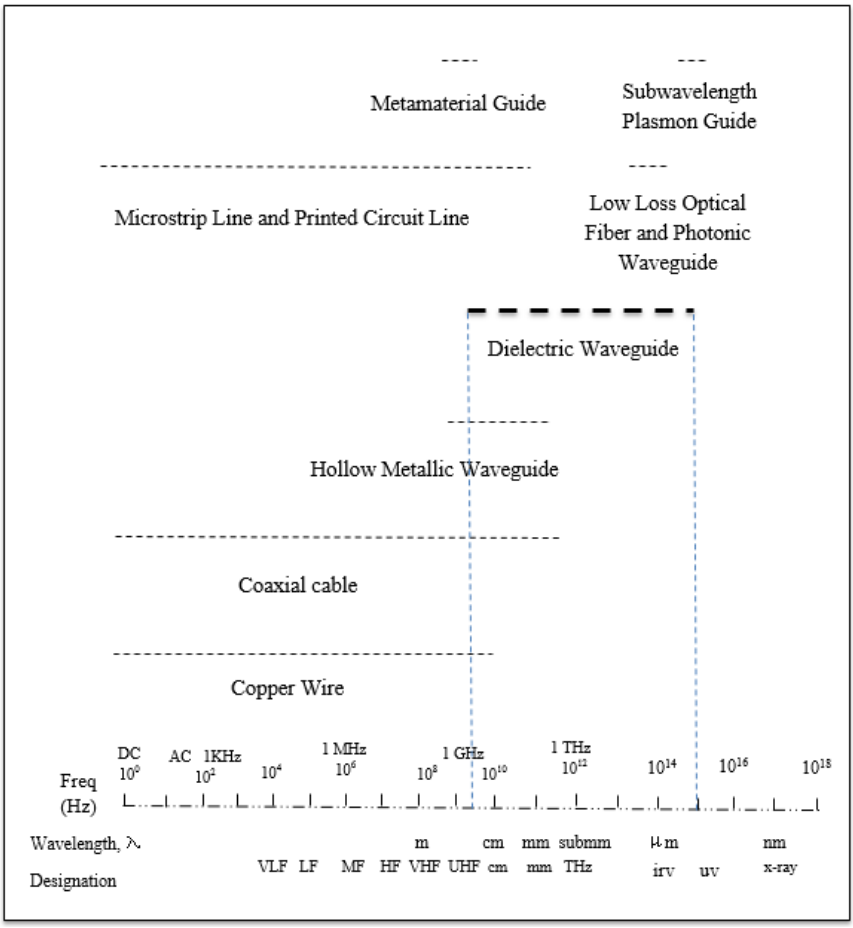

Fig. 1.3 spectral regions for various waveguides [1-13]

Reviewing the wave guiding structures over the whole electromagnetic spectrum (see Fig. 1.3) shows that the spectrum where dielectric waveguides are used spans from about 10^9 to 10^{15} Hz. For frequencies below 30 GHz, up to now mostly metal-based structures are used. In the beginning, the closed metal waveguide was widely applied in centimeter frequency bands but it met difficulties to be integrated with planar circuits. Later in the 1960s, microstrips and striplines started to be the main tranmission medium for microwave integrated technology applications [1-14]. However, in high frequency applications, these transmission lines will meet some problems as the wavelength becomes very small. First, the structure dimensions are

reduced a lot and require very tight tolerances. Second, the influences from the skin effect and shrinking guiding cross sections can cause high current densities and thus significant conductor losses [1-15]. Also, the surface roughness will start to affect the losses and the transmission efficiency at high frequencies. Finally, the dispersion effect and the high-order modes will affect the design performance greatly with the frequency increase [1-16, 17].

In recent years, the substrate integrated waveguide has been proposed as a class of efficient integrated transmission lines compatible with planar structures and gained a great popularity with researchers [1-18]. SIW structures are usually fabricated by using two periodic rows of metal vias connecting the top and bottom ground planes of a dielectric substrate, as seen in Fig. 1.4. With a planar and metal-closed structure, they retain the low loss property of the rectangular metal waveguide and are widely used as interconnections in high speed circuits, filters, directional couplers and antennas. One potential disadvantage for SIW is that leakage losses can be substantial. This is related to how tight the vias are spaced.

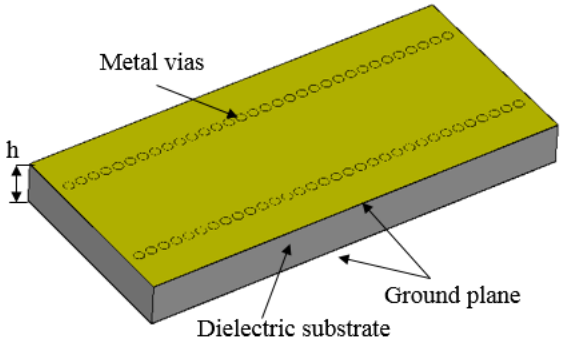

Fig.1.4 Structure of substrate integrated waveguide

In contrast, dielectric waveguides have attracted a great interest for microwave and millimeter-wave hybrid circuits due to the need for low-loss and low-cost transmission media [1-19, 20]. In comparison, there are some significant merits which can be listed as follows:

1. The sectional dimensions are in the order of the wavelength for a dielectric waveguide with single mode transmission, while they are in the order of one tenth of a wavelength for microstrips [1-21]. Therefore, dielectric waveguides are more easily fabricated than metal strip lines at high frequencies.

2. The transmission mechanism for the dielectric waveguide is based on reflections at the interfaces instead of relying on the existence of metallic lines [1-13]. In theory, there are thus no conductor losses.

3. The losses in dielectric transmission lines mainly come from dielectric losses and radiations. Hence, the transmission losses can be reduced a lot by using the low-loss materials, as shown in Fig. 1.5. Radiation is produced by the waveguide discontinuities like bendings, rough surface, and joints [1-22, 23], which can be used to generate radiation by adding some modulations to the waveguide structures.

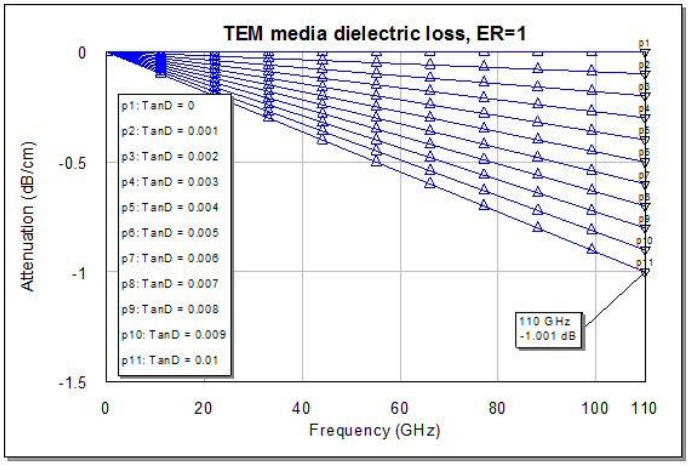

Fig. 1.5 Dielectric losses of dielectric materials with different loss tangent [1-24]

Therefore, when dielectric waveguides are used as substrate feeders in an antenna or array design, conductor losses for example coming from

a conventional complex feeding network can be avoided, which may help to improve the efficiency and performance of the antenna design.

1.2 Review of Dielectric Waveguides

The concept of guiding electromagnetic waves along a dielectric rod or slab has been known for a long time. Different from the closed metal waveguide, the dielectric waveguide does not require EM waves to be constrained inside the waveguide. It is a type of open or semi-open structure with a surface transmission mode, and allows the guiding wave to be distributed along the waveguide. The field at the outside of the waveguide is evanescent and decays exponentially away from the guiding structure [1-25].

In 1910, Hondros and Debye demonstrated analytically that it was possible to propagate a TM wave along a lossless dielectric cylinder [1-26]. Zahn in 1915 and his two students, Ruter and Schriever, confirmed the existence of such TM waves experimentally [1-27]. Around 1936, the propagation properties of asymmetric waves on a dielectric rod were obtained by Carson et al., who proved that the fundamental mode was the hybrid mode called HE_{11} mode, which possesses no cutoff frequency and can propagate at all frequencies [1-28], while all other circularly symmetric or nonsymmetric modes have cutoff frequencies. Later in 1936, Southworth described more detailed experimental results on the phase velocity and attenuation of the circularly symmetric TM wave in a circular dielectric guide [1-29]. Soon afterwards, in 1938, Schelkunoff wrote a paper on the coupled transmission line representation of the waves and the impedance concept, which became the foundation of the development of microwave circuits [1-30].

In 1943, Mallach published his results on the use of the dielectric rod as a directive radiator [1-31]. He showed experimentally that the radiation pattern obtained by the use of the symmetric HE_{11} mode produced only one lobe in the principal direction of radiation. Later,

Wegener presented a dissertation in which the asymmetric HE_{11} mode, together with the lowest order circularly symmetric TE and TM modes, were analyzed in detail [1-32]. Both the numerical results of the propagation constants and the attenuation characteristics of these waves were also obtained. In 1949, Chandler verified experimentally the attenuation properties of the dominant HE_{11} mode [1-33]. He found that the guiding effect was kept even when the rod was only a fraction of a wavelength in diameter. Little loss was observed since the greater part of the guided energy was outside the dielectric rod. It was also the first time that the cavity resonator technique for open dielectric structures was used to measure the attenuation constant of the HE_{11} mode. Yeh gave the correct expression for α and Q for the hybrid mode in 1962 [1-34].

Wave propagation characteristics in periodic structures were summarized in a book by Brillouin in the mid-1940s [1-35]. In 1951, Sensiper studied a periodic structure of helical wire waveguides [1-36]. In 1954, Pierce also provided results on the interaction of an electron beam with slow waves guided by a periodic structure [1-37]. The fundamental theory on wave propagation in a periodic transmission line was well founded by these works.

At the same time, with the increasing demand for high bandwidth and low-loss transmission lines for transcontinental and long-distance communications, lots of efforts were put in finding a new way to transmit microwaves efficiently. King and Schlesinger investigated the dielectric image line in 1954 [1-38], while Goubau experimented with a conducting wire coated with a thin dielectric material [1-39]. The further development of these methods was hampered by the high loss and instability. During the 1950s, significant research on the excitation of surface waves was carried out [1-40, 41]. These investigations offered the basic understanding of how to excite a surface wave on a dielectric structure.

Explorations of using optical fibers as a viable optical waveguide was

first studied by Snitzer and Hicks in 1959 [1-42]. In 1964, Kao and Hockham recognized that if the impurities in optical fibers could be eliminated, the fiber could become a very low-loss transmission waveguide for optical signals [1-43]. In 1970, Kapron successfully made an optical fiber with optical transmission losses of approximately 20 dB/km [1-44]. These progresses encouraged many researchers to put efforts on exploring optical glass fibers. Because of the superior dispersion property of the solid core single-mode fiber, it is now worldwide used as the standard long-distance fiber. At that time, researchers also started the persuit of an all-optical communication system based on integrated optical circuits and planar imbedded optical dielectric waveguides [1-45]. The H-guide transmission line received substantial attention after it had been proposed by Tischer. Tischer extensively studied properties of both single and double slab variants of the H-guide at X-band and millimeter-wave frequencies [1-46]. Since the 1980s, the emphasis of the research community has been changed to finding new ways to increase the bandwidth and to decrease the losses [1-47]. From the 1990s until now, we find an explosion of novel dielectric waveguides due to the discovery of new materials [1-48]. Yeh and Shimabukuro in 2000 found that the configuration of a high dielectric constant waveguide structure could greatly affect the loss behavior of the dominant TM-like mode [1-49].

Recently, a substrate-integrated image guide (SIIG) has been proposed for millimeter-wave applications [1-50]. The perforations of the dielectric slab at both sides of the guiding channel lower the effective permittivity and confine the power flow in a specified direction. Moreover, a gap layer of low permittivity dielectric between the ground-plane and the high permittivity electric slab creates an insulated image guide structure [1-51]. This gap layer can greatly reduce the transmission loss caused by the ground-plane conductivity.

Other modern application areas for dielectric waveguides include the photonic crystal waveguide, basically an air or dielectric core

surrounded by periodic dielectric structures [1-52]; the surface plasmon polaritons guide, a type of Sommerfeld guide [1-53]; the metamaterial waveguide, that is a dielectric waveguide whose core region is made with artificial dielectrics with negative permittivity and negative permeability [1-54, 55].

1.3 Dielectric waveguide antenna

As most of the dielectric waveguides are open guiding structures, leakages of energy will occur when the uniformity of these waveguides is perturbed. Although the leakage effect will influence the transmission efficiency, it could be an advantage for antenna designers. By introducing the perturbations to the waveguide structure, radiation can be generated and controlled to satisfy specific applications [1-56]. Benefiting from the low profile and simple structure, these types of antennas usually can be easily integrated with RF systems. In this section, several types of antennas based on dielectric materials will be discussed.

1. Tapered dielectric rod antenna

The dielectric rod antenna was first proposed in the 1940s [1-57]. The common structure of the dielectric rod antenna can be seen in Fig. 1.6. According to the cross section, it can be divided into two types: rectangular and spherical. For the rectangular antennas, the dielectric rod can be tapered into one or two directions [1-58, 59]. In practical applications, the travelling wave from the feeding structure will be smoothly transmitted to the tapered part. With the decrease of the sectional area to the end, the phase velocity of the travelling wave will be gradually increased to light speed. Then the constrained power along the dielectric rod can be radiated into free space. As this type of antenna gradually leaks a guided mode into free space to form a large effective aperture, a single tapered dielectric rod antenna can be employed to achieve a high-gain [1-60].

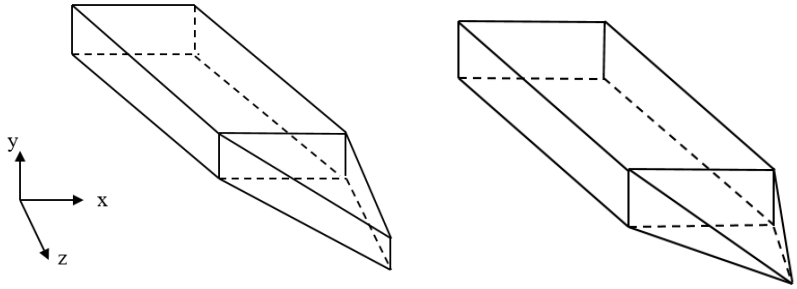

(a) (b)

Fig. 1.6 Tapered dielectric rod antenna, (a) x taper, (b) x-y taper

2. Dielectric resonant antenna

With the fast development of wireless communications, more stringent requirements of miniaturisation, broadband and low-loss are needed in antenna design. Although various types of microstrip antennas have been widely studied and applied because of the advantages of low profile, small size and easy integration, these antennas typically suffer from additional ohmic losses with the increase of the working frequency. In comparison, dielectric resonant antennas (DRAs) are promising candidates to replace the traditional radiation elements at high frequencies as they do not rely on metal strips and are characterized by a high radiation efficiency when excited properly [1-61].

DRAs are based on dielectric resonators, devices that were previously used for energy storage. By using a suitable excitation technique, they can become radiators to transform guided waves into radiation. After the first study on cylindrical DRAs by Long S. A in 1983 [1-62], People started to focus on DRAs more and more. The most two popular DRAs are the cylindrical and the rectangular ones (Fig. 1.7(a) and (b)). The basic principles and design rules for radiating dielectric resonators have been thoroughly discussed [1-63]. The main advantages of DRAs are summarized as follows:

1) The size of DRAs is proportional to $\lambda_0 / \sqrt{\varepsilon_r}$, with $\lambda_0 = c / f_0$

being the free-space wavelength at the resonant frequency λ_0 and ε_r denotes the relative permittivity of the material forming the radiating structure [1-64]. When compared with traditional metallic antennas whose size is proportional to λ_0 /2, DRAs are characterized by a smaller form factor, especially when a material with high dielectric constant is chosen for the design.

2) Due to the absence of conducting material, the inherent conductor losses can be avoided. Therefore, DRAs are distinguished by a high radiation efficiency when a low-loss dielectric material is chosen. This characteristic makes them very suitable for applications at very high frequencies[1-65], especially for millimeter wave antennas where the loss in metal fabricated antennas can be quite high.

3) DRAs can be characterized by a large impedance bandwidth if the dimensions of the resonator and the material dielectric constant are chosen properly [1-66].

4) DRAs can be excited using various feeding techniques which is helpful in different applications and for array integration [1-67]. Different types of the feeding mechanism are presented in Fig. 1.7. In Fig. 1.7(a), the dielectric resonator is directly disposed on the ground plane and excited by a coaxial probe through the substrate. In Fig. 1.7(b), the dielectric resonator is placed on a microstrip transmission line which is printed on a PCB substrate. The coplanar excitation was first introduced in [1-68], where a CPW circular-loop network that feeds a cylindrical DRA is presented. The similar feeding structure is used in Fig. 1.7(c) to feed a rectangular DRA. Fig. 1.7(d) is the most popular feeding technique for DRAs coupled through a slot in the ground plane. This excitation method is known as aperture coupling. The guided wave propagating along the transmission line is coupled, through the slots, to the resonant modes of the dielectric resonators.

5) The gain, bandwidth, and polarization characteristics of a DRA can be easily controlled with different techniques. The most direct way to increase the gain performance of a DRA is to array the individual DRAs [1-69]. Besides, integration with additional structures can be also an efficient way for gain improvement. One example of such design approach (Fig. 1.8) can be the surface mounted short horn DRA [1-70]. The impedance bandwidth of DRAs can be broadened by combining different dielectric resonators and shaping the dielectric resonators [1-71, 72]. Also, different feeding configurations can be used to achieve linear or circular polarizations of DRAs [1-73].

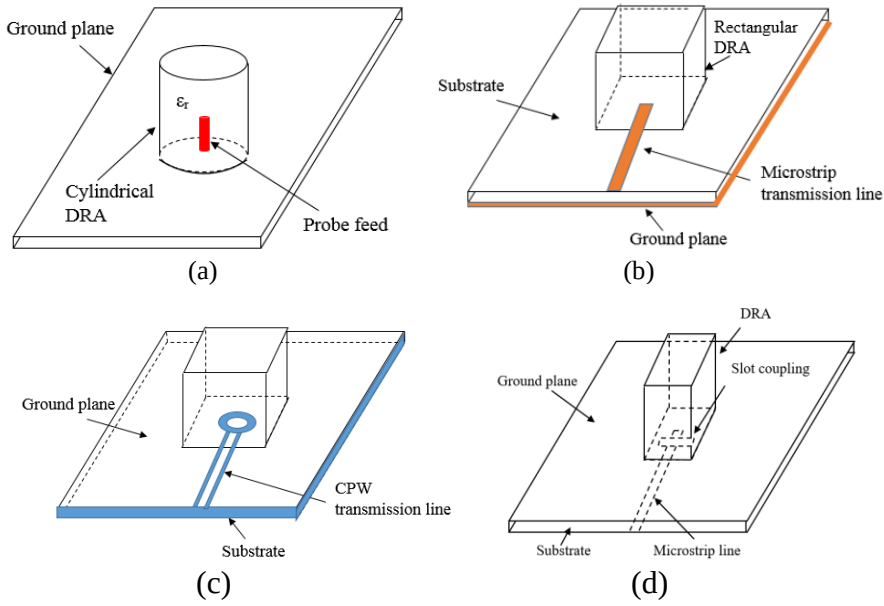

Fig. 1.7 Two types of DRAs and the different feeding mechanism, (a) cylindrical DRA fed by probe, (b) rectangular DRA fed by microstrip transmission line, (c) rectangular DRA fed by CPW transmission line, (d) slot aperture-coupled DRA

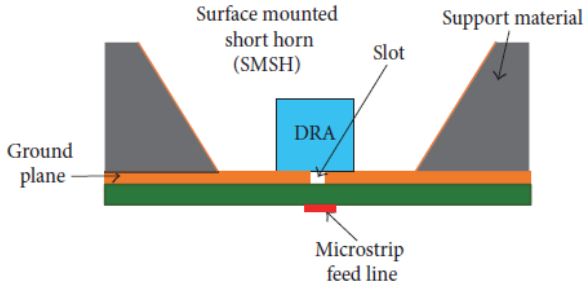

Fig. 1.8 Surface mounted short horn for gain improvement

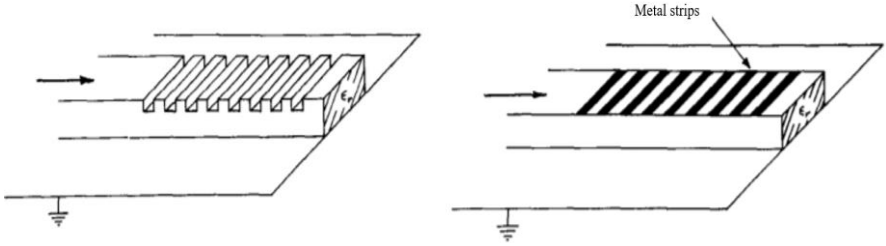

(a) (b)

Fig. 1.9 Periodic dielectric antenna, (a) periodic dielectric gratings, (b) periodic metal strips

3. Periodic dielectric antennas

As discussed, the leakage effect of DWs can be employed in the design of antennas. By introducing perturbations along the waveguide, they can radiate in a controlled fashion. Dielectric grating antennas, see Fig. 1.9, consist of a uniform dielectric waveguide with periodic surface perturbations and belong to the class of radiating structures [1-74].

The waveguide is mainly excited with the fundamental mode and its width is usually chosen smaller than a wavelength to avoid the excitation of higher order modes [1-75]. The surface perturbations can be in the form of dielectric gratings or metal strips, see Fig. 1.9(a) and (b), respectively. These gratings will transform the guiding mode into a leaky wave and generate the radiation [1-76]. Dependent on the frequency, the main beam direction can be scanned from backfire through broadside and into the forward quadrant, even reaching an

endfire situation, if the parameters are chosen appropriately [1-77]. Note that these periodic antennas usually do not radiate in the exact broadside direction, since an internal resonance inhibits radiation there [1-78, 79]. This associated "stopband" effect is narrow for typical antennas and is only noticed when scanning near the broadside direction.

4. Uniform waveguide leaky-wave antennas

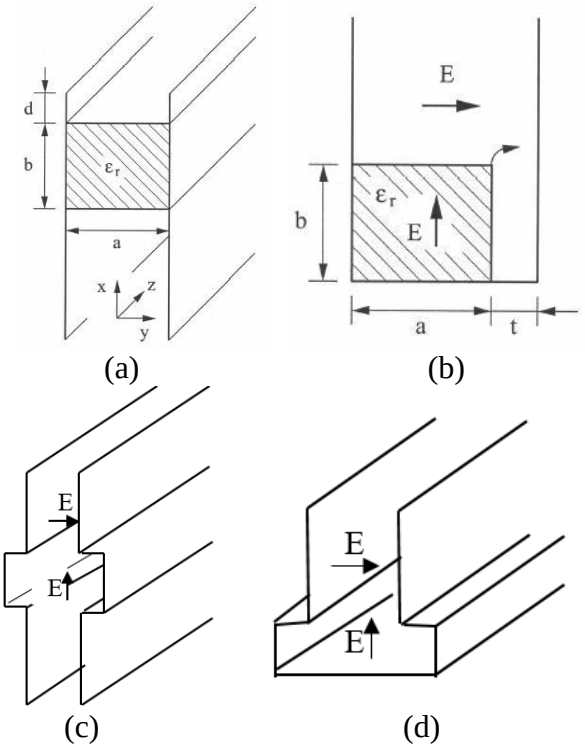

Fig. 1.10 uniform dielectric antennas, (a) and (b) groove guide, (b) and (d) NRD guide

Similar to periodic dielectric antennas, Fig. 1.10 shows a group of DW-based antennas which are basically operated as leaky-wave line sources that scan with frequency. Instead of periodic gratings, these antennas use uniform open waveguides that have been partially opened to allow radiation to occur. The guided wave on the structure is a fast wave, and thus radiates as it propagates. The theory and

design rules of these antennas have been systematically studied by Oliner et al [1-80, 81].

These antennas are based on two types of dielectric waveguide, more specifically the non-radiative dielectric (NRD) guide and the groove guide. In Fig. 1.10(a), the NRD guide is made of a dielectirc slab and two metal plates. The spacing between the metal plates is designed less than $\lambda_0 / 2$ to maintain the structure symmetry. When the metallic paltes are sufficiently extended, the dominant mode field will be exponentially decayed and bound inside. However, if the upper waveguide arms are foreshortened, a travelling wave field then can exist at the upper end and radiate away. Another way to generate radiation from the groove guide is the structure asymmetry as shown in Fig. 1.10(b). An air gap is introduced to the dielectric region and a certain amount of electric field is created horizontally, which propagates at an angle between the parallel plates until it reaches the open end and leaks away.

The groove guide shown in Fig. 1.10(c) and (d) is somewhat similar to the NRD guide. The dielectric central region is replaced by air. The field also decays exponentially in the regions of narrower width above and below. The leaky radiation can be obtained through shortening the arms or bisecting the groove guide horizontally.

The radiation direction for both the NRD antenna and the groove guide antenna varies with frequency. Because of the uniformity in the longitudinal direction, the scan range is confined to the forward quadrant. Compared with periodic antennas, these antennas have the benefit of greater structural simplicity.

1.4 Objectives and Contents

1.4.1 Objectives

Aiming at the development of RF systems towards higher frequencies

and the emerging problem of conductive losses from traditional metal feeding networks for antenna design, this doctoral work contributes to two main objectives: 1. The exploration of dielectric transmission media to satisfy the low loss communication requirement at high frequencies. 2. The design and analysis of DW-based antennas for different applications.To direct the research towards these goals, we are mainly studying the three major research questions as below:

- Research question 1: how to generate radiation from the rectangular dielectric waveguide with mounted metal patch at microwave frequencies?

- Research question 2: how to improve the radiation performance of antennas fed by a dielectric substrate?

- Research question 3: how to improve the mode conversion efficiency to the waveguide substrate from the mode excitation structures?

Based on the research methodology of exploration-analysis--validation-application flow, we make the following key contributions in this thesis to these research questions.

Contibution 1: Design of a patch antenna fed by a rectangular dielectric waveguide for the first time at X band frequencies on the basis of the coupling effect between the patch and the travelling wave inside the rectangular dielectric waveguide. Previous studies have given some approximation analysis of the transmission mode inside a rectangular dielectric waveguide and the applications are focusing on using RDW as planar optical waveguides. As dielectric waveguides are always regarded as low-loss transmission media, we consider to use them as the substrate feeder for antenna design, and therefore to avoid the conductive losses from metal feeding networks. Through the design of the patch antenna, we verified this idea and proved the possibility of employing the dielectric waveguide in antenna design at

microwave frequencies.

Contribution 2: Design of a four-element array with nonuniform topology to avoid the stopband effect in the broadside direction. Based on the design of the dielectric waveguide antenna, a four-element array is proposed for specific applications with an improvement of the far field radiation. To obtain a directive radiation in the normal direction, the elements are designed with different dimensions to eliminate the stopband effect from periodic structures.

Contribution 3: Adoption of electromagnetic bandgap (EBG) units to create the guiding channel for a planar dielectric waveguide design. EBG structures are widely used to control the wave propagation in specific bands. In our work, we propose a new type of transmission line in combination with the dielectric image guide. The mushroom-like EBG untis at the edges of the wave guide yield a transmission efficiency that is almost the same as in the case of a real dielectric waveguide. This new dielectric waveguide is used in the design of a periodic leaky wave antenna array and offers a good radiation efficiency and gain performance.

Contribution 4: Design of different feeding structures to excite the propagation mode inside the dielectric waveguide. There are different propagation modes with corresponding field distribution for the different dielectric waveguides. Therefore, we also design different feeding structures to excite the transmission mode inside the dielectric waveguides. A printed dipole is used to exicite the dominant E_{11}^{x} mode inside the RDW, while a transition from coplanar waveguide (CPW) to substrate integrated waveguide (SIW) is applied as the feeding structure to achieve a smooth mode conversion to the guiding channel of the EBG-based waveguide.

1.4.2 Contents

In the first part of Chapter 2, the working mechanism and the

transmission mode inside the rectangular dielectric waveguide will be studied. Influences from the design parameters of the dielectric waveguide on the guided mode are analyzed. After that, the coupling effect between the travelling wave and a metal patch will be discussed. A sensitivity analysis on the radiation efficiency in terms of different parameters, i.e. the width and length of the metal patch, is given. In the fabricated prototype, the fundamental mode inside the RDW is excited by a printed dipole, and a high coupling and radiating efficiency is obtained with a metal patch. However, it is difficult to achieve a directive beam normal to the waveguide with a single unit.

Next, in chapter 3, in order to achieve a directive radiation, a non-uniform antenna array with elements with different design parameters is proposed. These elements extract a certain power of the travelling wave inside the waveguide and radiate into space. An optimization of the design in terms of far field pattern and gain performance is conducted. A four-elements array is obtained with a bi-directional radiation, which can be used for in-house x band radar and localization purposes. To further improve the gain performance, a ground plane is added to the antenna topology for WiFi applications from about 5.60 GHz to 5.75 GHz. The influence from different ground sizes on the radiation efficiency is analyzed, and a single direction radiation is obtained with a significant improvement of the gain performance. The main features of these two designs are the low profile, low cost and easy fabrication and integration.

In the second part of this thesis, we propose a new type of dielectric transmission medium, which is the dielectric image guide combined with EBG units, and a periodic leaky-wave antenna. The design details of this new waveguide are given in Chapter 4. The idea is to eliminate the side leakages from surface waves propagated in the DIG by aligning two rows of EBG units along the guiding channel. While the specific frequency band allows a single mode transmission inside the waveguide, it is also designed as the “stop band” for the EBG units. To achieve this target, a transmission mode analysis inside the DIG

and an eigenmode analysis for the mushroom-like EBG unit are conducted. Meanwhile, a wideband feeding structure, a tapered CPW to SIW transition with a V slot, is employed to excite and convert the transmission mode inside the DIG efficiently and smoothly.

In Chapter 5, based on this new dielectric transmission medium, a leaky wave antenna array is proposed for Ku band applications. From the measured results of the fabricated antenna prototype, a high gain and radiation efficiency as well as a wide working band, are achieved by this antenna. At the same time, more than 30 degrees of beam scan can be reached with a working frequency increase from 12 GHz to 12.8 GHz.

Finally, the main findings of the doctoral work are summarized and a view of possible future research is outlined.

References

[1-1] P. Dhande, Antennas and its applications, *DRDO Science Spectrum*, Mar. 2009, pp. 66-78

[1-2] C. A. Balanis, Advanced Engineering Electromagnetics, 2nd Edition, John Willy and Sons, May 1989.

[1-3] Wikipedia. Heinrich Hertz. https://en.wikipedia.org/wiki/Heinrich_Hertz

[1-4] Wikipedia. G. Marconi. https://en.wikipedia.org/wiki/Guglielmo_Marconi

[1-5] S. H. Gold, G. S. Nusinovich, "Review of high-power microwave source research," *Review of Scientific Instruments*, Vol. 68, iss. 11, Aug. 1997, pp: 3945–3974.

[1-6] H. Iwasaki, T. Nakajima and Y. Suzuki, "Gain improvement of circularly polarized array antenna using linearly polarized elements," *IEEE Trans. Antenn. Propaga.*, Vol. 43, No. 6, Jun. 1995, pp: 604 – 608.

[1-7] L. Shafai, M. Barakat and A. Sebak, " Beam shaping using multiple linear arrays of microstrip slot antennas," *IEEE Antenn. Propagat. Society Int. Symposium.* Jul. 1997, Montreal, Canada, pp：1268 – 1271.

[1-8] K. L. Wong, Planar Antennas for Wireless Communications. John Willy and Sons, Jan. 2003.

[1-9] Y. Shiau, "Dielectric rod antennas for millimeter-wave integrated circuits," *IEEE trans. Microwave Theory and Techniq.*, Vol. 24, iss. 11, Nov. 1976, pp: 869 – 872.

[1-10] D. N. Black and J. C. Wiltse, "Millimeter-wave characteristics of phase correcting Fresnel zone plates," *IEEE trans. Microwave Theory and Techniq.*, Vol. 35, iss. 12, Dec. 1987, pp: 1122 – 1129.

[1-11] E. J. Rothwell and R. O. Ouedraogo, "Antenna miniaturization: definitions, concepts, and a review with emphasis on metamaterials," *J. of Electromagnetic Waves and Applications*, Vol. 28, No. 17, Nov. 2014, pp: 2089 – 2123.

[1-12] Y. P. Zhang and D. X. Liu, "Antenna-on-chip and antenna-in-package solutions to highly integrated millimeter-wave devices for wireless communications," *IEEE Trans. Antenn. Propaga*., Vol. 57, No. 10, Oct. 2010, pp: 2830 – 2841.

[1-13] C. Yeh and F. Shimabukuro, The Essence of Dielectric Waveguides, Springer, 2008.

[1-14] D. M. Pozar, Microwave Engineering, 3th Edition, John Willy and Sons, Jan. 2007.

[1-15] J. C. Rautio, and V. Demir, "Microstrip conductor loss models for

electromagnetic analysis," *IEEE trans. Microwave Theory and Techniq.,* Vol. 51, No. 3, Mar. 2003, pp: 915 – 921.

[1-16] M. Riaziat, R. Majidi-Ahy and I. J. Feng, "Propagation modes and dispersion characteristics of coplanar waveguides," *IEEE trans. Microwave Theory and Techniq.,* Vol. 38, No. 3, Mar. 1990, pp: 245 – 251.

[1-17] J. Zhang and T. Y. Hsiang, "Dispersion characteristics of coplanar waveguides at subterahertz frequencies," *Proc. of PIERS*, Mar. 2006, Cambridge, USA.

[1-18] F. Xu and K. Wu, "Guided-wave and leakage characteristics of substrate integrated waveguide," *IEEE Trans. Antenn. Propaga*., Vol. 53, No. 1, Jan. 2005, pp: 66 – 73.

[1-19] L. Jin, R. M. A. Lee and I. Robertson, "Analysis ande design of novel low-loss hollow substrate integrated waveguide," *IEEE trans. Microwave Theory and Techniq.,* Vol. 62, No. 8, Jun. 2014, pp: 1616 – 1624.

[1-20] N. Dolatsha and A. Arbabian, "Analysis and design of multi-mode dielectric waveguide interconnect with planar excitations," *Proc. of PIERS*, Aug. 2013, Stockholm, Sweden.

[1-21] E. Silvestre, P. S. J. Russell, T. A. Birks and J. C. Knight, "Analysis and design of an endlessly single-mode finned dielectric waveguide," *J. of Optical Society of America*, Vol. 15, iss. 12, 1998, pp: 3067 – 3075.

[1-22] R. Elio and E. El-Sharawy, "Reducing losses in dielectric waveguide discontinuities," *IEEE trans. Microwave Theory and Techniq.,* Vol. 46, No. 8, Aug. 1998, pp: 1045 – 1054.

[1-23] P. Bienstman, E. Six, M. Roelens, M. Vawolleghem and R. Baets, "Calculation of bending losses in dielectric waveguide using eigenmode expansion and perfectly matched layers," *IEEE Photonics Technology and Letters*, Vol. 14, No. 2, Feb. 2002, pp: 164 – 165.

[1-24] https://www.microwaves101.com/encyclopedias/transmission-line-loss

[1-25] J. Sharma and A. De, "Full-wave analysis of dielectric rectangular waveguides," *Progress in Electromagnetic Research M*, Vol. 13, 2010, pp: 121 – 131.

[1-26] D. Hondros and P. Debye, "Elektromagnetische wellen an dielektrischen drahten," *Ann. Phys.,* Vol. 30, 905, 1910, pp: 465 – 476.

[1-27] H. Zahn, "Dielectric of electromagnetic waves along dielectric wires," *Ann. Phys.,* Vol. 49, 907, 1915, pp: 907 – 933.

[1-28] J. R. Carson, S. P. Mead and S. A. Schelkunoff, “Hyperfrequency waveguides mathematical theory,” *Bell Syst. Tech. Jour.,* Vol. 15, No. 2, 1936, pp: 310 -333.

[1-29] G. C. Southworth, “ Hyperfrequency waveguides – general considerations and experimental results,” *Bell Syst. Tech. Jour.,* Vol. 15, Apr. 1936, pp: 284 -309.

[1-30] S. A. Schelkunoff, “The impedance concept and its application to problems of reflection, refraction, shielding and power absorption,” *Bell Syst. Tech. Jour.,* Vol. 17, Jan. 1938, pp: 17 - 48.

[1-31] Mallach, “Dielektrische richstrahler,” *Bericht des V. I. F. S.* , 1943.

[1-32] G. F. Wegener, “Ausbreitungsgescgwindigkeit wellenwiderstand und dampfung elektromagnetischer wellen an dielekrischen zylindern,” Dissertation, *Air Material Command Microfilm ZWB/FB/RE/2018*, 1946.

[1-33] W. M. Chandler, “An investigation of dielectric rod as waveguides,” *J. Appl. Phys.,* Vol. 20, iss. 12, Jan. 1949, pp: 1188 – 1192.

[1-34] C. Yeh, “A relation between α and Q,” *Proc. IRE,* Vol. 50, 2143, 1962.

[1-35] C. H. Brillouin, Wave Propagation in Periodic Structures, Dover Publications, New York, 1983.

[1-36] S. Sensiper, “Electromagnetic wave propagation on helical conductors,” *Research Lab for Electronics, Mass. Inst. Of Tech*., Rept. No. 194, May 1951.

[1-37] J. R. Pierce, Theory and Design of Electron Beams, D. Van Nostrand Co., Prinston, 2nd Edition, 1954.

[1-38] S. P. Schlesinger and D. D. King, “Dielectric image line,” IRE Trans. On Microwave Theory and Techniques, Jul. 1958, pp: 291 – 299.

[1-39] G. Goubau, “Surface waves and their application to transmission lines,” *J. Appl. Phys.,* Vol. 21, iss. 11, Nov. 1950, pp: 1119 – 1128.

[1-40] J. R. Wait, “Excitation of surface waves on conducting, stratified, dielectric-clad, and corrugated surfaces,” *J. Of Research of the National Bureau of Standards,* Vol. 59, Dec. 1957, pp: 365 – 377.

[1-41] S. Crampin, “The dispersion of surface waves in multilayered anisotropic media,” *Geophysical Jour. Of the Royal Astronomical Society,* Vol. 21, 1958, pp: 387-402.

[1-42] E. Snitzer and J. W. Hicks, “Optical waveguide modes in small glass fibers. I. Theoretical,” *J. Opt. Soc.,* Am. 49, 1128, 1959.

[1-43] K. C. Kao and G. A. Hockham, “Dielectric fiber surface waveguides for optical frequencies,” *IEE J – Optoelectronics*, Vol. 133, iss. 3, Jun. 1986, pp: 191-98.

[1-44] F. P. Kapron and D. B. Keck, “Radiation losses in glass optical waveguides,” *Appl. Phys. Lett.*, vol. 17, iss. 10, Dec. 1970, pp: 423 – 425.

[1-45] T. T. Fong and S. W. Lee, “Planar dielectric strip waveguide for millimeter-wave integrated circuits,” *S-MTT International Microwave Symposium*, Jun. 1974, Atlanta, USA, pp: 191–194.

[1-46] F. J. Tischer, “Groove guide and H-guide: supplementary information,” *Inter. J. Of Infrared and millimeter waves*, vol. 5, iss. 6, Jun. 1984, pp: 869-874.

[1-47] E. Liek and T. S. Pettersen, “A novel type of waveguide polarization with large cross-polar bandwidth,” *IEEE Trans. on MTT*, vol. 36, no. 11, Nov., 1988, pp: 1531–1534.

[1-48] Y. J. Cheng, X. Y. Bao and Y. X. Guo, “LTCC-based substrate integrated image guide and its transition to conductor-backed coplanar waveguide,” *IEEE Microwave and Wireless Compo. Lett.*, vol. 23, no. 9, Sep. 2013, pp: 450 – 452.

[1-49] C. Yeh, F. Shimabukuro, P. Stanton and V. V. Jamneiad, “Communication at millimeter-submillimeter wavelengths using a ceramic ribbon,” *Nature*, vol. 404, Apr. 2000, pp: 584 – 588.

[1-50] A. Patrovsky and K. Wu, “Substrate integrated image guide (SIIG) – A planar dielectric waveguide technology for millimeter-wave applications,” *IEEE Trans. on MTT*, vol. 54, no. 6, Jun. 2006, 2872 – 2879.

[1-51] A. Patrovsky and K. Wu, “Substrate integrated image guide (SIIG) – A low-loss waveguide for millimeter-wave applications,” *EuMC 2005*, Paris, France.

[1-52] H. S. Dutta, A. K. Goyal, V. Srivastava and S. Pal, “Coupling light in photonic crystal waveguides: A review,” *Photonics and Nanostructures – Fundamentals and Applications*, vol. 20, Jul. 2016, pp: 41 -48.

[1-53] W. B. Shi, T. Y. Chen, H. Jing and M. Wang, “Dielectric lens guides in plane propagation of surface plasmon polaritons,” *Optical Express*, vol. 25, iss. 5, Mar. 2017, pp: 5772 – 5780.

[1-54] C. Jin, A. Alphones and M. Dhirendra, “TM mode analysis in a metamaterial based dielectric waveguide,” *Proc. PIERS*, vol. 24, Aug. 2012, Mosco, Russia, pp: 221–234.

[1-55] J. Carbonell, L. J. Rogla, V. E. Boria and D. Lippens, “Design and experimental verification of backward-wave propagation in periodic waveguide structures,” *IEEE Trans. on MTT*, vol. 54, iss. 4, pp: 1527 – 1533.

[1-56] P. Modal and K. Wu, "A leaky-wave antenna using periodic dielectric perforation for millimeter-wave applications," *IEEE Trans. Antenn. Propagat*., vol. 64, no. 12, Dec. 2016, pp: 5492 – 5495.

[1-57] D. F. Halliday and D. G. Kiely, "Dielectric-rod aerials," *J. of the Institution of Electrical Engineere – Part IIIA: Radiocommunication*. vol. 94, iss. 14, Mar. 1947, pp: 610 – 618.

[1-58] S. Kobayashi, R. Mittra and R. Lampe, "Dielectric tapered rod antennas for millimeter-wave applications," *IEEE Trans. Antenn. Propagat*., vol. 30, no. 1, Jan. 1982, pp: 54 – 58.

[1-59] J. Richter, J. U. Garbas and L. P. Schmit, "Mean and differential phase centers of rectangular dielectric rod antennas," *34th EuMC*, 2004, Amsterdam, Netherlands.

[1-60] N. Ranjkesh, A. Taeb and M. A. Bash, "High-gain integrated tapered dielectric antenna for millimeter-wave application," *IEEE Antenn. And Propagat. Socie.* 2014, pp: 1045 – 1046.

[1-61] B. Ahn, T. D. Yeo, S. C. Chae and J. W. Yu, "High gain spherical dielectric resonator antenna using higher-order resonant mode," *Proc. ISAP 2017*, Phuket,Thailand.

[1-62] S. A. Long, M. W. McAllister and L. C. Shen, "The resonant cylindrical dielectric cavity antennas," *IEEE Trans. Antennas Propagat.*, vol. 31, May 1983, pp: 406 - 412.

[1-63] S. Keyrous and D. Caratelli, "Dielectric resonator antennas: basic concepts, design guidelines, and recent developments at millimeter-wave frequencies," *Inter. Jour. of Antenn. And Propagat.*, vol. 2016, Aug, 2016, pp: 1 – 20

[1-64] G. Ramzi, G. Mohamed and G. Ali, "Design and parametric analysis of a very compact UWB antenna using a simple DRAtopology," *Eighth Int. Multi-Conf. Systems, Signals and Devices*, Mar. 2011, Sousse, Tunisia.

[1-65] W. M. Abdel-Wahab, D. Busuioc and S. S. Naeini, "Millimeter-wave high radiation efficiency planar waveguide series-fed dielectric resonator antenna (DRA) array: analysis, design and measurements," *IEEE Trans. Antennas Propagat.*, vol. 59, iss. 8, Aug. 2011, pp: 2834 – 2843.

[1-66] A. Buerkle, K Sarabandi and H. Mosallaei, "A novel approach to enhance the bandwidth of miniaturized dielectric resonator antennas," I*EEE Antennas Propagat. Socie. Sym.*, vol. 2, Jun. 2004, Monterey, Canada, Pp: 1359 -1362.

[1-67] I. A. Eshrah, A. A. Kishk, A. B. Yakovlev and A.W. Glisson, "Excitation of dielectric resonator antennas by a waveguide probe: modeling technique and wideband design," *IEEE Trans. Antennas Propagat.*, vol. 53, iss. 3, Mar. 2005, pp: 1028 – 1037.

[1-68] R. A. Kranenburg, S. A. Long and J. T. Williams, "Coplanar waveguide excitation of dielectric resonator antennas," *Electronics Letters*, Vol. 39, no. 1, 1991, pp. 119-122.

[1-69] A. S. Al-Zoubi, A. A. Kishk and A. W. Gilsson, "A linear rectangular dielectric resonator antenna array fed by dielectric image guide with low cross polarization," *IEEE Trans. Antennas Propagat.*, vol. 58, no. 3, 2007, pp: 697-705.

[1-70] Nasimuddin and K. P. Esselle, "Antennas with dielectric resonators and surface mounted short horns for high gain and large bandwidth," *IEEE Trans. Antennas Propagat.*, vol. 1, no. 3, 2007, pp: 723 – 728.

[1-71] R. Chair, S. L. S. Yang, A. A. Kishk, K. F. Lee and K. M. Luk, "Aperture fed wideband circularly polarized rectangular stair shaped dielectric resonator antenna," *IEEE Trans. Antennas Propagat.*, vol. 54, no. 4, 2006, pp: 1350–1352.

[1-72] S. Dhar, R. Ghatak, B. Gupta and D. R. Poddar, "A wideband Minkowski fractal dielectric resonator antenna," *IEEE Trans. Antennas Propagat.*, vol. 61, no. 6, 2013, pp: 2895–2903.

[1-73] Y. X. Guo and K. M. Luk, "Dual-polarized dielectric resonator antennas," *IEEE Trans. Antennas Propagat.*, vol. 51, no. 5, May 2003, pp: 1120 – 1123.

[1-74] A. Vashishtha, A. Yadav and D. Chaudhary, "A review of 1-dimensional and 2-dimensional leaky wave antenna and recent advancements in LWAs," *Int. J. of Conputer Application*s, Vol. 155, no. 9, Dec. 2016, pp: 7-12.

[1-75] S. Fan, J. N. Winn and J. D. Johannopoulos, "Guided and defect modes in periodic dielectric waveguides," *J. Optical Society of America*, vol. 12, iss. 7, 1995, pp: 1267 -1272.

[1-76] J. Zhang, F. Xu, G. Hua and K. Wu, "Turning substrate integrated nonradiative dielectric waveguide into leaky wave antenna," *IEEE 4th APCAP*, Jul. 2015, Kuta, Indoesia.

[1-77] H. Yu and D. Yang, "An analytical array scaning method for field computations of sources within a periodic structure," *IEEE Antennas Propagat. Int. Sym*., vol. 4, Jul. 1999, Orlando, USA, pp: 2204 – 2207.

[1-78] F. Siaka, J. J. Laurin and R. Deban, “New broad angle frequency scanning antnena with narrow bandwidth based on a CRLH structure,” I*ET Microwaves, Antennas and Propagat.,* vol. 11, iss. 11, Sep. 2017, pp: 1644 – 1650.

[1-79] P. Burghignoli, G. Lovat and D. R. Jackson, “Analysis and optimization of leaky-wave radiation at broadside from a class of 1-D periodic structures,” *IEEE Trans. Antennas Propagat.*, vol. 54, iss. 9, Sep. 2006, pp: 2593 – 2604.

[1-80] A. A. Oliner and P. Lampariello, “Theory and design considerations for a new millimeter-wave leaky groove guide antenna,” *12th EuMC*, 1982, Helsinki, Finland, pp: 367 – 371.

[1-81] C. D. Nallo, F. Frezza, A. Galli and A. A. Oliner, “Properties of NRD-guide and H-guide higher-order modes: physical and nonphysical ranges,” *IEEE Trans. MTT*, vol. 42, iss. 12, Dec. 1994, pp: 2429-2434.

CHAPTER 2 PATCH WITHIN RECTANGULAR DIELECTRIC WAVEGUIDE

Inspired by the success of dielectric waveguides in optical communications, a RDW-based antenna is proposed for X-band applications. The coupling effect between the travelling wave inside the substrate guide and the middle patch is verified by simulations from the standalone waveguide to the complete structure within CST MWS. The influence on the coupling efficiency of the dimensional parameters of the metal patch is analyzed. The analysis is also validated with measured results from fabricated samples. To the knowledge of the authors, this is the first design of a rectangular dielectric waveguide based antenna for X-band.

This chapter is based on the following publication:
[1] Linghui Kong, Xuezhi Zheng, Sen Yan, Guy A. E. Vandenbosch. “Design of a dielectric waveguide antenna at microwave frequencies.” EuCAP 2017, Paris, France, pp: 2017 – 2019.

2.1 Introduction

The rectangular dielectric waveguide has been commonly used in integrated optics, especially in semiconductor diode lasers. Demands for new applications such as high-speed data backplanes, waveguide filters, multiplexors and switches are driving technology toward better materials and processing techniques for planar waveguide structures [2-1]. The infinite slab and circular waveguides have been studied a lot but are not practical for use on a substrate: the slab waveguide has no lateral confinement, and the circular fiber is not compatible with planar technology being used to make planar integrated circuits [2-2]. Compared with them, the rectangular waveguide is the natural structure.

In this chapter we will first investigate the methods for analyzing the transmission mode inside the RDW, and then verify with the simulation results in CST. After that, the fundamental mode will be excited by a feeding structure and be coupled with a middle patch. Prototypes will be fabricated and measured to compare with the obtained simulation results.

2.2 Mode analysis of RDW

2.2.1 Marcatili's approximation method

A metal waveguide is a hollow structure with closed boundaries in which waves can propagate without any distortion or attenuation along the direction of the guide. Such waves are generally dispersive and the dispersive relationship can be obtained by solving the self-adjoint eigenvalue problem [2-3]. However, for open dielectric waveguides, there is no exact analytical solution for the case of wave propagation along a dielectric waveguide of rectangular shape. Eigen-modes have to be calculated either numerically or using an approximate method.

Pioneering work was conducted by Marcatili with a wave analysis on the eigenmodes of rectangular structures [2-4]. In this method, there is a prior assumption for a well guided mode in a dielectric waveguide with cross section like in Fig. 2.1., that is, most of its guided power is constrained within the core region of the guide. Very little power of that mode stays in the adjacent region of the guide. So, if the boundary conditions are satisfied by most of the assumed fields that carry most of the guided power, then, the assumed fields can be used to approximate the solutions of the eigenmodes. In the shaded corners, very little power is contained in these regions of the guide. Marcatili created an approximate approach to this problem by ignoring the matching of fields along the edges of the shaded areas.

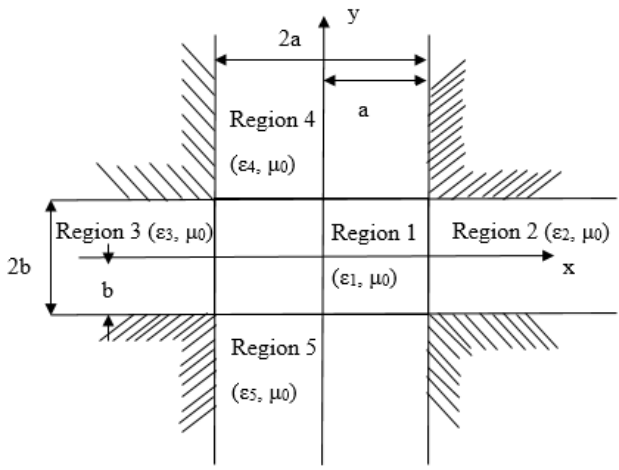

Fig. 2.1 Cross-sectional geometry of RDW for Marcatili's approximate method

There are mainly two independent families of modes, the E_{mn}^{y} modes ($\overrightarrow{E_y}$, $\overrightarrow{E_z}$, $\overrightarrow{H_x}$ and $\overrightarrow{H_z}$) and the E_{mn}^{x} modes ($\overrightarrow{E_x}$, $\overrightarrow{E_z}$, $\overrightarrow{H_y}$ and $\overrightarrow{H_z}$), on this rectangular dielectric waveguide, which have most of the electric field polarized in the *y* and *x* directions, respectively [2-5]. The subscripts *m* and *n* individually represent the number of extrema that the field components for this mode have along the *y* and *x* directions.

In Marcatili's approach, he first gives the five groups of wave

equations for the core region and the closed four sides along the longitudinal direction (see Eq. 2.1) with the assumption that the factor $e^{j\omega t}$ is attached to all the field components and suppressed. These equations can be solved with the method of the separation of variables. Then, the eigenvalue equations can be obtained when the tangential electric and magnetic fields at the boundaries are matched. Finally, the propagation constant of the modes can be calculated. The wave equations can be written as below.

$$\begin{cases} \nabla_t^2 \vec{E}_{zi} \pm (k_i^2 - \beta^2)\overrightarrow{E_{zi}} = 0 & \text{i = 1, 2, 3, 4, 5} \\ \nabla_t^2 \overrightarrow{H}_{zi} \pm (k_i^2 - \beta^2)\overrightarrow{H_{zi}} = 0 & \text{if i = 1, it is '+'} \end{cases} \tag{2.1}$$

where $k_i^2 = \omega^2 \mu \varepsilon_i = k_{xi}^2 + k_{yi}^2 + \beta^2$. Now we can consider the example with $\varepsilon_2 = \varepsilon_3 = \varepsilon_4 = \varepsilon_5 < \varepsilon_1$. The electric field distribution of the E_{11}^x and E_{11}^y modes, in the regions shown in Fig. 2.1, can be expressed as:

$$\overrightarrow{E_x}\ ,\ \overrightarrow{E_y} = \begin{cases} \vec{E}_0 \cos(k_{x1}x)\cos(k_{y1}y) & |x| \le \text{a},\ |y| \le \text{b} \\ \vec{E}_0 \cos(k_{x1}a)\cos(k_{y1}y)e^{-k_{x2}(|x|-a)} & |x| > \text{a},\ |y| \le \text{b} \\ \vec{E}_0 \cos(k_{x1}a)\cos(k_{y1}y)e^{-k_{y2}(|y|-a)} & |x| \le \text{a},\ |y| > \text{b} \\ 0 & |x| > \text{a},\ |y| > \text{b} \end{cases} \tag{2.2}$$

Then, the degenerate fundamental modes of E_{11}^x and E_{11}^y are shown in Fig. 2.2.

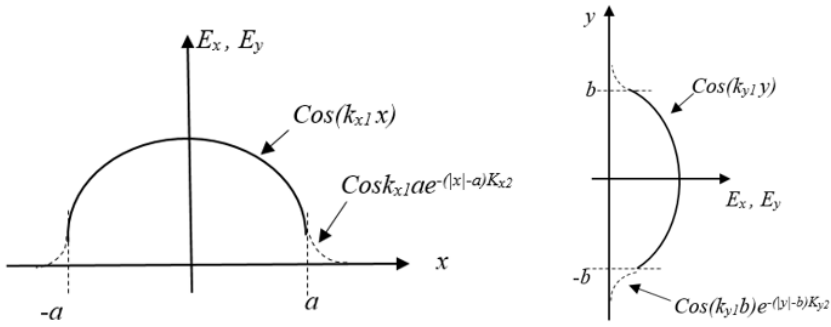

Fig. 2.2 Electric field distribution along *x* and *y* direction for E_{11}^x and E_{11}^y modes

2.2.2 Launch of E_{11}^{x} mode

As the design is targeted towards substrates with very low losses, for example alumina or glass, therefore, in a first approximation, the material is assumed to be lossless, with zero loss tangent and no losses in the metals. In practice, the waveguide takes the form of a thin dielectric strip (Fig. 2.3) made of substrate with a dielectric constant of 10.2. A higher permittivity can lead to an increased field concentration within the waveguide core [2-6].

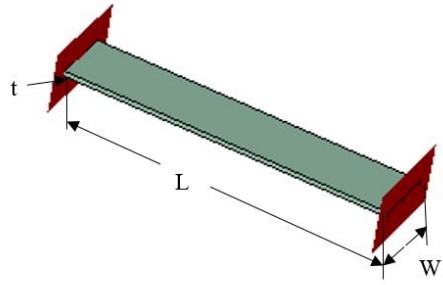

Fig. 2.3 Rectangular dielectric waveguide (L = 80, W = 15, t = 1.27, unit: mm)

As the field distribution is determined by the permittivity and the waveguide dimensions, we choose the design parameters for this waveguide as shown in Fig. 2.3 and conduct the transmission analysis in CST MWS at the target design frequency of 10 GHz. Waveguide ports are defined at both sides to mimic the mode transition to the waveguide.

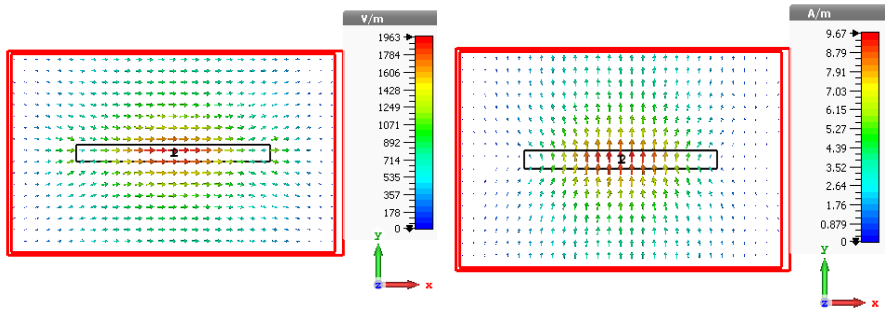

(a) (b)

Fig. 2.4 Port mode at 10 GHz, (a) electric field, (b) magnetic field

Fig. 2.4 presents the polarization of the dominant mode propagating inside the waveguide. Compared with the approximate analysis in Macartili's method, it is matched with the field distribution of the E_{11}^{x} mode. In order to excite this mode exactly, a printed dipole connected with microstrips (Fig. 2.5) is employed as the feeding structure [2-7]. The two branches followed by the 3 dB power divider are designed to achieve the 180 degrees of phase shift by the difference in length $W_4 - W_3 = \lambda_g / 4$, with λ_g the guided wavelength in the microstrip at the center of working band, i.e. 10 GHz. The propagation of the excited E_{11}^{x} mode inside the waveguide is shown in Fig. 2.6, and the design parameters for this feeding structure are listed in Table 2.1.

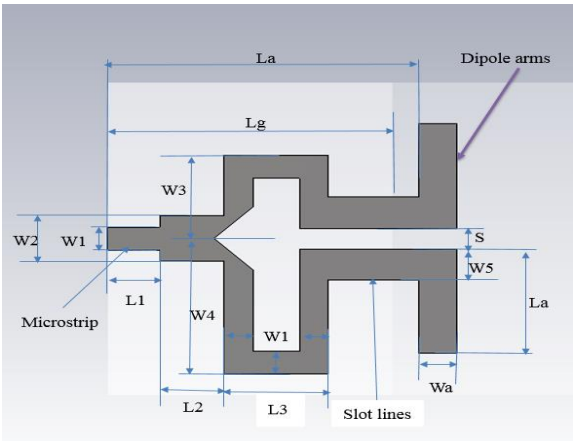

Fig. 2.5 Top view of the feeding structure to excite the E_{11}^{x} mode

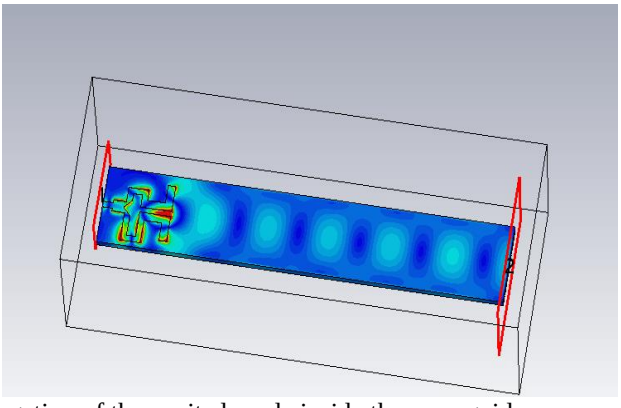

Fig. 2.6 Propagation of the excited mode inside the waveguide

Table 2.1 Dimensions of the feeding structure (unit: mm)

Parameter	L1	L2	L3	W1	W2	W3	W4	W5	La	Wa	Lb	Lg	s
Value	2	2.5	4	1.1	2.2	4	6.5	1.5	5	1.5	12	11	1

2.3 Coupling effect with patch

2.3.1 Simulation analysis

1) Simulations for the waveguide

Simulations are conducted with CST. First a stand-alone waveguide is considered (Fig. 2.3). The simulated results of the S parameters are depicted in Fig. 2.7. From the simulated results, we can find that almost all of the power (about 99.28%) can be transmitted inside the waveguide in this ideal situation.

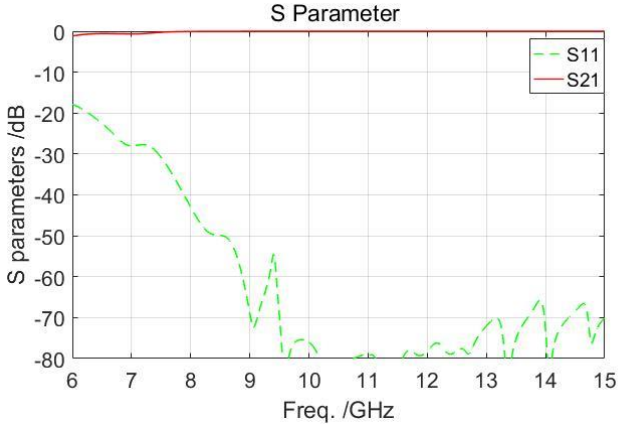

Fig. 2.7 S parameters of the waveguide (at 10 GHz, S_{21} = -0.001 dB, S_{11} = -76.03 dB)

2) Simulations with feeding structure

Then, we consider the case where a feeding structure is added on one side of the waveguide port (Fig. 2.8), while the other side is still defined as a pure waveguide port. Although some radiation losses are inevitable for this semi-open structure, it is seen that this feeding structure still can work in the frequency band of 9.0 to 11.0 GHz.

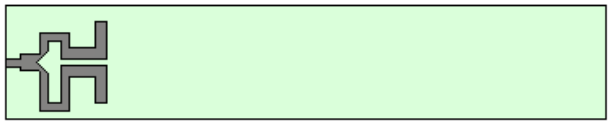

Fig. 2.8 Waveguide with feeding structure

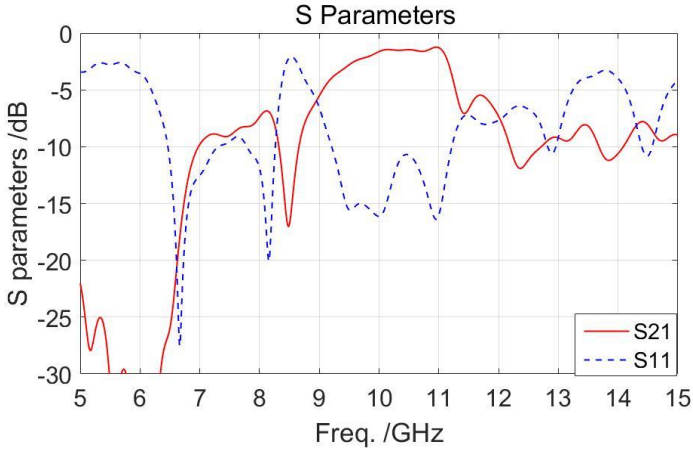

Fig. 2.9 S parameters with feeding structure (at 10 GHz, S_{21} = -1.62 dB, S_{11} = -16.54 dB)

In order to verify the coupling effect of the transmitted mode with metal elements and in order to generate the radiation, a patch scatterer is placed in the middle part of the waveguide (Fig. 2.10). An optimization of the design parameters was conducted to persue a high radiation efficiency. The resulting S parameters for several values of the length and width at the target frequency are listed in Table 2.2. It is observed that the length can influence the results much more than the width. As a best compromise, the optimized values for the length and width are chosen as 6 mm and 4 mm, respectively.

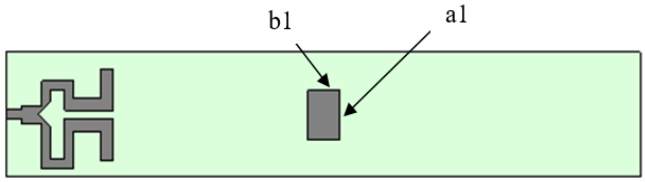

Fig. 2.10 Waveguide with feeding structure and the scatterer

Table. 2.2. S parameters for several lengths and widths of the patch (mm)

Dimension	a1 (b1= 4mm)				b1 (a1= 6mm)			
	3	4	5	6	1	2	3	4
S11/dB	-24.69	-24.59	-14.42	-11.39	-9.14	-9.69	-10.43	-11.39
S21/dB	-2.15	-3.09	-6.15	-10.30	-10.74	-10.90	-10.76	-10.30

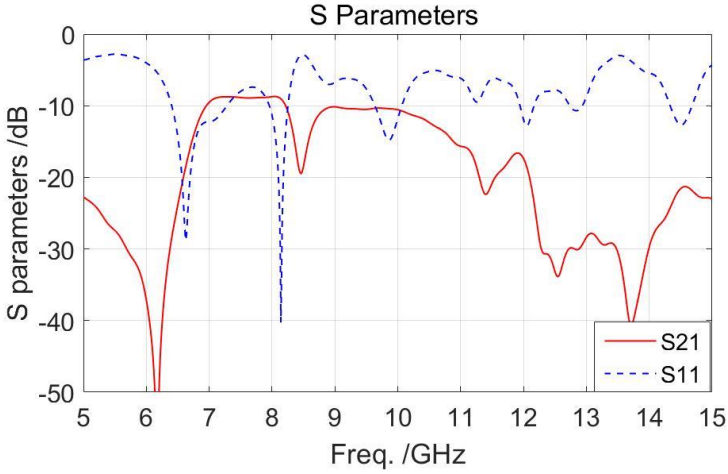

Fig. 2.11 S parameters with scattere (at 10 GHz, S_{21} = -10.44 dB, S_{11} = -11.40 dB)

The simulated S parameters of the patch with the optimized values are shown in Fig. 2.11. Both S_{21} and S_{11} are decreased below – 10 dB. This proves that the transmitted wave inside the RDW can be efficiently coupled with the middle patch and radiated into space.

3) Simulations with feeding and absorbing structure

In order to realize a structure that can be manufactured, the same feeding structure is used at the other side of the waveguide too (Fig. 2.12). One port emits the guided wave and the other one absorbs the

guided wave.

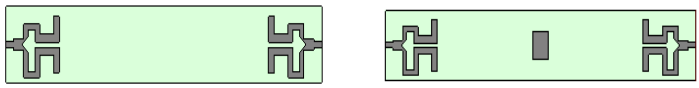

(a) (b)

Fig. 2.12 (a) waveguide with feeding and absorbing parts, (b) the complete structure

The simulated S parameters are presented in Fig. 2.13 and 2.14 for the waveguide and the patch scatterer. Although the transmission coefficient has decreased from -1.62 dB to -4.49 dB when the ideal waveguide port is replaced by the absorbing structure (see Fig. 2.9 up to 2.13), there is no significant change in the results of the patch structure (see Fig. 2.10 and 2.14). This means that radiation from the absorbing structure is suppressed while the patch is put in the middle of the waveguide. Based on these simulated results, the power balance is calculated and given in Table 2.3.

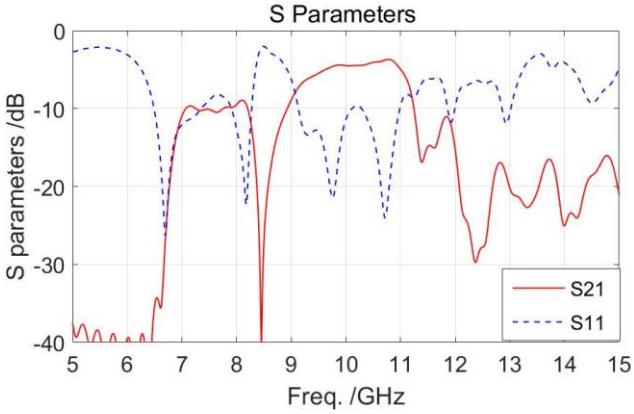

Fig. 2.13 S parameters with feeding and absorbing parts (at 10 GHz, S_{21} = -4.49 dB, S_{11} = -11.39 dB)

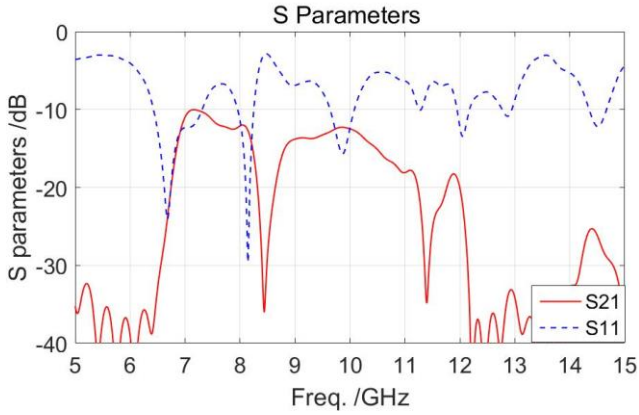

Fig. 2.14 S parameters of the complete structure (at 10 GHz, S_{21} = -12.05 dB, S_{11} = -12.12 dB)

Table. 2.3 Percentage of each power components at 10 GHz

	Waveguide (WG)	WG + feeding	WG + feeding + patch	WG + feeding + absorbing	Complete structure
Return loss	0.02%	2.2%	7.3%	7.3%	6.1%
Transmitted power	99.28%	68.9%	9.0%	35.5%	6.3%
Radiated power	0.70%	28.9%	83.7%	57.2%	87.6%

In this table, we can clearly see that most of the power (68.9%) can be fed into the waveguide by the selected feeding topology. When this topology is also put on the other side as the absorbing port, the radiated power almost doubles while the transmitted power declines to 35.5%. For the structure with feeding topology and patch, and the complete structure, the percentages are quite similar with a significant increase of radiation (83.7% and 87.6%, respectively) and a great decrease of the transmitted power (less than 10%), which means that most of the power is coupled to the middle patch and radiated into space. The radiation from the absorbing port is suppressed. The return loss always remains at a low level below 8% for all these structures.

2.3.2 Measured results and comparisons

On the basis of the previous designs, we manufactured two prototypes and measured them carefully, see Fig. 2.15 and 16. The measurement of the transmission and reflection of the prototypes was conducted in our lab with the vector network analyzer (VNA) HP8510. Before the measurement, the short-load-open-thru (SLOT) calibration method was used to eliminate the system errors. An absorbing material was put besides the the prototypes to reduce the environmental influences.

Fig. 2.15 Sample of waveguide and measurement setup

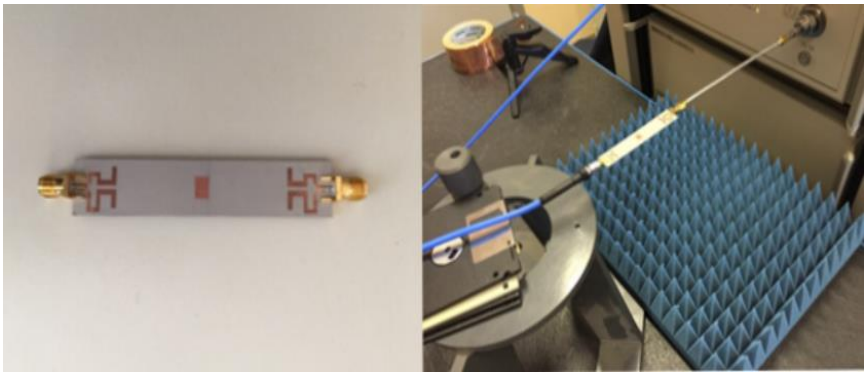

Fig. 2.16 Sample of patch scatterer and measurement setup

Comparisons of the measured and simulated results (S_{21}) are plotted in Fig. 2.17 and 18 for these two samples, respectively. Considering the changes on the given permittivity values of the substrate material, there is a frequency deviation (about 0.5 GHz) in the results. But the tendency matches well, and it is confirmed by the experimental results

that the guided wave is coupled with the patch and radiated into free space.

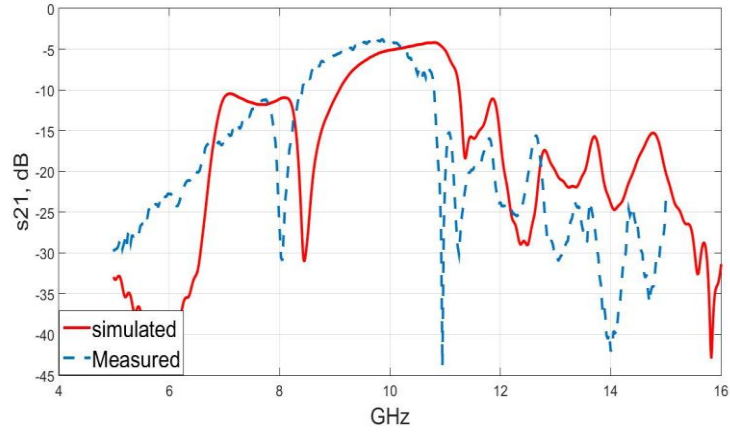

Fig. 2.17 Comparison of measured and simulated results for waveguide sample

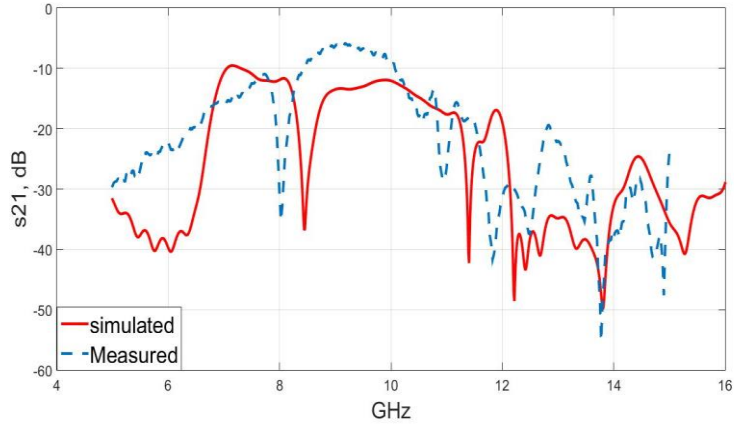

Fig. 2.18 Comparison of measured and simulated results for scatterer sample

2.4 Conclusion

In this chapter we have investigated in detail the wave propagation characteristics in a rectangular dielectric waveguide in the presence of a top-mounted patch scatterer. The scatterer couples to the propagating EM wave and, if properly designed, is able to generate radiation, just as an antenna element. First, this idea was verified by simulations in CST. Then, we designed a feeding structure in order to be able to

fabricate a real prototype. This prototype was measured and used to validate the concept of this type of antenna. As far as we know, this is the first antenna of this type realized in X band.

Reference

[2-1] Y. Rong, K. A. Zaki, M. Hageman, D. Steven and J. Gipprich, "Low-temperature cofired ceramic (LTCC) ridge waveguide band pass chip filters," *IEEE Trans. Microwae Theory Tech.*, vol: 47, iss. 12, Dec. 1999, pp: 2317 – 2324.

[2-2] J. D. Love and C. Winkler, "Power attenuation in bent multimode step-index slab and fiber waveguides," *Electronics Lett.*, vol. 14, iss. 2, Jan. 1978, pp: 32 – 34.

[2-3] D. M. Pozar, Microwave Engineering, 3th Edition, John Willy and Sons, Jan. 2007.

[2-4] E. A. J. Marcatili, "Dielectric rectangular waveguide and directional coupler for integrated optics," *Bell Labs Technical Journal*, vol. 48, iss. 7, Sep. 1969, pp: 2071 – 21025

[2-5] J. Sharma and A. De, "Full-wave analysis of dielectric rectangular waveguides," *Proc. PIERS*, vol. 13, Jan. 2010, Cambridge, USA, pp: 121 -131.

[2-6] A. Oliner, S. T. Peng, T. I. Hsu and A. Sanchez, " Guidance and leakage properties of a class of open dielectric waveguides: Part II – New physical effects," *IEEE Trans. Microwae Theory Tech.*, vol: MTT-29, no. 9, Sep. 1981, pp: 855 – 861.

[2-7] Y. Qian and T. Itoh, "A broadband uniplanar microstrip-to-CPS transition," *Asia-Pacific Microwave Conf. Dig*., Dec. 1997, pp: 609-612.

CHAPTER 3 NONUNIFORM ANTENNA ARRAY

In this chapter, two types of planar antenna array fed by RDW are proposed for X-band and WiFi applications, respectively. Based on the coupling effect between the travelling wave inside the waveguide and printed metal elements, the non-uniform antenna elements are placed in series along the waveguide to achieve a directive radiation and avoid the ‘stop band’ effect of the 1-D periodic leaky waveguide antenna array. Prototypes are manufactured and measured to prove the concept. A very reasonable performance is achieved with a simple planar structure without feeding network, which is easily manufactured with mass-production Printed Circuit Board (PCB) technology.

This chapter is based on the following publications:

[1] Linghui Kong, Sen Yan, Vladimir Volski and Guy A. E. Vandenbosch, “Linear non-uniform antenna array of planar elements fed by a dielectric waveguide,” Microwave and Optical Technology Letters (MIOTL), Vol 60, iss. 4, Apr., 2018, pp: 849 - 854.

[1] Linghui Kong, Sen Yan and Guy A. E. Vandenbosch, “Directive planar antenna array fed by dielectric waveguide for WiFi applications,” Microwave and Optical Technology Letters (MIOTL), Vol 60, iss. 8, Jun., 2018, pp: 1963 - 1967.

3.1 Introduction

In the first part, we aimed at designing a cheap, low loss, medium sized array topology that meets the antenna requirements for radar and localization purposes, operating in corridors and elongated rooms in X band.

The X-band frequency range (8 – 12 GHz) plays an important role in applications related to localization and positioning. This includes surveillance, logistics, drive support, monitoring of vehicular movements, entertainment, etc. [3-1, 2]. Among the technologies used for radio localization and positioning, we distinguish between outdoor scenarios and indoor environments. Considering the former one, commonly used techniques are based on satellite systems, WiFi access points, and celluar networks [3-3, 4]. For indoor localization, wireless sensor networks offer an innovative solution to achieve a high accuracy. Such a system could consist of hundreds of sensor nodes, each node integrated with an antenna for signal transferring [3-5].

Inspired by the advantages of the low-loss dielectric waveguide, the single dielectric strip as a substrate waveguide is chosen to feed four planar elements of a linear non-uniform array in X band. The non-uniformity of the elements is absolutely crucial in order to reach the proper power distribution over the elements. Although the antenna uses a very generic form of series feeding, its operating principle is totally different from the directly coupled array, cfr. the Yagi-Uda antenna [3-6], since the energy is coupled to each radiating element separately from the guided wave propagating in the dielectric waveguide. In a Yagi-Uda, all coupling in between the elements is via free space. To the best knowledge of the authors, this concept is presented for the first time. Another novel point in this design is using the non-uniformity to avoid the “stopband effect” and the poor broadside radiation of 1-D open periodic structures, as reported in [3-7]. It allows a well-behaving broadside radiation. The optimization

of the design also involved the achievement of a high radiation efficiency, and minimum side lobes.

In the following sections, first the electromagnetic coupling and scattering effects are studied for a single antenna element in the strip waveguide. Afterwards, the topology is extended to a series-fed 4-element non-uniform antenna array, and finally the feeding launching structure is incorporated in the design, and the fabricated prototype is discussed.

Then, in the second part, a conceptually new, low-cost antenna topology with compact and low profile is proposed to meet the requirements in the indoor and outdoor fixed point scenarios for WiFi applications.

Wireless fidelity (WiFi) is a superset of the IEEE 802.11 standards for communications in the 2.4 and 5 GHz industrial, scientific and medical (ISM) bands [3-8, 9]. In a typical WLAN network, a WiFi connection is built up through the wireless stations including fixed access points (APs) and mobile or fixed devices such as laptops, IP phones or personal digital assistants [3-10]. According to the different scenarios, WiFi antennas can be mainly divided into three groups for outdoor, indoor and mobile applications. The indoor and outdoor antennas include backhaul and fixed base-station antennas. They usually need to provide a gain up to 10 dBi for point to point links and are commonly mounted on towers or buildings for line of sight (LOS) communications with reduced multipath interference. Some typical directional antennas like Yagi antennas, dish/grid reflector antennas, or circular polarized endfire helix antennas [3-11], are employed for this application.

For the indoor and outdoor point to point connections, design of antennas with high directivity and gain performance is desirable. The most common way to achieve this target is to configure a series of single radiators as an array topology [3-12]. According to the different

types of feeding method, these antennas can be divided into the types of series and corporate feeding networks. Compared with the corporate-fed array, the size of the series feeding network can be usually reduced significantly. Also, it usually allows a slight steering of the main beam with frequency [3-13].

The rectangular dielectric strip is chosen as the substrate waveguide to feed four planar elements of a linear non-uniform array. The non-uniformity of the elements is absolutely crucial in order to reach the proper power distribution over the elements.

3.2 Bidirectional antenna design

In this section, the proof of concept is given by simulation results, first for a single patch, and then for a 4-element non-uniform array. These antenna elements are optimized in such a way that each element radiates the required power in order to provide a medium gain broadside beam. All designs are performed with CST Microwave Studio. Waveguide ports are used to launch the wave in the dielectric.

3.2.1 Single element

First, the coupling between the wave traveling in the rectangular dielectric substrate and a single element is studied. The structure is shown in Fig. 3.1.

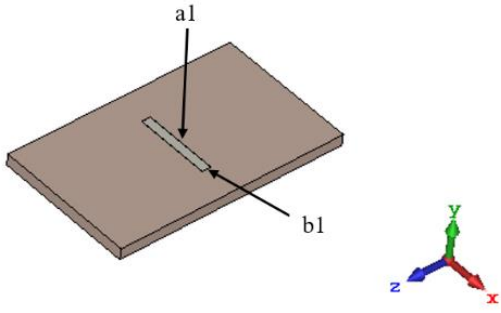

Fig. 3.1 Single antenna element

The dielectric strip waveguide is still designed on the basis of a piece of low-loss high permittivity Rogers RT 6010 substrate (permittivity 10.2, tg δ = 0.0023, thickness 1.27 mm). The dimensions are chosen so that a final prototype will be obtained that is easily mountable in a monopole like fashion, for example on the ceiling of a corridor or a room.

The occupied ratios of the radiation, reflection and transmission over the incident power (the power in the incident wave) for a 1 mm wide strip as a function of the strip length *a1* are given in Fig. 3.2. It is clearly shown that around 7.0 mm a considerable amount of power (about 35%) is radiated due to the resonating current on the strip. Note that the effect on this radiated power of changing the width is marginal. Essentially, this means that it is indeed possible to extract the necessary power from a wave traveling in the dielectric to assemble an array structure. Further, the far field patterns with different lengths of the printed strip are presented in Fig. 3.3, it is seen that maxima occur in the two directions normal to the substrate, as is needed to construct an array with radiation in the front and back broadside directions.

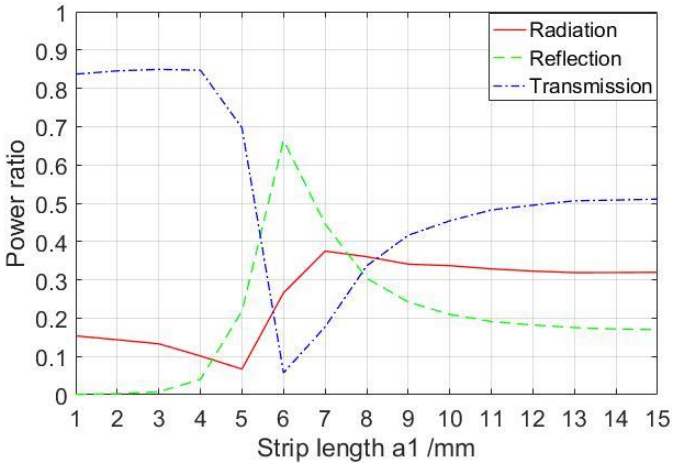

Fig. 3.2 Ratios of radiation, reflection and tranmission over incident power as a function of the strip length for 1 mm wide at 9.5 GHz

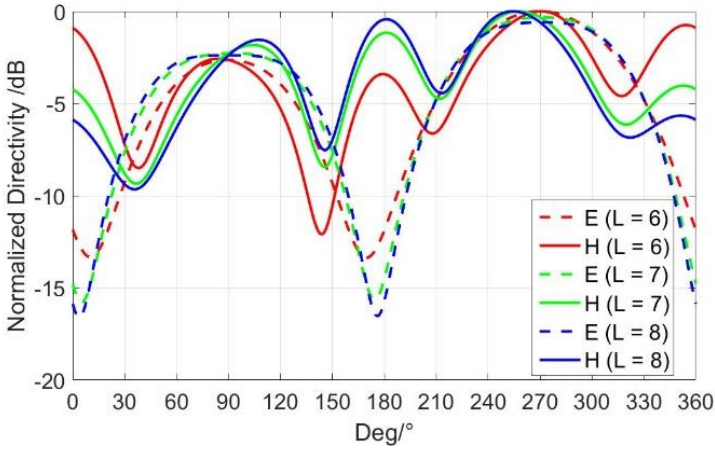

Fig. 3.3 Simulated far field pattern of the single element for different strip lengths at 9.5 GHz, both in E and H plane. E plane = xy plane, H plane = yz plane.

3.2.2 Four elements

In order to increase the gain in the broadside directions, the concept is extended and used in a 4-element non-uniform linear array, as shown in Fig. 3.4. The idea is that at one side the wave in the dielectric waveguide is launched and that, while the wave is travelling to the other end, each patch element extracts a certain amount of power from this wave. This extraction of partial power is very similar as in the antennas described in [3-14, 15]. However, in these publications the concept is worked out with a traditional feeding network involving conductors. The waveguide ports are added in CST at both sides of the substrate for excitation and absorbing. The dimensions of the elements and the distances between them are optimized in such a way that the realized gain in the broadside directions is maximized while the wave reflection and transmission are kept at a low level. The research problem can be described as an optimization problem within the frequency range from 9.0 GHz to 10.0 GHz. The Genetic Algorithm optimization available in CST Microwave Studio is employed. The resulting dimensions are listed in Table 3.1

$$PI \quad Find \ (a1, a2, a3, a4, b1, b2, b3, b4, d1, d2, d3, d4)$$

$$Max \quad RlzGain(\vartheta = 90°, \varphi = 90°)$$

$$S.t. \quad S_{11} < -10dB$$

$$S_{21} < -10dB$$

$$9.0GHz \le f \le 10.0GHz$$

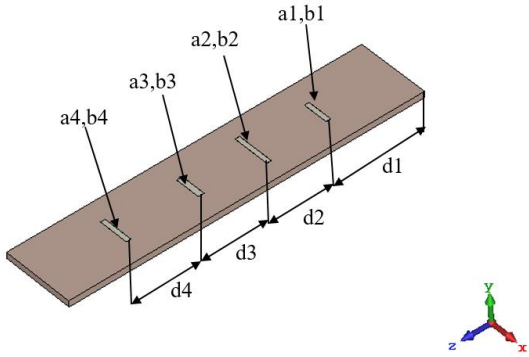

Fig. 3.4 The 4-element antenna array of strips in the waveguide, substrate length = 87 mm, substrate width = 15 mm.

Table. 3.1 Dimensions of the optimized 4-element array

Parameter	Values (mm)	Parameter	Values (mm)
a1	5.2	b3	1.1
a2	7.8	b4	0.9
a3	5.6	d1	14.5
a4	6.5	d2	13.9
b1	1.0	d3	13.3
b2	0.9	d4	15.6

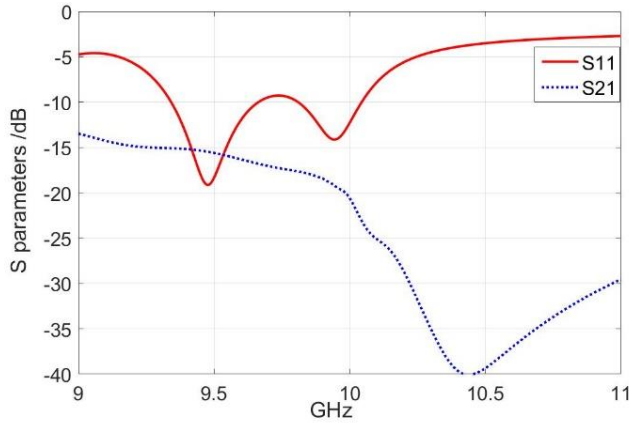

Fig. 3.5 Simulated S parameters of the 4-element array

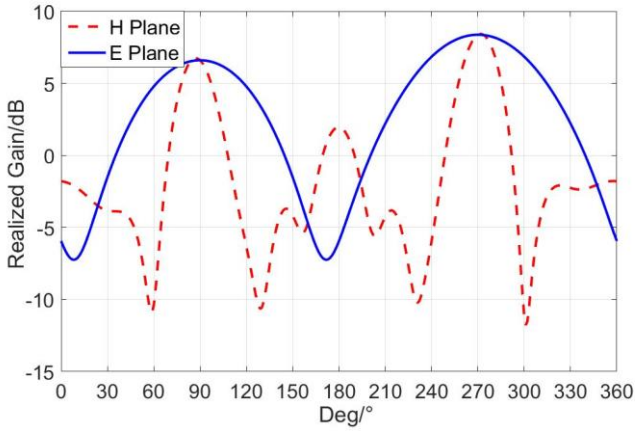

Fig. 3.6 Simulated far field pattern at 9.5 GHz for H plane (yoz) and E plane (xoy)

Fig. 3.5 presents the simulated S parameters and Fig. 3.6 gives the far field pattern at 9.5 GHz. The main lobe directs to 270 degrees and the magnitude achieves to 8.4 dBi. Compared with the single patch antenna, the array configuration not only provides a broadside beam, but also achieves a high radiation efficiency (92%).This study extends the proof of the proper working of the new concept also to medium sized non-uniform arrays.

3.3 Comparison of simulation and measurement

3.3.1 Prototype

In this section, a practical prototype is designed, built, and measured. The simulated model and the real prototype are shown in Fig. 3.7 and 8, respectively. It involves a more practical finite structure with a realistic single feeding topology to launch the wave. The feeding structure of the printed dipole connected with microstrips (Fig. 3.9) is used again as the feeding part to excite the transmission mode. The frequency targeted is part of the radio location sub-band in X band, i.e. 8.75 – 9.75 GHz. As the feeding structure itself contributes to the radiation pattern and affects the final result, a new optimization has been performed with the dimensions of the feeding structure (as

shown in Fig. 3.9) included in the list of optimization parameters. The resulting optimized dimensions are listed in Table 3.2.

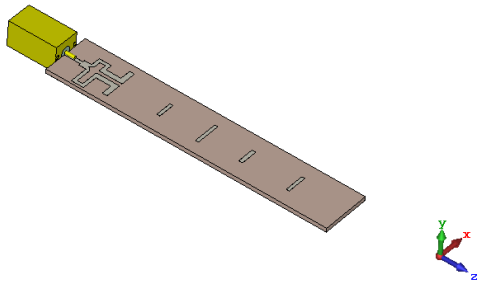

Fig. 3.7 Simulation model for the real prototype

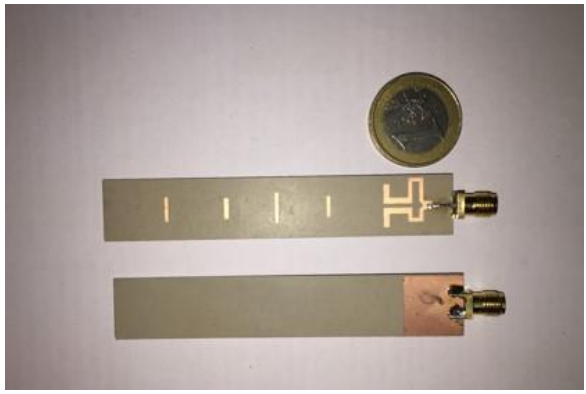

Fig. 3.8 Fabricated prototypes

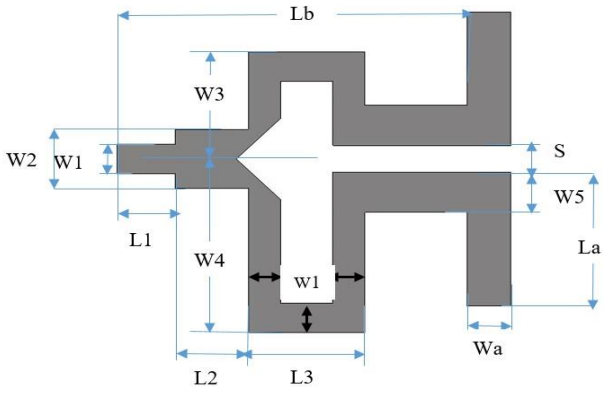

Fig. 3.9 Top view of the feeding structure

Table 3.2 Dimensions of the optimized 4-element array with feeding structure

Parameters	Values (mm)	Parameters	Values (mm)
a1	5.2	L1	5.0
a2	7.6	L2	2.3
a3	5.2	L3	3.8
a4	6.2	La	5.0
b1	1.0	Wa	1.5
b2	0.9	Lb	15.7
b3	1.2	s	1.0
b4	0.9	w1	1.1
d1*	31.0	w2	2.2
d2	12.9	w3	4.1
d3	12.5	w4	6.9
d4	14.8	w5	1.5

d1 represents the distance from the edge of the dielectric waveguide to the first element. The distance between the last element and the edge of the waveguide is 15.3 mm.

3.3.2 Results analysis

It is very important to emphasize the following. At first the permittivity for the Rogers RT 6010 substrate (i.e. 10.2, as provided by the manufacturer) was used in the design. However, this gave a quite poor agreement between simulations and measurements. After investigating this issue a bit deeper, it was discovered that Rogers actually gives several and different permittivities, the "common" one in the direction normal to the substrate sheet (to be used in regular designs, i.e. 10.7) and another one in the directions parallel to the sheet (i.e. 13.3) [3-16]. The fact that this substrate is anisotropic had to be rigorously taken into account in order to obtain a good agreement between simulations and measurements. This is a consequence of the fact that the main electric field component in the dielectric waveguide is directed parallel to the sheet.

In Fig. 3.10, the simulated and measured reflection coefficients are presented. When the material permittivity is changed with the anisotropic values of $\varepsilon_x = \varepsilon_z = 13.3, \varepsilon_y = 10.6$. The simulated results of S parameters can reach a good match with the measurement at 9.20

GHz. In a bandwidth of about 160 MHz, the measured reflection is below -10 dB. The simulations yield that at 9.2 GHz about 86% of the energy is radiated. The effect of the anisotropy is clearly illustrated by also simulating the structure with a 10.2 permittivity.

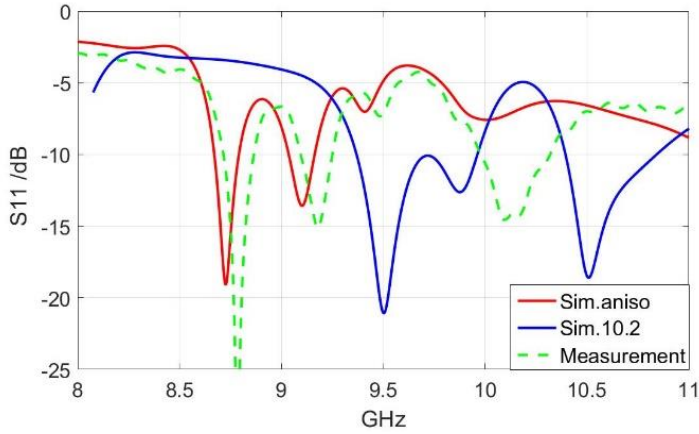

Fig. 3.10 Simulated and measured reflections of the prototype. Sim. Aniso indicates the simulation with the anisotropic permittivity, and Sim. 10.2 indicates the simulations with default value of 10.2. dashed green line is the measured results.

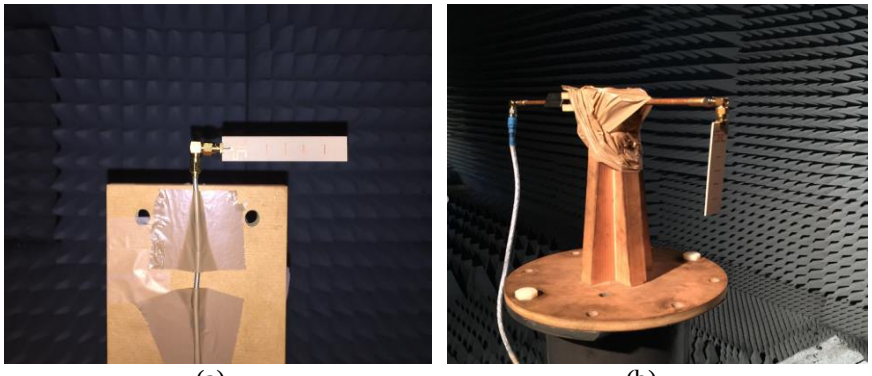

(a) (b)

Fig. 3.11 Far field measurement setup, (a) E plane (b) H plane

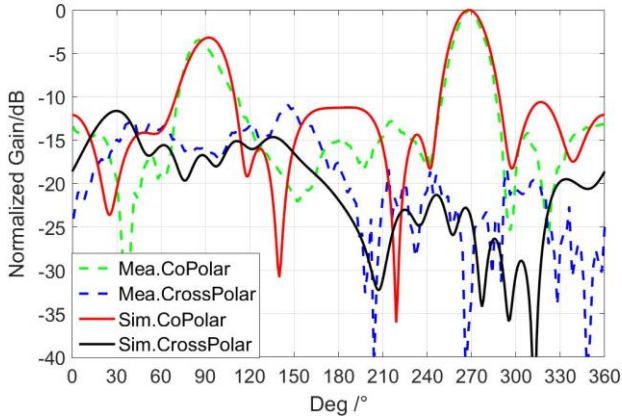

Fig. 3.12 Normalized measured and simulated H-plane (yz plane) pattern of the prototype at 9.2 GHz

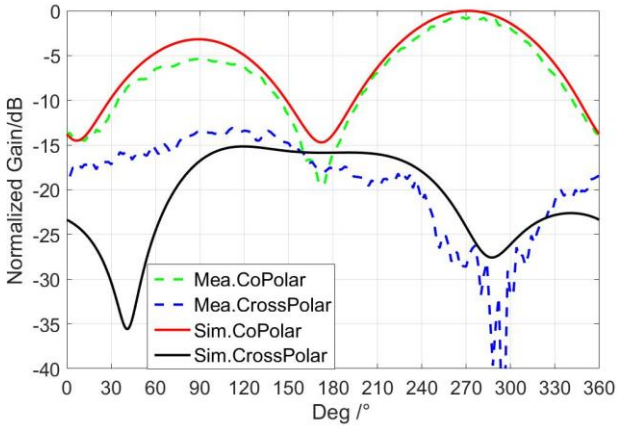

Fig. 3.13 Normalized measured and simulated E-plane (xy plane) pattern of the prototype at 9.2 GHz. Normalization is with respect to the maximum in the H-plane at 270 degrees

Fig. 3.11 is the setup for the far field measurement in the anechoic chamber. The signal source is an HP83630A with a working frequency range from 10 MHz to 26.5 GHz. The antenna under test (AUT) is connected by a coaxial cable to the receiver. The far field pattern is measured at 9.2 GHz, which is practically in the middle of the targeted band. and the normalized results in the H and E planes are given in Fig. 3.12 and 13, respectively. In each plane, the far field pattern is measured in the whole space with a rotation angle of 2 degrees for each step to ensure the continuity of the curve. The positions 90° and

270° correspond to the top and bottom direction, respectively.

The measured results of the co-polarization agrees well at the broadside front and back side directions, while the cross-polarization is at levels of more than 10 dB below the co-polar main beam. With the measured far field pattern of the AUT, a standard horn antenna is used for the calculation of the realized gain of the AUT. The maximal value of the measured realized gain is 8.51 dB to the back. It is clearly shown that this non-uniform antenna array achieves a bidirectional normal radiation pattern with a quite high efficiency.

3.4 Grounded antenna design

To further improve the gain performance, a metal ground is added to the proposed RDW-based antenna array for WiFi applications. Compared with omnidirectional antennas, directional antennas usually focus more energy in one direction, and are typically used to extend the WiFi network into hard-to-reach corners of buildings or other specific situations.

3.4.1 Antenna design

The geometry of the antenna array is shown in Fig. 3.14. The same feeding structure (Fig. 3.9) is used to launch the propagated E_{11}^{x} mode. The low-loss and high permittivity Rogers RT 6010 is chosen as dielectric waveguide material with the dimensions of 100 x 24.5 mm. This is an anisotropic material with different permittivities in the different directions ($\varepsilon_x = \varepsilon_z = 13.3, \varepsilon_y = 10.6$, $tg\ \delta$ = 0.0023, thickness = 1.91 mm).

A finite ground plane with length 105 mm and width 68.5 mm is applied to shield from the underground and to boost the directivity. In previous work, the electromagnetic coupling between this wave and a patch mounted at the surface of the dielectric was validated [3-17]. Although a high coupling and a high radiation efficiency can be obtained from a single patch, it is not possible to achieve a high

enough gain in the broadside direction. Hence, four patch elements are placed in series. Furthermore, a finite ground based on an FR4 slab is used as the reflector to improve the gain performance in the broadside direction. The distance between the ground and the substrate waveguide is 11.0 mm aiming at half a wavelength at 5.7 GHz. It reflects the backside radiated wave in phase with the top radiation.

The Genetic Algorithm optimization tool available in CST Microwave Studio is employed. The optimization involves the targets of a high radiation efficiency, and minimum side lobes. The resulting optimized parameters are listed in Table 3.3. The feeding structure used to excite the E_{11}^{x} mode inside the waveguide is based on a printed dipole [3-18]. As this dipole also contributes to the far field, the optimization incorporated the dimensions of the complete launcher topology together.

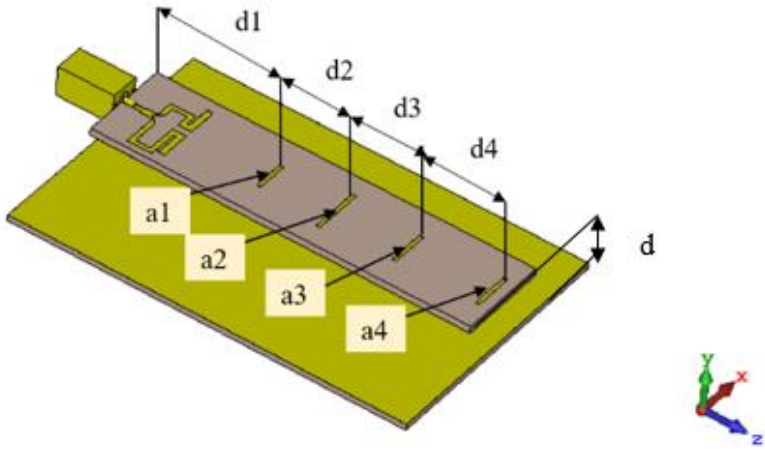

Fig. 3.14 Geometry of the antenna, a1 to a4 are the lengths of the four elements, all widths are kept at 1 mm, d1 to d4 refer to the distances between the elements, the distance between ground and the substrate waveguide is d = 11 mm.

Table 3.3 Optimized dimensions of the antenna array including the feeding structure

Parameter	Values (mm)	Parameter	Values (mm)
a1	8.5	L3	6.6
a2	13.5	La	8.1
a3	10.2	Wa	1.6
a4	10.4	Lb	15.7

d1	38.8	S	1.9
d2	17.5	w1	1.3
d3	18.8	w2	2.0
d4	21.7	w3	5.7
L1	5.1	w4	10.4
L2	3.3	w5	1.7

3.4.2 Ground size influence

Considering that the ground size can be changed greatly in the real environment, we conducted the simulations of the model with different ground sizes. The simulated results of return loss are plotted in Fig. 3.15, from which we can see there is little influence on the return loss from the change of the ground size. Also, in Fig. 3.16 and 17, we present the simulated results on the far field gain performance with different ground sizes. The simulated maximal realized gain in the broadside direction are listed in Table 3.4. Compared with the original topology, we can also find that the changes on the gain performance are quite small for the different ground sizes. Based on these results, we can conclude that there is little influence from the ground size for the antenna performance on the real installation environment.

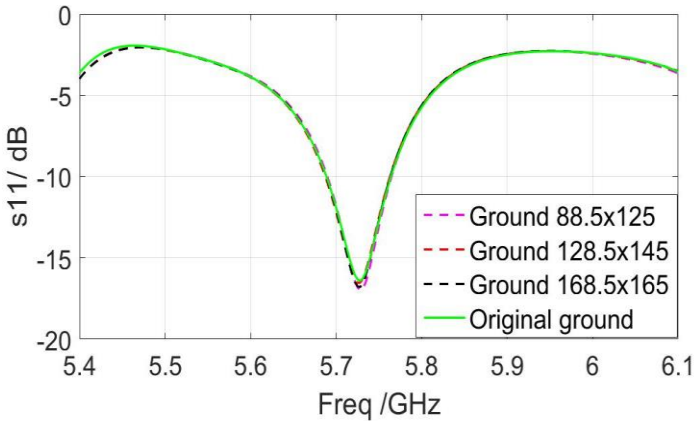

Fig. 3.15 Simulated results of S_{11} with different ground sizes

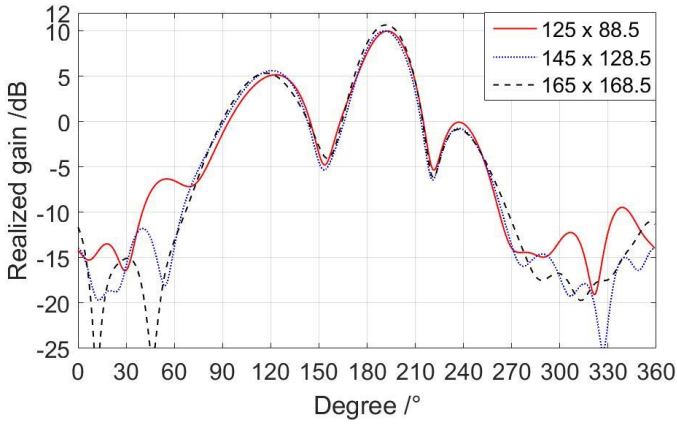

Fig. 3.16 Simulated gain performance (H plane) with different ground sizes

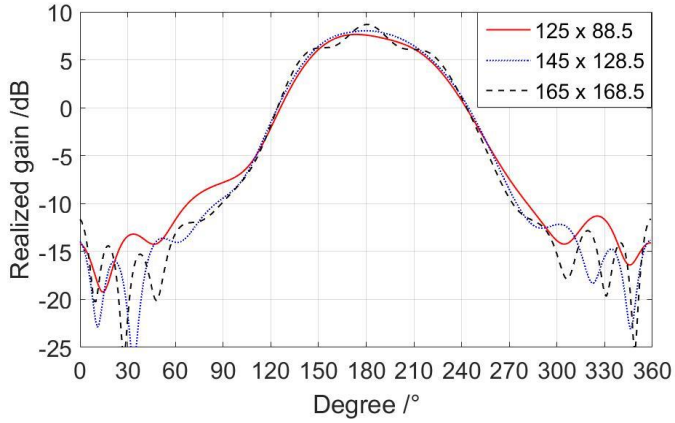

Fig. 3.17 Simulated gain performance (E plane) with different ground sizes

Table 3.4 the simulated maximal realized gain in the broadside direction with different ground sizes (unit: mm, dBi)

Ground sizes	68.5 x 100	88.5 x 125	128.5 x 145	168.5 x 165
Realized gain	10.9	10.0	10.0	10.7

3.5 Comparison of simulation and measurement

3.5.1 Prototypes

A prototype based on the design is built and measured, see Fig. 3.18. The plastic screws, with a low permittivity, are used to connect the antenna with the metal ground. The far field pattern and the gain

performance are measured in the anechoic chamber and the setup is presented in Fig.3.19.

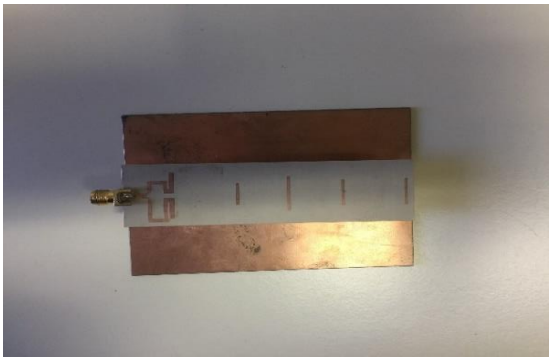

Fig. 3.18 Fabricated antenna sample

Fig. 3.19 Far field measurement setup

3.5.2 Results analysis

The comparison of the simulated and measured reflection coefficients are presented in Fig. 3.20. The frequency shift is about 40 MHz or 0.7%. The -6 dB bandwidth is about 150 MHz and the -10 dB bandwidth is about 80 MHz. This is sufficient to cover several channels in the 5 GHz WiFi band.

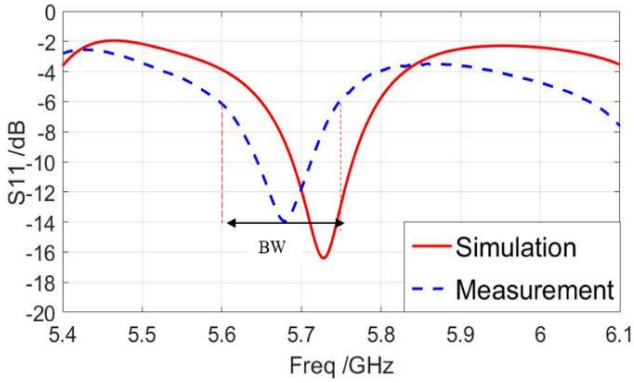

Fig. 3.20 Simulated and measured S_{11}

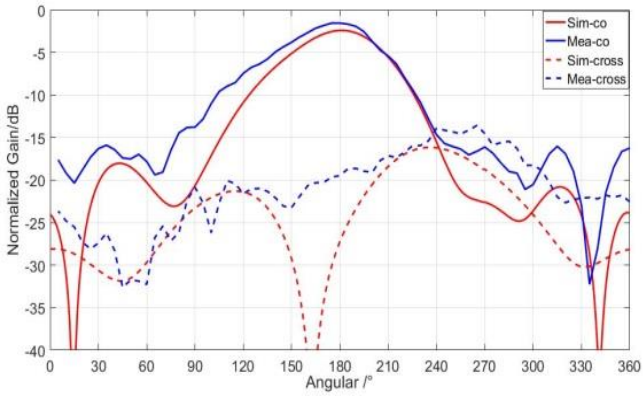

Fig. 3.21 Normalized measured and simulated E-plane (XY plane) pattern of the proposed antenna array at 5.7 GHz.

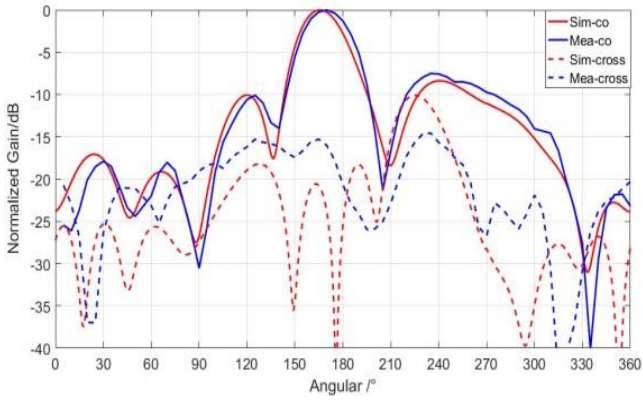

Fig. 3.22 Normalized measured and simulated H-plane (YZ plane) pattern of the proposed antenna array at 5.7 GHz.

The E-plane and H-plane patterns at 5.7 GHz are shown in Fig. 3.21

and 22, respectively. Simulated and measured co-polarization components agree well. The measured cross-polarization component always stays below the -10 dB threshold. The measured realized gain in the broadside direction is 9.58 dBi. The 3 dB angular beam widths are 60 degrees in the E-plane and 30 degrees in the H-plane. The calculated radiation efficiency reaches 84.0%. It is clearly seen that this non-uniform antenna array achieves a directional radiation pattern with a quite high efficiency.

3.6 Conclusion

In this chapter, a single rectangular dielectric substrate is employed as the waveguide feeder for the design of planar antenna arrays, which could improve the gain performance significantly in the far field. It is first used for a 4x1 X-band non-uniform antenna array with the antenna elements in different design parameters and spaces. This non-uniformity is essential in order to reach the design target of broadside beams with high efficiency. This mitigates one of the disadvantages of a periodic uniform array configuration in such a dielectric waveguide feeder: the poor radiation in the broadside direction.

Then, this antenna topology is extended for outdoor point to point WiFi scenarios. The proposed antenna operates around 5.7 GHz with a bandwidth of 80 MHz. A metal ground plane is added to reach the design target of broadside beams with sufficient gain. Analysis of the ground size influence from the real environment installation are also validated with simulations.

Reference

[3-1] O. Losito, L. Mescia and M. A. Chiapperino, "X-Band SIW cavity-backed patch antenna for radar applications," in *Proc. 43rd Eur. Microw. Conf.*, Nuremberg, Germany, Oct. 2013, pp. 199-202.

[3-2] R. Y. Hermansyah, F. Y. Zulkifli and E. T. Rahardjo, "Radiation characteristics of slotted waveguide array antenna for x-band dual-polarized weather radar," in *Proc. PIERS*, Shanghai, China, Nov. 2016, pp. 3988-3991.

[3-3] M. Lazecky, I Hlavacova and M. Bakon, "Bridge displacement monitoring using space-borne x-band SAR interferometry" *IEEE Journal of Selected Topics in Applied Earth Obervations and Remote Sensing*, vol. 10, no. 1, Jan. 2017, pp. 205-210.

[3-4] X. Fu, A. P. Engel, D. Arnitz and C. M. Watts, "Simultaneous imaging, sensor tag localization, and backscatter uplink via synthetic aperture radar," *IEEE Trans. MTT*, vol. 66, iss. 3, Mar. 2018, pp: 1570 – 1578.

[3-5] S. Arianos, G. Dassano and F. Vipiana, "Propagation study and antenna design for wireless sensor networks in train environment," in *Proc. EuCAP*, Hague, Netherlands, Apr. 2014, pp. 2899-2900.

[3-6] P. Cheong, K. Wu, W. W. Choi and K. W. Tam, "Yagi-Uda antenna for multiband radar applcations," *IEEE Antennas and Wireless Propagat. Lett.*, vol. 13, Jun. 2014, pp: 1065 – 1068.

[3-7] P. Baccarelli, S. Paulotto, D. R. Jackson and A. Oliner, "A new brillouin dispersion diagram for 1-D periodic printed structures," *IEEE Trans. Microw. Theory Tech.*, vol. 55, no. 7, pp. 1484-1495, Feb. 2007.

[3-8] Z. N. Chen, X. M. Qing, T. S. P. See and W. K. Toh, "Antennas for WiFi connectivity," *Proc. The IEEE*, 2012, 100, (7), pp. 2322-2329

[3-9] [2] M. K. Usman, K. Zain and A. H. Syed, "Wireless health monitoring using passive WiFi sensing," *Proc. Of 13th IWCMC*, Valencia, Spain, Jun. 2017, pp. 1771-1776.

[3-10] G. V. Ricardo, J. A. Hildeberto and L. M. Roberto, "Broadband PIFA antenna for mobile communication terminals," *Proc. Of 11th Conf. on Electrical Engineering, Computer Science and Automation Control*, Campeche, Mexico, Sep. 2014.

[3-11] Y. X. Gu, M. Zhou, S. L. Fu and Y. Wan, "Airborne WiFi network through directional antenna: an experimental study," *Proc. Of IEEE WCNC, New*

Orleans, LA, USA, Mar. 2015, pp. 1314-1319.

[3-12] M. M. I. Shekh, A. Q. Farhan, F. I. Magdy and S. Galen, "Advanced directional networking: LTE vs WiFi radios," *2017 IEEE AP-S Symposium on Antennas and Propagation and USNC-URSI Radio Science Meeting*, California, USA, Jul. 2017, pp. 189-190.

[3-13] Y. J. Cheng, Y. X. Guo, X. Y. Bao and N. N. Kung, "Millimeter-wave low temperature co-fired ceramic leaky-wave antenna and array based on the substrate integrated image guide technology," *IEEE Trans. Antennas. Propag.*, 2014, 62, (2), pp. 669-676.

[3-14] Z. Ma, V. Volski, and G. A. E. Vandenbosch, "Optimal design of a highly compact low-cost and strongly coupled 4 element array for WLAN", *IEEE Trans. Antennas Propagat.,* Vol. 59, no. 3, Mar. 2011, pp. 1061-1065.

[3-15] Z. Ma and G. A. E. Vandenbosch, "Low-cost wideband microstrip arrays with high aperture efficiency," *IEEE Trans. Antennas Propag*., vol. 60, no. 6, Jun. 2012, pp. 3028-3034.

[3-16] Rogers Corp.: General information of dielectric constants for circuit design using rogers high frequency materials. [Online]. Available: https://globalcommhost.com/rogers/semiprivate_test/docs/General_information_of_design_dk_rev4.pdf.

[3-17] L. H. Kong, X. Z. Zheng, S. Yan and G. A. E. Vandenbosch, "Design of a dielectric waveguide antenna at microwave frequencies," *Proc. Of EuCAP*, Paris, France, Mar, 2017, pp. 2017-2019.

[3-18] N. Dolatsha and J. Hesselbarth, "Power divider based on grounded dielectric slab waveguide operating in E_{11}^{x} mode," *Proc. Of the 6th German Microwave Conf.*, Darmstadt, Germany, Mar. 2011.

CHAPTER 4 EBG-BASED DIELECTRIC IMAGE GUIDE

In this chapter, electromagnetic bandgap (EBG) structures are studied and used in the design of new transmission media for 5G applications. Combined with the dielectric image guide (DIG), the mushroom-like EBG units at the edges of the wave guide yield a transmission efficiency that is almost the same as in the case of a real dielectric waveguide. Besides, a tapered CPW to SIW transition structure is used as the mode launcher to achieve a broadband and smooth mode conversion to the guiding channel. Simulation results show that this new proposed waveguide can be efficiently working in the targeted frequency range.

This chapter is based on the following paper:
[1] L. H. Kong, S. Yan, V. Volski and G. A. E. Vandenbosch, “A new design of EBG-based dielectric image guides for 5G applications,” manuscript in preparation.

4.1 Introduction

With the rapid development of the next generation (5G) mobile communication networks, there is a large demand to increase the overall system bandwidth as well as the connectivity at all levels, from individual ICs to backplanes. As aggregate link data rates and capacity requirements are coming to the Tbps level, current physical channels are facing severe limitations [4-1]. A bottleneck of power is appearing on the horizon because of maximum data flux density and link efficiency when the bandwidth of conventional planar on-board transmission lines are pushed to tens of GHz. To achieve a high data-rate, wideband and large-capacity communications, the 5G system will introduce the use of higher frequency bands such as the unused millimeter wave bands [4-2].

At higher frequencies, several figures must be considered when assessing communication channels: bandwidth, data rate, overall energy efficiency and the associated cost. To improve the bandwidth, it is necessary to eliminate the influences from the high-loss, dispersion, cross-talk and reflections from the conventional planar TEM electrical channel [4-3]. In these lines, the capacity of the link is mainly restricted by the skin effect and the impedance mismatches. Meanwhile, the line width is selected based on the wavelength of the guided wave, which poses limitations on the data flux density and energy efficiency. The frequency increase will also cause fabrication and mounting problems [4-4]. Although optical fiber links have been extensively used in long-distance communications, they are slowly making the way into the short-range arena as the associated power and cost overhead influence the adaptability for board-level interconnectors [4-5].

To solve these concerns, we propose a new dielectric transmission medium combining the dielectric image guide with EBG units, as seen in Fig. 4.1. The complete topology of the transmission medium is composed of three parts: the middle guiding channel, the feeding part

and the EBG units.

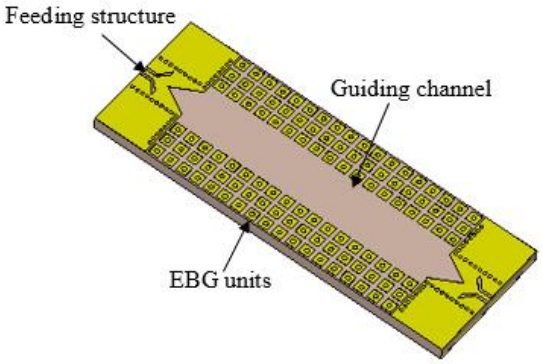

Fig. 4.1 Complete structure of the EBG-based DIG

The idea is to design the middle guiding channel to work in a specific frequency band. At the same time, by carefully choosing the parameters, we can make the stop band of the EBG units cover this frequency range. In this way, a higher transmission efficiency can be expected from this topology. All designs are performed with full wave analyses in CST Microwave Studio. The new medium offers a planar topology with low profile and easy integration for applications such as chip-to-chip interconnectors and antenna array feeders.

A common DIG is using a rectangular dielectric slab placed on a ground plane as shown in Fig. 4.2, which is the most widely used dielectric guide structure in component development and of increasing interest for millimeter-wave and sub-millimeter wave applications. The conducting plane beneath the dielectric can act as heat sink and be used for DC biasing of the integrated circuit device. The waves within DIGs are travelling along the interface between the dielectrics and air, and can be seen as a type of surface wave [4-6]. However, the power transferred into these surface waves will be scattered off the edges of the finite ground plane and lead to some deep nulls and ripples in the radiation pattern, increased back radiation, gain deterioration, low polarization purity, etc [4-7].

Fig. 4.2 Dielectric image guide

Aiming at this problem, we propose to add an additional shielding with EBG units to suppress surface wave propagation to the sides for this open structure. EBG structures are periodic structures that exhibit special properties in a band of frequencies called the band gap [4-8, 9]. When they interact with electromagnetic waves, different electrical properties are observed at different frequencies. These structures can pass certain frequency bands, reject some frequency bands, and behave like a magnetic conductor [4-10]. In the band gap, the EBG structures have a very high surface impedance, which makes them a good candidate to replace the ground plane and suppress the undesired surface wave in microwave components [4-11, 12].

A common type of EBG structure is realized by etching periodic mushroom-like square patches on a dielectric board (Fig. 4.3), with or without metal vias connecting the patches to the ground plane [4-13]. With adequate design parameters, materials and shapes, it can be used to control the propagation of electromagnetic waves [4-14]. In the following sections, the mushroom-like EBG unit will be discussed and analyzed, and finally adopted in the design of the new transmission medium.

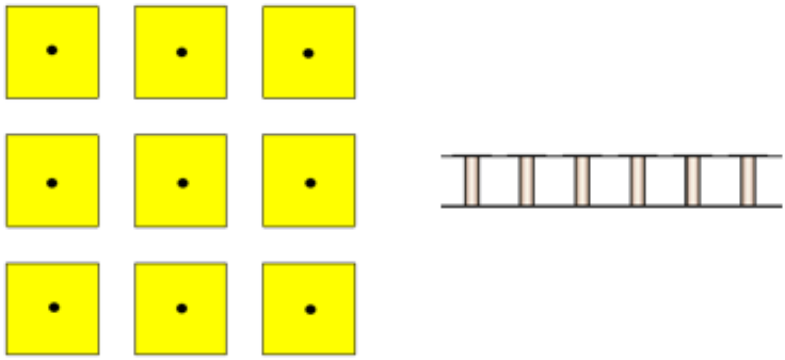

(a) (b)

Fig. 4.3 Mushroom-like EBG structure, (a) top view, (b) side view

4.2 Analysis of dielectric image guide

The dielectric image guide, as shown in Fig. 4.4, is designed with a piece of low-loss high permittivity Rogers RT 6010 substrate (permittivity 11.4, loss tangent 0.0023, thickness 1.27 mm). Structure dimensions are listed below the figure.

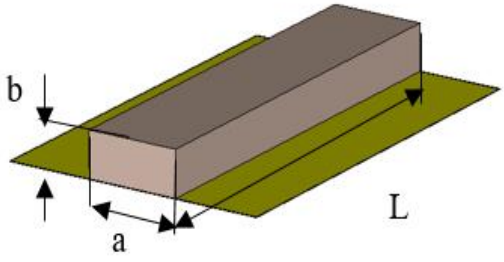

Fig. 4.4 The guiding channel of dielectric image guide in CST (a = 4.4, b = 1.27, L = 15, unit: mm)

As discussed in Chapter 2, there are two groups of transmission modes, the E_{mn}^{y} and E_{mn}^{x} modes, existing in the RDW. With a metal ground, DIGs can keep the same transmission properties as RDWs but take

only half of the thickness of the dielectric strip [4-15]. By choosing the appropriate design parameters for the cross-section shape, the degenerate mode of E_{11}^{x} can be avoided, and only the E_{11}^{y} mode leaves as the dominant mode. Fig. 4.5 shows the port mode field distribution of this mode. In the simulation model, the open (add space) boundary conditions are used at the edges of the simulation model, which extends the touching geometry virtually to infinity by using the perfectly matched layer boundary. Waves can pass this boundary with minimal reflections. Fig. 4.6 shows the simulated S parameters. We can see that this image guide can work in a broad frequency range from 20.0 GHz to 30.0 GHz.

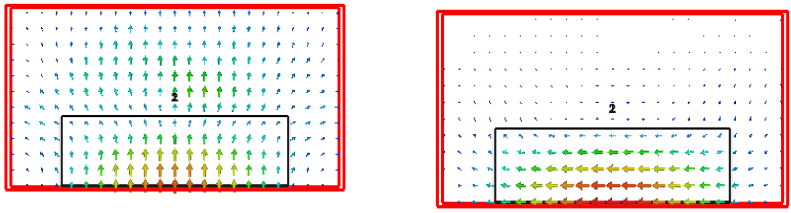

(a) (b)

Fig. 4.5 Port field distribution of E_{11}^{y} mode inside DIG, (a) electric field, (b) magnetic field

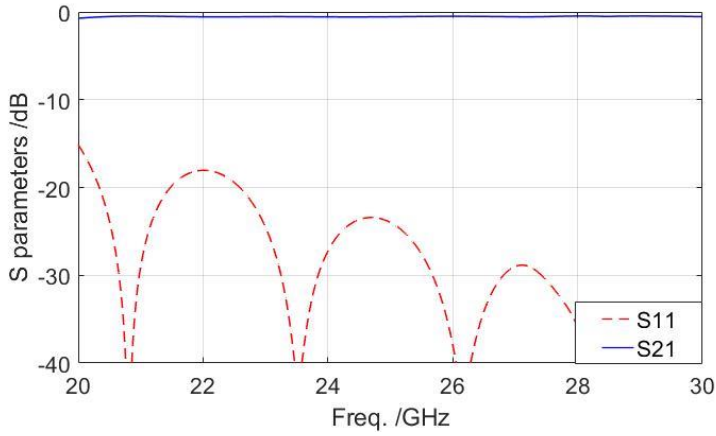

Fig. 4.6 Simulated S parameters of the DIG

4.3 Eigenmode analysis of EBG units

4.3.1 Analyzing methods

The mushroom-like EBG unit typically consists of metal patches that are separated by a gap on a dielectric substrate with vias connecting the metal patches to the ground plane, as shown in Fig. 4.7. Different methods have been proposed to analyze EBG structures. By analyzing the unit cell and using appropriate boundary conditions, there are mainly three ways, related to the reflection phase, the dispersion diagram, and the transmission characteristics, to determine the electromagnetic band gap of an EBG structure [4-16,17].

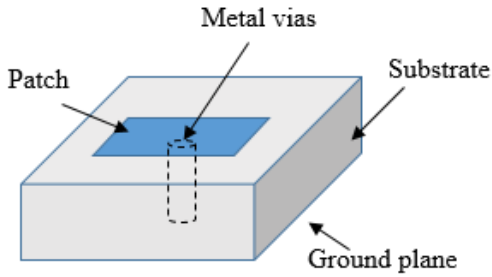

Fig. 4.7 The mushroom-like EBG unit

The electromagnetic nature of a surface is predictable from the reflection phase characteristic [4-18]. The reflection phase is defined as the phase of reflected electric field when plane waves normally incident on EBG structures. Such that a 180 degree reflection phase implies a perfect electric conductor (PEC) surface and a 0 degree reflection phase represents a perfect magnetic conductor (PMC) surface. As a result, the reflection coefficients are equal to -1 and +1 for PEC and PMC, respectively [4-19]. Since the PMC surface does not exist in nature, the reflection phase of an EBG surface varies from $+180^\circ$ to -180° with increasing frequency [4-20], and the identification of the electromagnetic forbidden band to the frequency band where the phase of the reflected wave is equal to $0 \pm 45^\circ$ with

criterion of Sievenpiper [4-21], or to $90 \pm 45°$, criterion of Rahmat-Samii [4-22]. The bandwidth in both cases corresponds to the excursion of $\pm 45°$ around the resonance frequency. Fig. 4.8 is an example of a typical reflection phase diagram.

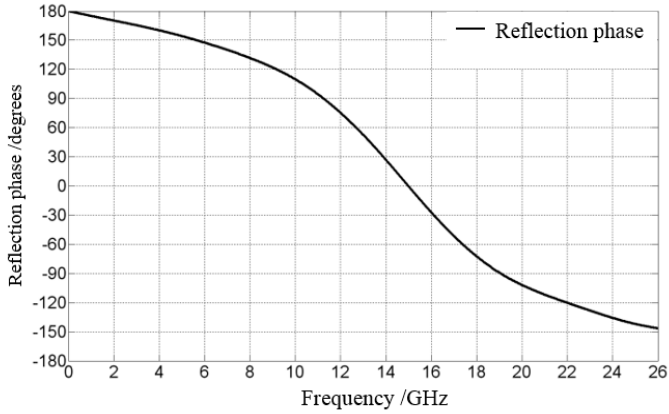

Fig. 4.8 Reflection phase of an EBG unit

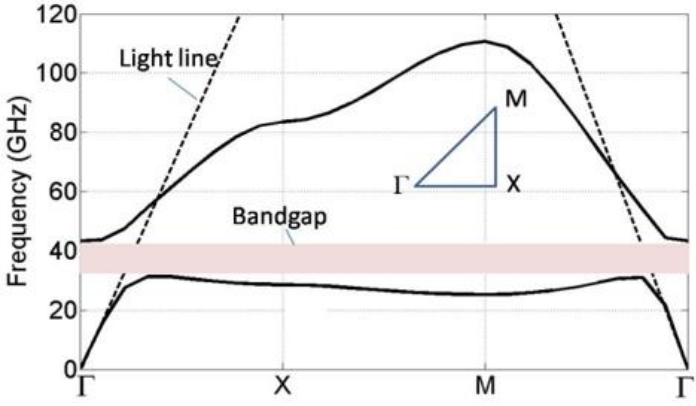

Fig. 4.9 Dispersion diagram of an EBG unit

Also, the dispersion characteristics can be used to extract the band gap of a periodic structure, which is often calculated from the eigenmode slover in a full wave analysis software. For a given wavenumber, the eigenmode solver can calculate all the resonant frequencies. At the same frequency point, the different propagation constants are known

as the different modes with their own values of phase velocity and group velocity, and the field distribution. The relationship between phase constant and resonant frequency is often plotted out and referred to as the dispersion diagram [4-23]. As shown in Fig. 4.9, the gray area is the resulting band gap for a structure.

Commonly, there are two ways, based on the suspended microstrip line and the directive transmission method, that can be used to obtain the transmission characteristics of an EBG structure. In the suspended line method, the band gap is characterized by using the EBG array as a ground plane for a microstrip transmission line which is suspended above the array [4-24]. This method is similar to the implementation of an EBG as a filter to find the surface wave suppression characteristics of EBG structures [4-25]. As shown in Fig. 4.10, the measured EBG material is inserted between the microstrip and ground, forming a sandwich-like structure. The suspended microstrip is soledered with connectors to measure the *S* parameters. In Fig. 4.11, the frequency range with attenuation losses of less than -10 dB or -20 dB is usually considered as the band gap. The directive transmission line method considers a finite number of unit cells into a two port TEM waveguide with periodicity along the main direction of propagation, and the transmission result is calculated [4-26].

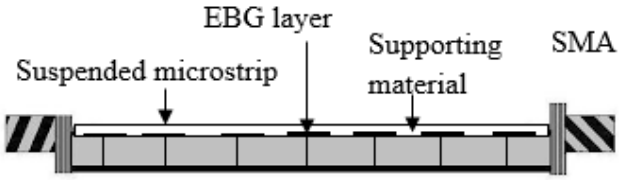

Fig. 4.10 Sketch of the suspended microstrip structure

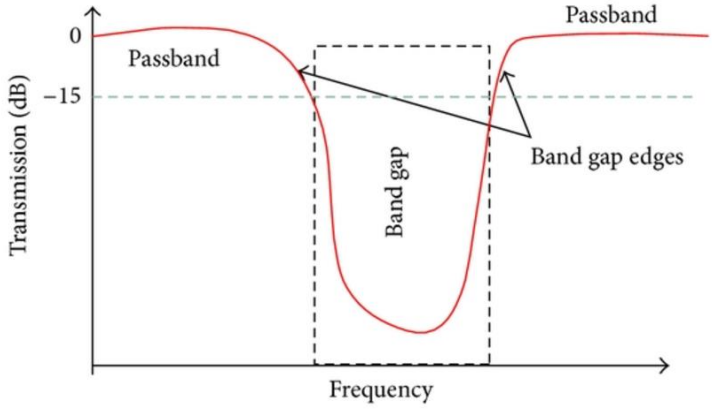

Fig. 4.11 Transmission loss of an EBG unit

4.3.2 Dispersion diagram

Analysis of EBG structures is based on the Bloch-Floquet theorem which describes the wave propagation in infinite media consisting of periodical unit cells. The theory reveals that the properties of wave propagation in a periodic structure can be fully calculated from a single unit cell with periodic boundary conditions at the edges [4-27]. Fig. 4.12 is the equavilent circuit model of the mushroom-like EBG unit. The capacitance of the EBG structure is coming from the gap between the patches, while the inductance is coming from the via. The values of the capacitance and inductance of the EBG structure are determined by its geometric parameters [4-28].

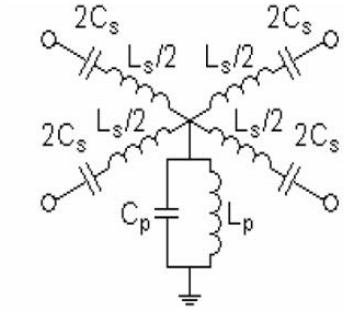

Fig. 4.12 Equivalent circuit model of the mushroom-like EBG unit

However, it is usually difficult to give an explicit expression for the wavenumber *k* of a surface wave propagating in an EBG structure. We have to either solve the eigen-value equations or perform a full wave simulation to determine this wavenumber. In a loss-free structure, there exists the relationship that the phase constant equals the real part of the wavenumber $k = 2\pi / \lambda = \beta$ [4-29], where the phase constant β is a function of frequency ω. This relation is plotted as the dispersion diagram to determine the pass and stop bands of the periodic structure.

From the dispersion diagram, we can find the phase changes of a material at a given frequency. The Brillouin zone is the fundamental region to define the propagation vectors for a unit cell [4-30]. Basically, if all the propagation vectors can be defined in the Brillouin zone, we can obtain the entire characteristic of the periodic structure. Therefore, for a two-dimensional periodical structure, the dispersion diagram can be depicted in three directions from Γ (0, 0) to X (0, π), then to M (π, π) and back to Γ, as shown in Fig. 4.13, by the path in the Brillouin zone [4-31].

In CST MWS, we can describe the directions (Γ to X, X to M, M to Γ) with a pair of defined variations of *phase_x* and *phase_y*. These two parameters are the phase variations of the slow surface wave in the periodic structure in the *x* and *y* directions, respectively. The relationship with wave numbers is:

$$Phase\ \mathrm{x} = \beta_x \cdot d\ ,\ \ Phase\ \mathrm{y} = \beta_y \cdot d \qquad (4\text{-}1)$$

Then, by sweeping the parameters of *phase x* and *phase y,* we can calculate all the possible values of the phase constants along the *x* and *y* directions.

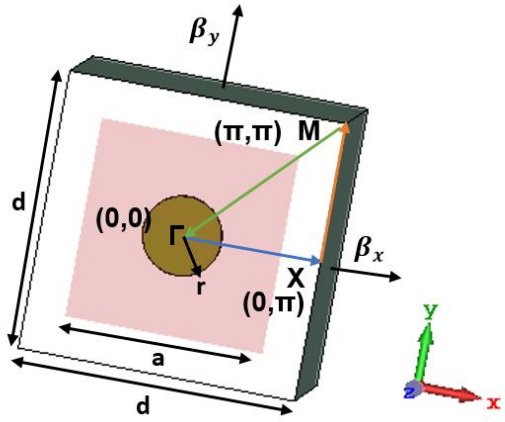

Fig. 4.13 Brillouin zone (a = 1.0, d = 1.4, r = 0.15, unit: mm)

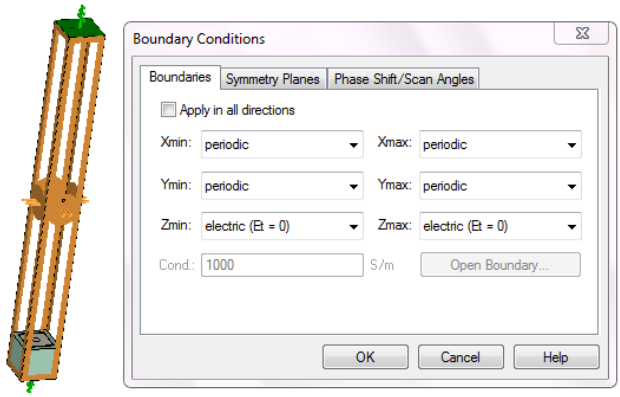

Fig. 4.14 Boundary conditions

To mimic the periodicity of the structure, the boundary conditions of the unit for *x* and *y* plane are set to "periodic" while the *z* direction is defined with an electric wall, as seen in Fig. 4.14. Since the eigenmode solver in CST does not support open boundary conditions, they have to be replaced by an electric wall at the top. It is important to define a proper height, i.e. more than ten times the substrate thickness [4-32], of the air space above the structure to allow the correct field distribution of the eigenmodes.

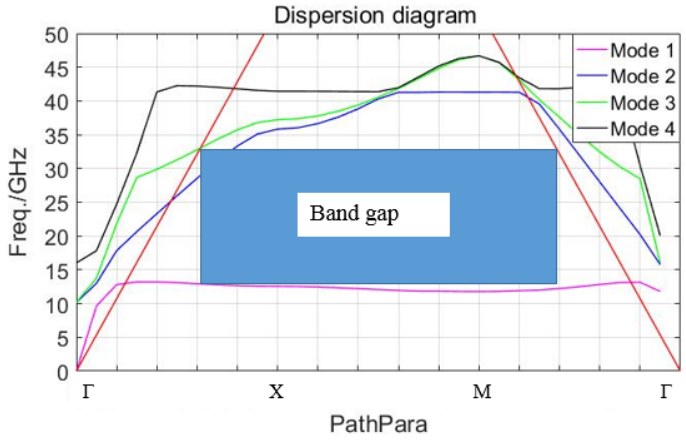

Fig. 4.15 Dispersion diagram

The design parameters of the EBG unit are also optimized and listed below Fig. 4.13. The dispersion diagram for this unit is obtained and plotted in Fig. 15. As discussed, it incorporates three intervals (Γ to X, X to M, M to Γ), in order to be able to describe all possible propagation directions in the xy plane. It is known that the mushroom EBG allows the propagation of TM waves at low frequencies and TE waves at high frequencies [4-33]. The first mode is thus a TM mode, which starts as a forward propagating TEM mode at very low frequency and low wavenumber, and changes into a forward TM surface wave. Modes 2, 3 and 4 are hybrid modes that start as TE waves at a very low wavenumber and transform into TM waves at high frequencies.

Fig. 4.16 presents the electric field distribution in yz plane of the first four eigenmodes. We can see that the electric field of mode 2 is orthogonal to the electric field of the transmission mode inside the waveguide, mode 2 is not excited and does not need to be considered. Meanwhile, because the transmission mode is a slow wave, the band gap should be below the light line [4-34]. Hence, we obtain the band gap for this periodic structure as going from about 12.8 GHz to 33.0 GHz.

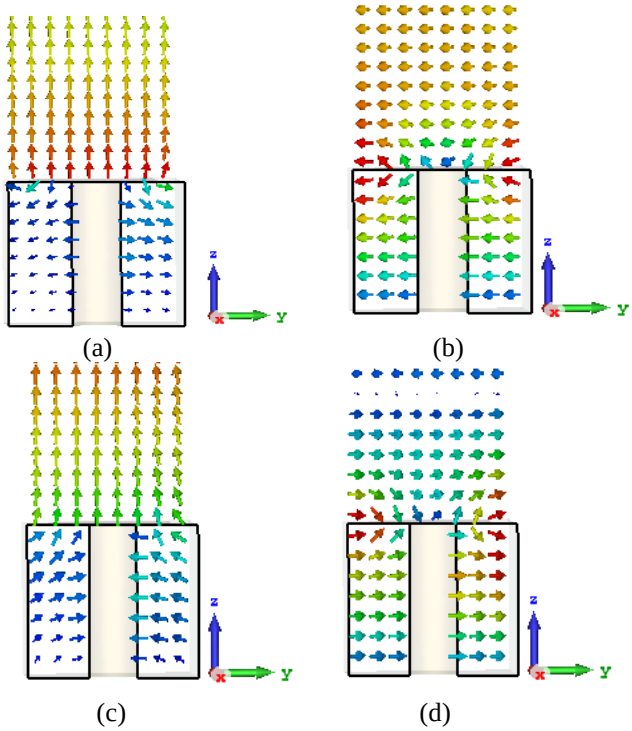

Fig. 4.16 Electric field distribution of the first four eigenmodes

4.3.3 Simulation results

(a) Comparison analysis of the rows of EBG units

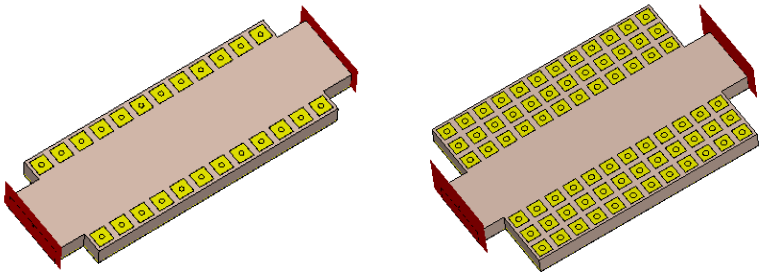

Fig. 4.17 DIG with different rows of EBG units, (a) single row of EBG units, (b) three rows of EBG units

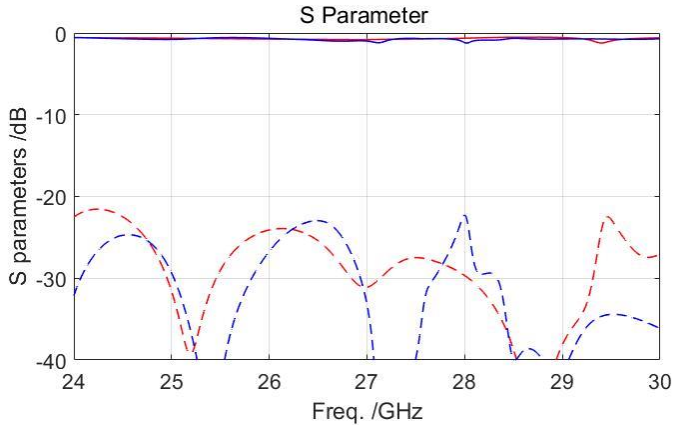

Fig. 4.18 Simulated *S* parameters (red lines: structure with single row, blue lines: structure with three unit cell rows, solid lines: S_{21}, dashed lines: S_{11}

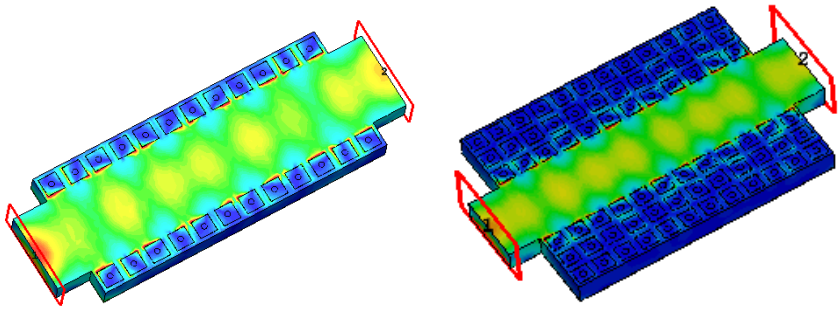

Fig. 4.19 Electric field of the propagating mode inside the structure

(b) Comparison with microstrip line

Based on the eigenmode analysis of the EBG unit, we compared the simulation results of two structures (Fig. 4.17) with single and three rows of the units, respectively. Fig. 4.18 presents the simulated *S* parameters, the excited waves can be efficiently propagated within both of these structures. From the simulated electric field distribution of the propagated wave in Fig. 4.19, we see that three rows of the units can well ensure the periodicity of the structure, and the electric field strength is decreased to a quite low level when compared with the propagated mode along the channel, which means that three rows of unit cells can well suppress the leakages at the structure edges.

The transmission efficiency of the proposed waveguide with three rows of EBG units (Fig. 4.17(b)) is compared with the microstrip transmission line (Fig. 4.20). The results are presented in Fig. 4.21. Although there are some ripples appearing in the transmission curve for the proposed waveguide, it is still seen that a transmission efficiency comparable with a microstrip line can be reached in this frequency range.

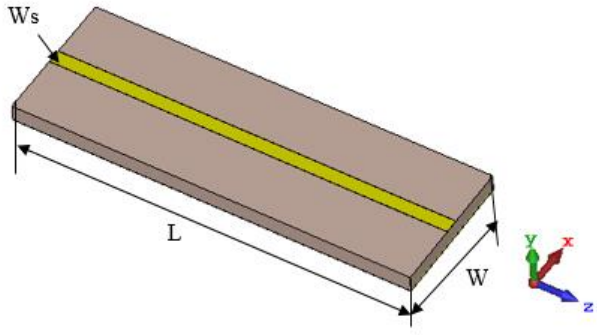

Fig. 4.20 Microstrip line (L = 20 mm, W = 10 mm, Ws = 1.0 mm, substrate material RT 6010)

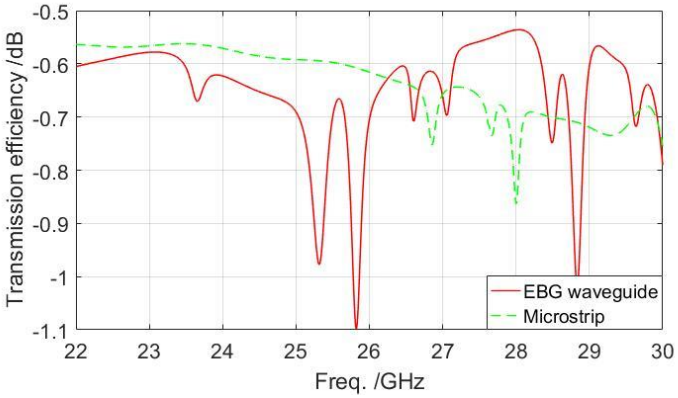

Fig. 4.21 Comparison of the transmission efficiencies of the proposed waveguide and the microstrip line

4.4 Feeding structure design

Although DIGs are known for their very low transmission loss in mm-wave bands, there are still some challenges lying in designing an efficient, wideband and low-cost coupling feeding structure that can excite the appropriate waveguide modes [4-35]. Here, we propose a novel planar structure to excite the E_{11}^{y} mode with a smooth mode conversion to the guiding channel. Fig. 4.22 gives the configuration of the proposed feeding structure and the design parameters are presented in Table 4.1. Such an interface can be regarded as an integrated SIW horn to excite the DIG, which can result in a wide bandwidth of the transition. The tapered CPW line is of the bottom ground type with a continuous impedance transition from coaxial cable to SIW, and achieves an impedance transition from 50 Ω to 29.9 Ω to match with the SIW.

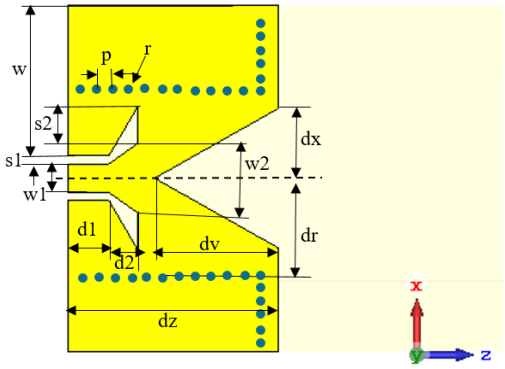

Fig. 4.22 Configuration and dimensions of the proposed feeding structure

Table 4.1 Dimensions of the proposed feeding structure

Parameters	Values (mm)	Parameters	Values (mm)
d1	1.2	s1	0.25
d2	0.85	s2	0.4
dz	5.2	w	5.9
dv	2.6	w1	0.4
dr	1.7	w2	2
dx	1.5	p	0.4
r	0.15		

4.4.1 Design of SIW

SIW is a new form of transmission line based on the metal rectangular waveguide [4-36]. As shown in Fig. 4.23, the SIW structure is created with a substrate by adding a top metal over the ground plane and using rows of plated vias on both sides. To the propagation wave, it looks like a dielectrically-filled rectangular waveguide (DFW). Because of these metal vias at the sidewalls, the TM modes do not exist and the TE_{10} mode becomes the fundamental mode [4-37]. To ensure a single mode transmission, we need to first explore the design rules for SIWs.

For a rectangular waveguide, the cut-off frequency of an arbitrary mode is found by the formula [4-38]

$$f_c = \frac{c}{2\pi}\sqrt{(\frac{m\pi}{a})^2 + (\frac{n\pi}{b})^2} \tag{4-2}$$

where c is the speed of light, m and n are the mode numbers, and a and b are the dimensions of the waveguide. For the TE_{10} mode, this becomes

$$f_c = \frac{c}{2a} \tag{4-3}$$

For the DFWs, we have $a_d = \frac{a}{\sqrt{\varepsilon_r}}$, ε_r is the relative permittivity of the substrate material. With this dimension, we can pass to the design formula for an SIW [4-39].

$$a_s = a_d + \frac{d^2}{0.95p} \tag{4-4}$$

where d represents the diameter of the vias and p is the periodicity. Now we can determine the cutoff frequency and the cutoff wavelength for the dominant mode of the SIW by using

$$f_c = \frac{c}{2\sqrt{\varepsilon_r}(a_s - \frac{d^2}{0.95p})} \tag{4-5}$$

with the conditions that $d < \lambda_g / 5$ and $p < 2d$ [4-40]. Here, we have the equivalent wavelength λ_g in the SIW as

$$\lambda_g = \frac{2\pi}{\sqrt{\frac{\varepsilon_r (2\pi f)^2}{c^2} - (\frac{\pi}{a_s})^2}} \qquad (4\text{-}6)$$

From the Eq. (4-5, 6), the SIW was dimensioned with parameters as listed in the caption of Fig. 4.23. We obtain $f_{cTE10} = 14.1\ GHz$, $f_{cTE20} = 28.2\ GHz$ and $\lambda_g = 3.59mm > a_s$. The computed results predict that only the dominant mode can propagate inside the waveguide in the operation frequency range of 24 to 28 GHz.

Based on the calculated results, the model SIW is developed and simulated in CST as shown in Fig. 4.23. Fig. 4.24 yields the simulation results of the transmission coefficients of the first two modes, while the electric field distributions inside the waveguide at 28.0 GHz are given in Fig. 4.25 (a) and (b). Both the simulation results show that only the single mode can be transmitted within the target frequency range, and also verify the correctness of the design rules. Fig. 4.25 (c) and (d) present the electric and magnetic field distribution of the first mode, while Fig. 4.25 (e) and (f) give the field distribution in the longitudinal direction. It can be clearly seen that the wave is well constrained and the field distribution is very similar to the TE_{10} mode.

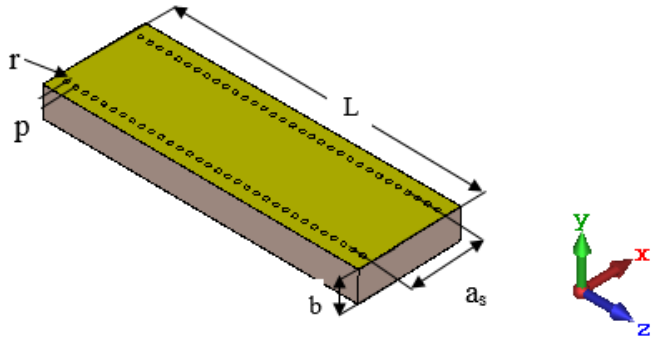

Fig. 4.23 Simulation model of SIW (a_s = 3.4, L = 15, p = 0.4, r = 0.15, b = 1.27, unit: mm), with r is the via radius and p is the distance between vias

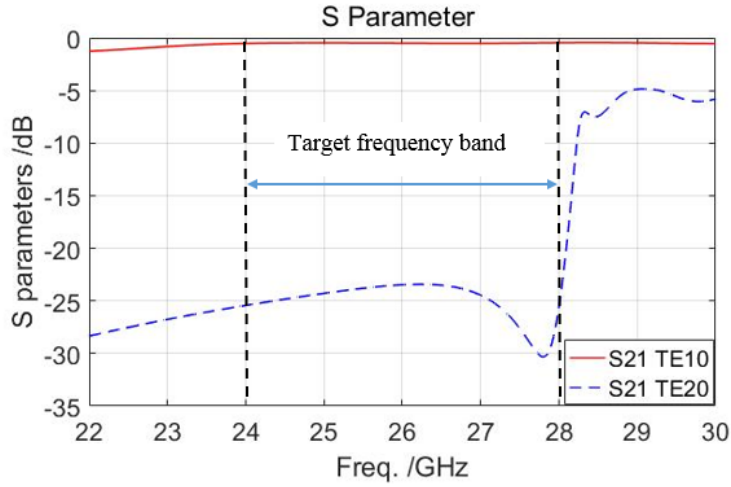

Fig. 4.24 Simulated S parameters of SIW

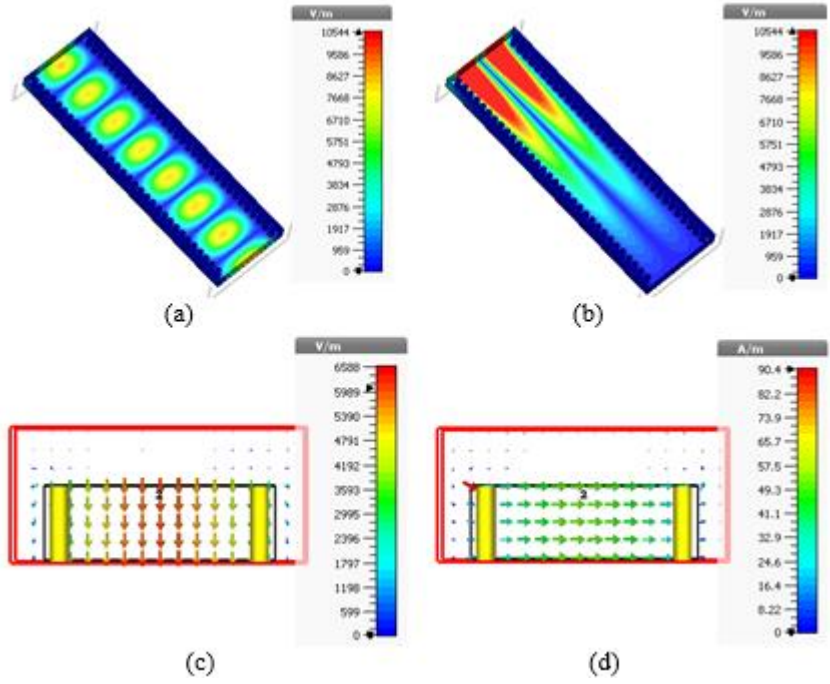

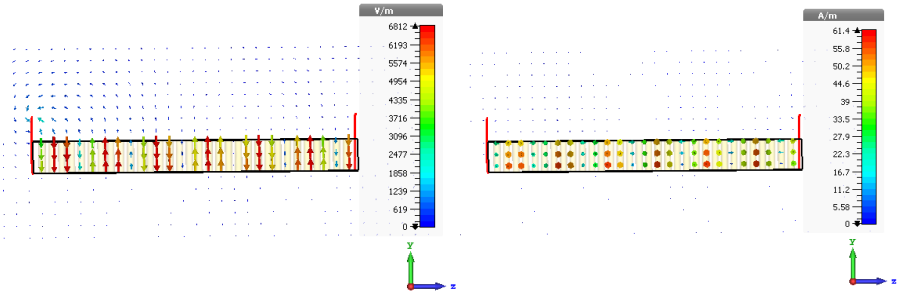

(e) (f)

Fig. 4.25 Transmission mode in the SIW, (a) electric field distribution of TE_{10} mode, (b) electric field distribution of TE_{20} mode, (c) electric field of TE_{10} mode at port, (d) magnetic field of TE_{10} mode at port, (e) electric field distribution of TE_{10} mode along the longtitudinal direction, (f) magnetic field distribution of TE_{10} mode along the longitudinal direction

4.4.2 Transition from GCPW to SIW

To obtain a connection with MMIC chips and coaxial cables, the CPW feed line with ground is employed as shown in Fig. 26. The input impedance extracted from the SIW model in Fig. 4.23 is 29.9Ω. to match with SIW. The design parameters *s1*, *s2*, *w1* and *w2* listed in Table 4.1 are well calculated with an impedance change from 50 Ω to 29.9Ω [4-41]. The width of the middle strip is increased gradually with a continuous impedance change, and thus leading to a wideband transition [4-42].

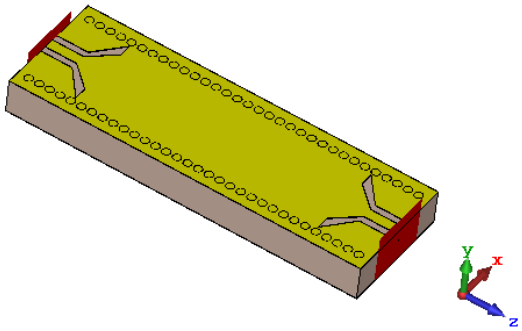

Fig. 4.26 Transition from GCPW to SIW

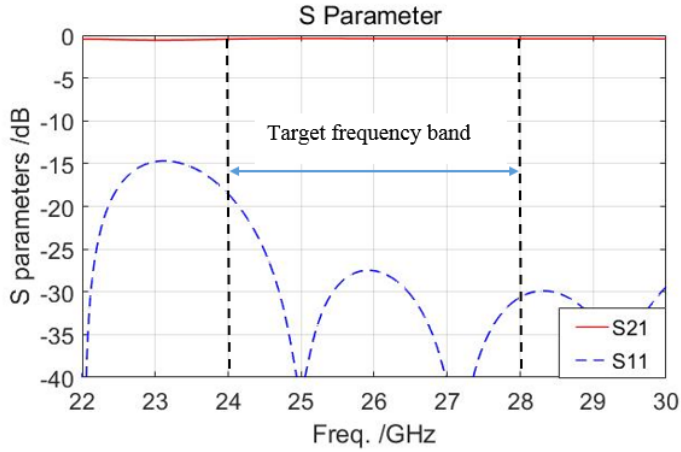

Fig. 4.27 Transmission efficiency of the GCPW to SIW transition

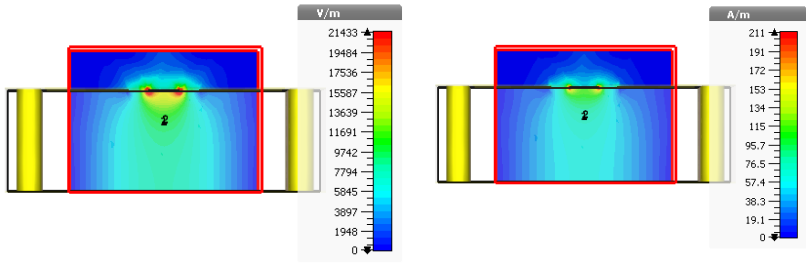

(a) (b)

Fig. 28 Mode field in GCPW, (a) electric field, (b) magnetic field

The simulation results of the transmission efficiency are presented in Fig. 4.27, from which we can see that a high efficiency and a wide bandwidth can be achieved with the structure. Fig. 4.28 is the common field distribution of the GCPW, the energy is well restricted and guided along the slots.

After that, the complete feeding structure is added to the DIG with a v-slot (Fig. 4.29). Fig. 4.30 presents the simulated *S* parameters. From the simulated results, we see that there is a little decrease of the transmission efficiency when compared with the DIG structure in Fig. 4.18. This is because some radiation losses are generated by the planar v slot.

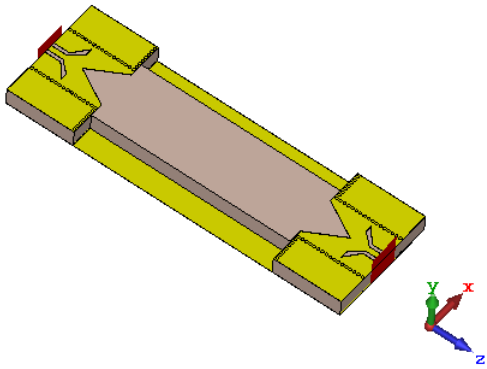

Fig. 4.29 Feeding structure with DIG

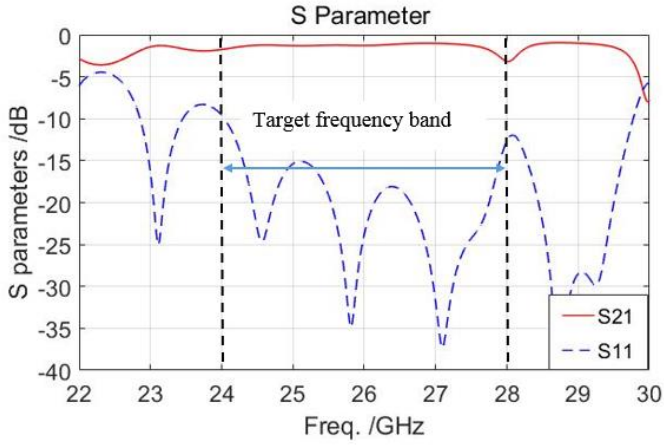

Fig. 4.30 Transmission efficiency of the feeding structure

4.5 Complete waveguide

4.5.1 Wave propagation

In this section the complete structure, with the feeding part and the EBG units, as shown in Fig. 4.1, is studied. The electric field distribution in the different parts of the structure is shown in Fig. 4.31. The transmitted TE_{10} mode within the SIW horn is well matched with the dominant E_{11}^{y} mode in the SIG, which delivers a smooth mode conversion. The simulated *S* parameters (Fig. 4.32) show that a reasonable transmission efficiency is achieved in the desired frequency range. Fig. 4.33(a) gives the propagation mode in the

proposed waveguide, (b) and (c) present the electric and magnetic field distribution in the longitudinal direction, respectively.

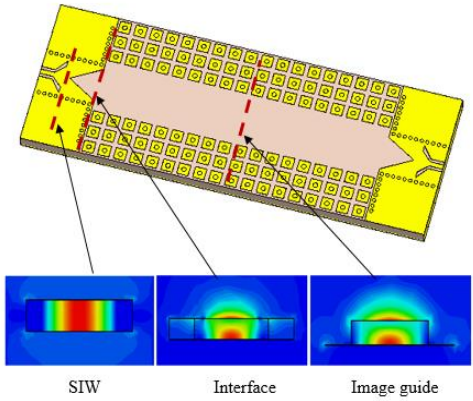

Fig. 4.31 Mode conversion of the complete waveguide

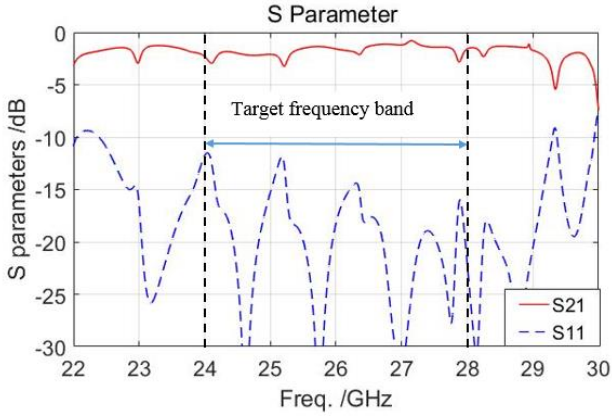

Fig. 4.32 Transmission efficiency of the proposed waveguide

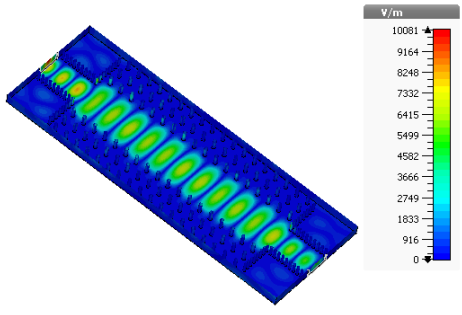

(a)

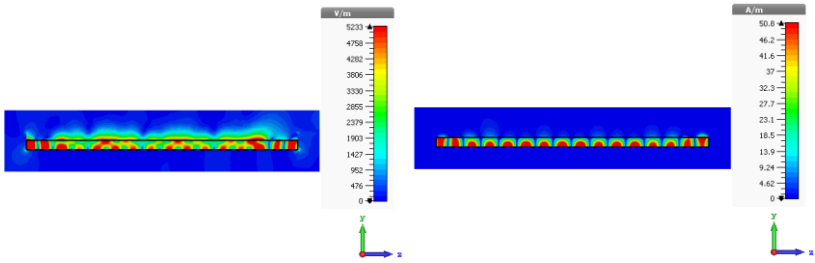

(b) (c)

Fig. 4.33 Propagation mode in the proposed waveguide, (a) propagation mode, (b) electric field distribution along the longitudinal direction, (c) magnetic field distribution along the longitudinal direction

4.5.2 Decoupling analysis

From Fig. 4.34 to 4.39, we studied and compared the coupling effects between two parallel waveguides. In situation (a), complete waveguide structures are compared with guiding channels with EBG units and air gap, respectively. The port numbers are all defined as the structure in Fig. 4.34(a) in these three situations. In situation (b), the feeding topology for mode excitation is removed, and in situation (c), the guiding channels are directly connected on the whole board.

(a) Air gap with feeding structure

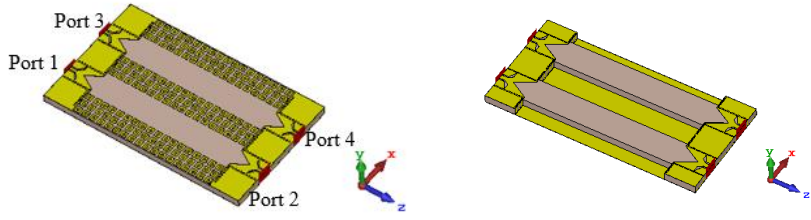

(a) (b)

Fig. 4.34 Waveguide structures, (a) isolation of EBG units, (b) isolation of air gap

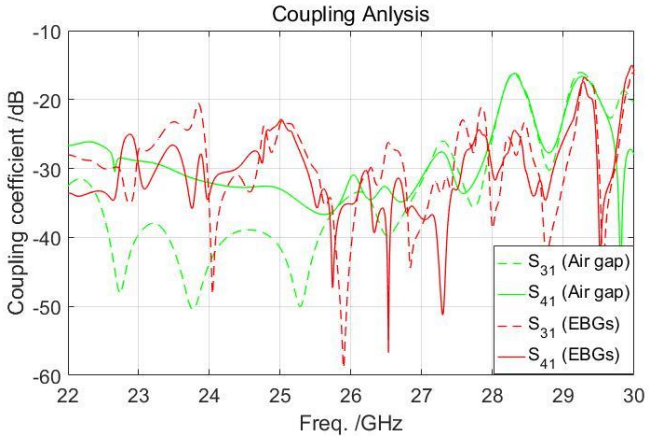

Fig. 4.35 Coupling comparison: green lines refer to (a) and red curves to (b)

(b) Air gap without feeding structure

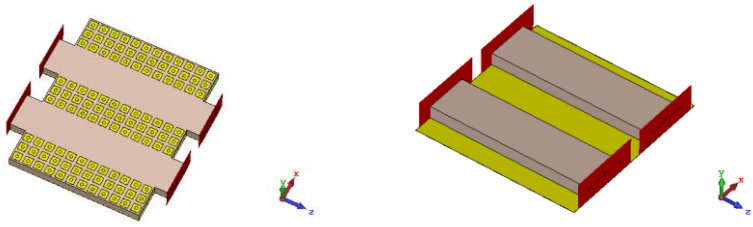

(a) (b)

Fig. 4.36 Waveguide structures without feeding part, (a) isolation of EBG units, (b) isolation of air gap

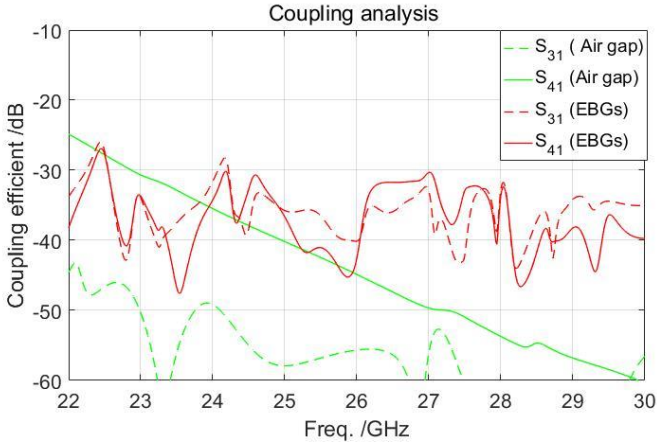

Fig. 4.37 Coupling comparison: green lines refer to (a) and red curves to (b)

From the simulated results in Fig. 4.35 and 4.37, we see that the coupling is kept at a very low level for the channel with EBG units

and air gap. It also can be seen that the feeding structure contributes little to the coupling effect to the channels. The added EBG units can only be used to suppress the surface wave propagation to the edge sides and thus generate the guiding channel. However, if the substrate material is removed together with the EBG units, the surface wave cannot exist any more. In other words, the air gap can be also used to generate the guiding channel and should have the best decoupling effect. But it will also influence the structure stability and the integration with other components.

In comparison, we also investigated the structure by removing the EBG units directly as shown in Fig. 4.36(b). We can see that the propagation characteristics have totally changed. The surface wave even cannot propagate in the target frequency band and the coupling effect increases a lot when compared with the structure with EBGs.

(c) Direct connection of guiding channels

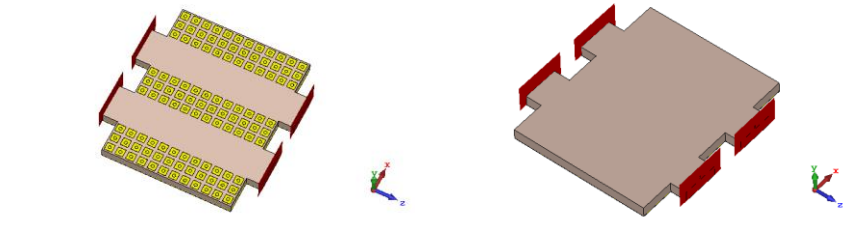

(a) (b)

Fig. 4.38 Waveguide structures, (a) isolation of EBG units, (b) direct connected channels

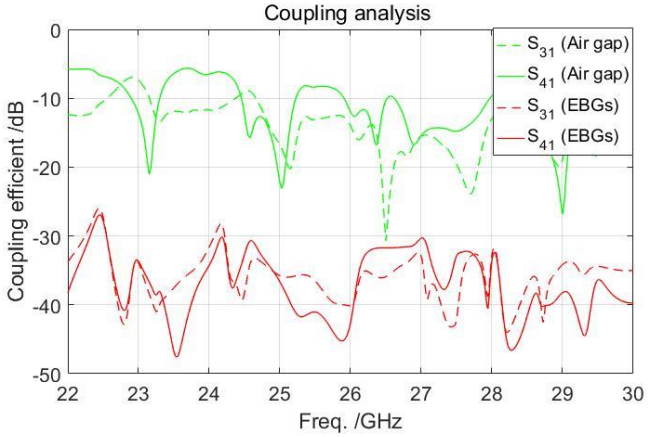

Fig. 4.39 Coupling comparison with green lines refer to (a) and red curves for (b)

In conclusion, the EBG units in combination with the dielectric image

guide are employed to create the guiding channel. This structure can achieve a reasonable transmission efficiency within the target frequency range. Meanwhile, by suppressing the surface wave propagation, it can also decrease the coupling effect from other integrated components on the same board. Although this decrease is not as good as with an air gap, it is sufficient for the isolation of the guiding channel when three rows of EBG units are used.

4.6 Conclusion

In this chapter, we introduced a new transmission line designed for 5G frequency applications. The topology combines a dielectric image guide and EBG units and achieves a single mode, broadband transmission with a reasonable transmission efficiency in the targeted frequency range. Besides, different methods for the eigenmode analysis of the EBG units are discussed. The dispersion diagram for the mushroom-like EBG unit is obtained with the full wave analyzing method. After that, a feeding structure is proposed with an impedance transition and smooth mode conversion, which ensures a wide bandwidth and the medium efficiency when exciting the propagation mode inside the guiding channel. Simulation results show that this structure satisfies the design requirements. The structure offers many potential applications, for example in planar connectors, substrate feeders etc.

In the design of this new transmission topology, we found that the EBG units can be used to design a full planar dielectric waveguide in a single layer PCB. The guiding channel can be generated by suppressing the surface wave propagation with the aligned EBG units. Despite that the decoupling effect of the EBG rows is not as good as with an air gap, it is enough to ensure that the guiding channel can be isolated from the influence from other integrated components. The EBG-based waveguide also performs almost at the same level of the transmission efficiency when compared with microstrip lines in this frequency range. However, some radiation losses are produced with the introducing of the mode excitation structure which lead to a

decrease of the transmission efficiency. Some further improvements still need to be explored to enhance the mode conversion efficiency from the metal feeding part to the guiding channel.

Reference

[4-1] A. Kumar, M. Gupta, "A review on activities of fifth generation mobile communication system," *Alexandria Engineering Journal*, vol: 57, iss. 2, Jun. 2018, pp: 1125–1135.

[4-2] T. Imai, K. Kitao, N. Tran and Y. Okumura et.al, "Development of high frequency band over 6 GHz for 5G mobile communication systems," *EuCAP 2015*, Lisbon, Portugal.

[4-3] A. Naeemi, A. V. Mule and J. D. Meindel, "Partition length between board-level electrical and optical interconnections," *IEEE Int. Conf.*, Jun. 2003, pp: 230–232.

[4-4] R. Ma, J. Fu, "Microstrip to coplanar strip double-Y balun with very high upper frequency limitations," *Proc. Of Asia-Pacific Conf. on Antenn. And Propagat.*, Jul. 2014, pp: 1402-1405.

[4-5] R. Reinosa, A. Allen, E. Benedetto and A. Mcallister, "Characterization mechanical performance of board level interconnects for in-circuit test," *IEEE Int. Test Conf.*, Nov. 2010, pp: 1–11.

[4-6] R. R. Kumar, D. Chadha and S. Aditya, "Analysis of dielectric image guide structures using method of lines," *J. of Electromagnetic Waves and Applications*, Vol. 10, iss. 6, 1996, pp: 835-844.

[4-7] E. H. Scheibe, B. G. King and D. L. V. Zeeland, "Loss measurements of surface wave transmission lines," *J. of Applied Physics*, Vol. 25, iss. 6, 1954, pp: 790-797.

[4-8] Wikipedia. Metamaterials. https://en.wikipedia.org/wiki/Metamaterial

[4-9] W. Huang and Z. Wu, "Study on band gap characterization of EBG structures with interdigital and spiral ground plane," *AIP Conf. Proc.*, Vol. 1890, iss. 1, Oct. 2017, pp: 1-5.

[4-10] Y. Toyata, A. E. Engin, T. H. Kim and K. Uriu, "Stopband prediction with dispersion diagram for electromagnetic bandgap structures in printed circuit boards," *IEEE Intern. Sympos. On EMC*, 2006, pp: 807-811.

[4-11] S. Lim, M. F. Iskander, "Design of a dual-band, compact Yagi antenna over an EBG ground plane," *IEEE Antennas and Wireless Propagat. Lett.*, vol. 8, Dec. 2008, pp: 88-91.

[4-12] A. Kumar, J. Mohan and H. Gupta, "Surface wave suppression of microstrip antenna using different EBG design," *Int. Conf. on Signal Processing and Communications*, 2015, pp: 355-359.

[4-13] P. Kovacs, Z. Raida and M. M. Vazquez, “Parametric study of mushroom-like and planar periodic structures in terms of simultaneous AMC and EBG properties,” *Radio Engineering*, Vol. 17, no. 4, Dec. 2008, pp: 19-24.

[4-14] A. R. Weily, K. P. Esselle, T. S. Bird and B. C. Sanders, “Experimental woodpile EBG waveguides, bends and power dividers at microwave frequencies,” *Electronics Letters*, Vol. 42, iss. 1, Jan. 2006, pp: 32-43.

[4-15] V. A. Katrich, A.A. Zvyagintsev and S. A. Pogarksy et al., “Dielectric image guide as basic electromadynamic structure for high-perfoemance radiation system design,” *2004 14th Int. Conf. Microwave and Telecom. Technology*, Sep. 2004, Crimea, Ukraine.

[4-16] M. S. Alam, N. Misran, B. Yatim and M. T. Islam, “Development of electromagnetic band gap structures in the perspective of microstrip antenna design,” *Int. J. of Antennas and Propagat.*, Vol. 2013, 2013, pp: 1-22.

[4-17] Y. Q. Fu and N. C. Yuan, “Reflection phase and frequency bandgap characteristics of EBG structures with anisotropic periodicity,” *J. of Electromagn. Waves and Appl*., Vol. 19, no. 14, 2005, pp: 1897-1905.

[4-18] D. R. Jackson, Plane Wave Propagation and Reflections, Houston, TX, Univ. Houston, pp: 3-12.

[4-19] N. Jaglan and S. D. Gupta, “Design and analysis of performance enhanced microstrip antenna with EBG substrate,” *Intern. J. of Microwave and Optical Lett.*, Vol. 10, iss. 2, Jan. 2015, pp: 79-88.

[4-20] I. T. McMichael, A. I. Zaghloul and M. S. Mirotznik, “A method for determining optimal EBG reflection phase for low profile dipole antennas,” *IEEE Trans. Antenna and Propagat.*, Vol. 61, no. 5, May 2013, pp: 2411-2417.

[4-21] D. Sievenpiper, L. Zhang, R. F. J. Broas, N. G. Alexopolous and E. Yablanovitch, “High-impedance electromagnetic surface with a forbidden frequency band,” *IEEE Trans. on Microwave Theory and Techiniques*, Vol. 47, No. 11, Nov. 1999, pp: 2059-2074.

[4-22] F. Yang, Y. R. Sami, “Reflection phase characterization of the EBG ground plane for low profile wire antenna applications,” *IEEE Trans. on Antennas and Propagat.*, Vol. 51, no. 10, Oct. 2003, pp: 2691-2703.

[4-23] A. Orlandi, B. Archambeault, F. D. Paulis and S. Connor, “Planar EBGs:

Fundamentals and Design,' in *Electromagnetic Bandgap Structures: Common Mode Filter for High Speed Digital Systems*, IEEE, 2017.

[4-24] O. Ayop and M. K. A. Rahim, "Analysis of mushroom-like electromagnetic band gap structure using suspended transmission line technique," IEEE Intern. RF and Microwave. Conf., Dec. 2011, Negeri Sembilan, Malaysia.

[4-25] M. Koledintseva, S. Radu and J. Nuebel, "Physical and technological aspects of microstrip EBG filter design," *IEEE Symp. On EMC, SI and PI*, Aug. 2018, CA, USA.

[4-26] M. S. Alam, M. T. Islam, N. Misran, "Performance investigation of a uni-planar compact electromagnetic bandgap (UC-EBG) structure for wide bandgap characteristics," *Proc. Of Asia-Pacific Symp. EMC*, May 2012, pp: 637-640.

[4-27] A. Giorgio, A. G. Perri and M. N. Armenise, "Design of guided-wave photonic bandgap devices by using the Bloch-Floquet theory," *Optical Engineering*, Vol. 42, iss. 4, Apr. 2003.

[4-28] G. Luo,E. Li, X. Wei and C. Xiang, "Modelling of planar EBG structure by using equivalent circuit method," *IEEE Symp. On EMC*, Aug. 2015, Dresden, Germany.

[4-29] https://www.microwave101.com/encyclopedias/propagation-constant

[4-30] J. J. Quinn, K. S. Yi, Solid State Physics, Principles and Modern Applications, Springer, 2009.

[4-31] Y. Abdo, M. R. Chaharmir, J. Shaker and Y. M. Antar, "Detailed study of millimeter wave EBG guide: broadbanding techniques, modal structure, and crosstalk behavior," *PIERS*, Vol. 50, Jan. 2013, pp: 141-156.

[4-32] P. Kovacs and T. Urbanec, "Electromagnetic band gap structures: practical tips and advice for antenna engineers," *Radio Engineering*, Vol. 21, no. 1, Apr. 2012, pp: 414-421.

[4-33] S. Enoch, G. Tayeb, and D. Maystre: 'Dispersion diagrams of Bloch modes applied to the design of directive sources'. in Proc. PIERS, 2003, Vol. 41, pp. 61–68.

[4-34] D. Sievenpiper, L. Zhang, R. F. J. Broas, N. G. Alexopolous and E. Yablonovitch, "High-impedance electromagnetic surfaces with a forbidden frequency band," *IEEE Trans. Microw. Theory Tech.*, vol. 47, no. 11, Nov. 1999, pp. 2059-2074.

[4-35] M. Basha, B. Biglarbegian, S. Gigoyan and S. Safavi-Naeini, "Design and fabrication of CPW to dielectric image-guide transitions at 60 GHz on

SOI," *IEEE Radio and Wireless Symp*., Jan. 2014, CA, USA.

[4-36] F. Xu, K. Wu, "Guided-wave and leakage characteristics substrate integrated waveguide," *IEEE Trans. Microw. Theory Tech.,* vol. 53, no. 1, Jan. 2005, pp. 66-73.

[4-37] S. Moitra and P. S. Bhowmik, "Modelling and analysis of substrate integrated waveguide and half-mode SIW band-pass filter using reactive longitudinal periodic structures," *Int. J. of Electronics and Communications*, Vol. 70, iss. 12, Dec. 2016, pp: 1593-1600.

[4-38] D. M. Pozar, Microwave Engineering, 3th Edition, John Willy and Sons, Jan. 2007.

[4-39] K. Wu, D. Deslandes and Y. Cassivi, "The substrate integrated circuits – a new concept for high-frequency electronics and optoelectronics," *6th Int. Conf. on Telecom. in Modern Satellite, Cable and Broadcasting*, Oct. 2003, Nis, Yugoslavia.

[4-40] J. E. Raya-Sanchez and V. Gutierrez-Ayala, "A general EM-based design procedure for single-layer substrate integrated waveguide interconnects with microstrip transitions," *IEEE MTT-s Int. Microwave Symp. Dig.*, Atalanta, GA, Jun. 2008. Pp: 983-986.

[4-41] R. Simons, "Coplanar waveguide circuits, components, and systems," Wiley, 2001, pp: 15-21.

[4-42] M. Nedil, T. A. Denidni and A. Djaiz, "Ultra-wideband microstrip to CB-CPW transition applied to broadband filter," *Electronics Letters*, Vol. 43, no. 8, Apr. 2007.

CHAPTER 5 PERIODICAL LWA FED BY EBG-BASED WAVEGUIDE

In this chapter we explore the potential use of the EBG-based waveguide, as introduced in the previous chapter, as a substrate feeder in antenna design. Leaky wave antennas are popular in the microwave band and above, as they can reach a high directivity with a simple structure without metallic feeding network. Also, they have the capability of beam scanning with changing frequency. Hence, we designed LWAs with six elements for Ku band applications.

This chapter is based on the following paper:

[1] L. H. Kong, S. Yan, V. Volski, B. K. Huang and G. A. E. Vandenbosch, "Leaky wave array in full planar substrate with EBG based wave guiding channel," IET Microwaves, Antennas & Propagation. Under review.

5.1 Introduction

Generally, LWAs can be categorized as one dimensional or two dimensional. In the former category, the travelling wave propagates in one direction and therefore the radiation pattern is conical or fan shaped. Two dimensional LWAs depend on a radially travelling wave and they produce a pencil beam in the broadside direction and conical beams otherwise [5-1,2]. LWAs are designed based on transmission lines. Different types of LWAs have been proposed and widely studied [5-3]. Examples include the dielectric waveguide, groove guides, rectangular waveguides, SIW and SIIG [5-4,5,6,7]. The level of interest and pace of development in the field of planar LWAs have recently accelerated significantly due to the surge of interest in metamaterials [5-8,9].

Research on the working mechanism of LWAs has been conducted decades ago [5-10]. Since a leaky wave is produced from the guiding structure, it becomes important to know the characteristics of the guiding waves. Explorations on how to control the leakages will help to guide the design of LWAs [5-11]. In Fig. 5.1, we assume that a guiding wave $e^{-j\beta z}$ propagates along the $+z$ direction with the phase constant β and a leaky mode is produced in x direction. Then

$$k_x^2 = k_0^2 - \beta^2 \tag{5-1}$$

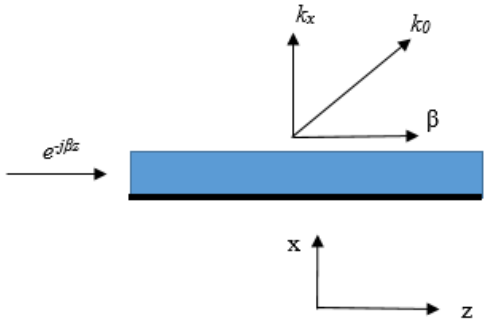

Fig. 5.1 Leaky conditions for structures

In Eq. 5-1, only when k_x is real, a leaky wave can be produced. Therefore, to have radiation, the propagation mode should be a fast mode with $\beta < k_0$. Then, the direction of the main radiation is determined by $\theta = \sin^{-1}(\beta / k_0)$, where θ is measured from broadside. It also should be noted that due to the existence of radiation loss, the propagated wave will be attenuated along the $+z$ direction. So it is necessary to introduce an attenuation constant α associated with β, which will influence the beam width of the radiation pattern [5-12].

As known, the travelling wave inside a pure dielectric rod is regarded as a slow wave ($\beta > k_0$) [5-13]. Therefore, it is not possible to generate leaky waves directly from the dominant mode, even if it is an open guiding structure. The leaky conditions can be changed with periodic modulations [5-14]. According to Floquet theory, periodicity can result in many space harmonics when periodic metal strips are added. Each of the harmonics has a phase constant β_n [5-15].

$$\beta_n = \beta_0 + \frac{2n\pi}{d} \tag{5-2}$$

where d is the periodicity length of the guiding structure and β_0 is the phase constant of the dominant mode. From Eq. 5-2, we find that other harmonics are of the fast wave type while the basic space harmonic is of the slow wave type. The phase constant of the first order spatial harmonic can be written as:

$$\beta_{-1} = \beta_0 - \frac{2\pi}{d} \tag{5-3}$$

By carefully designing the geometry of the leaky structure in a given frequency range, we can satisfy the leaky condition $\beta_{-1} < k_0$, and design a periodic LWA with a single beam. Then, the beam direction of the periodical LWA can be expressed as:

$$\sin\theta_m \approx \frac{\beta_{-1}}{k_0} \tag{5-4}$$

where θ_m is the angle of the main beam. So when $-k_0 < \beta_{-1} < 0$, the beam of the periodic LWA directs to the backside and changes to the broadside. With a frequency increase, it comes to the front side.

However, for a periodic structure, a stop band will appear at the broadside direction ($\beta_0 = 2\pi / d_0$) [5-16,17]. The reason is that the attenuation constant will increase significantly at broadside, and most of the power will be reflected.

5.2 Leaky wave antenna array

5.2.1 Substrate feeder

In Ku band, the antennas can be used in radar applications involving target tracking and detection, or satellite communications with a high transmitting and receiving data rate. This requires the antennas to operate in the wide bandwidth and with high efficiency [5-18]. Because of the planar topology and the broad bandwidth, the waveguide structure proposed in Chapter 4 is used here as a substrate feeder for an LWA working in Ku band. The design parameters of the feeding topology like in Fig. 4.17 are optimized and listed in Table 5.1

Table 5.1 Dimensions of the mode launching structure

Parameters	Values (mm)	Parameters	Values (mm)
d1	4	s1	0.8
d2	2.4	s2	1.8
dz	13.4	w	11.35
dv	5.6	w1	1.3
dr	3.8	w2	3.4
dx	3.4	p	1
r	0.3		

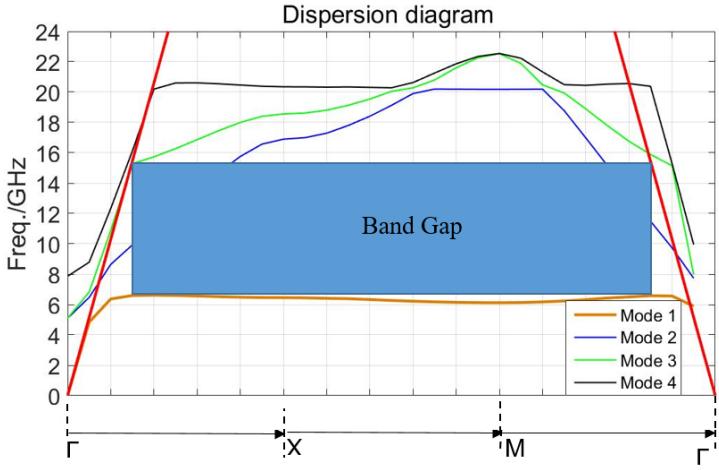

Fig. 5.2 Dispersion diagram of the mushroom-like EBG unit

The design parameters for the mushroom-like EBG unit are chosen with a = 2.8 mm, d = 2.0 mm, r = 0.3 mm as depicted in Fig. 4.10. The dispersion diagram is calculated and (Fig. 5.2) shows a band gap from about 6.5 GHz to 15.0 GHz. In Fig. 5.3, we present the simulated S parameters of the EBG-based waveguide. It is seen that a reasonable transmission efficiency over the frequency range 11.0 GHz - 16.0 GHz can be obtained.

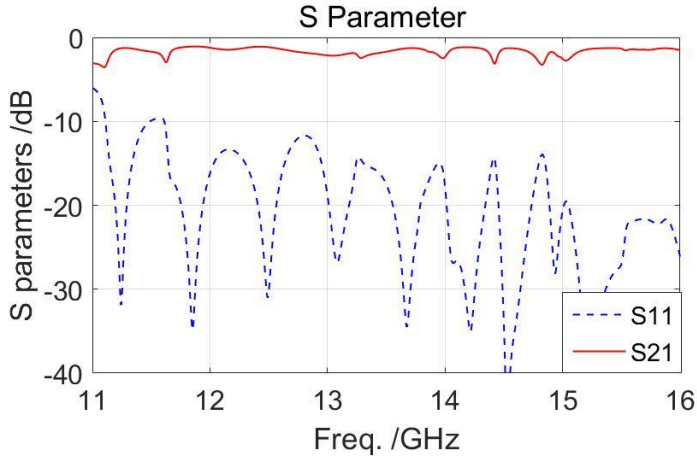

Fig. 5.3 Simulated S parameters of the EBG-based waveguide

5.2.2 Array design

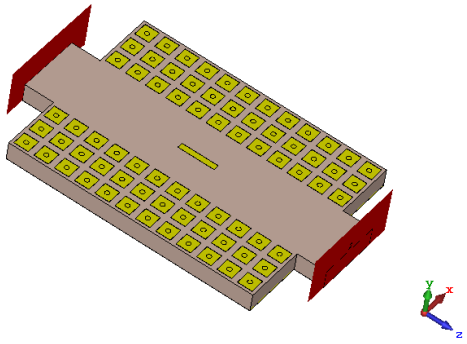

Fig. 5.4 Structure with single metal strip

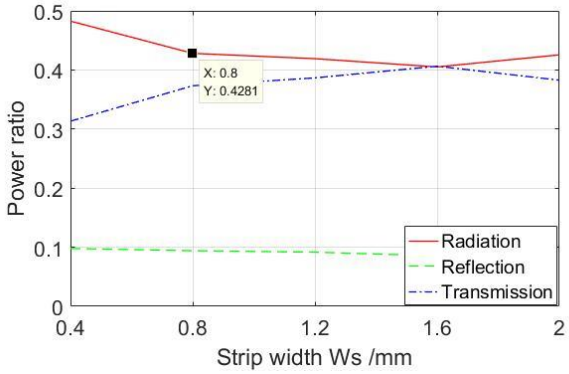

Fig. 5.5 Power relationship with different strip widths at 12.5 GHz

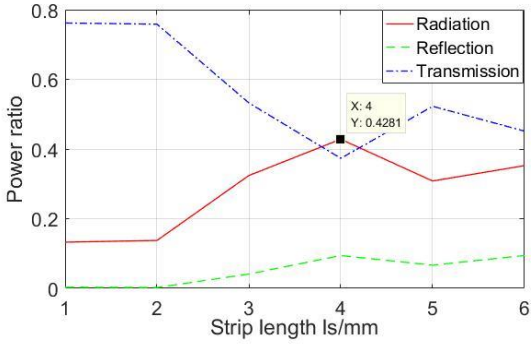

Fig. 5.6 Power relationship with different strip lengths at 12.5 GHz

LWAs usually have a simple structure, low profile and high gain performance, which allows them to be fabricated and integrated with

printed circuit board (PCB) technology easily and flexibly. For the periodic leaky wave antenna array, each antenna element can extract a part of the travelling energy to generate radiation. Therefore, the radiation property of a single strip is investigated firstly. The structure of a single metal strip fed by the substrate waveguide is presented in Fig. 5.4, and the power relationships of radiation, reflections and transmissons with changes of the strip dimensions are given in Fig. 5.5 and 5.6 for width and length, respectively. We can see that the curves are quite smooth when the strip width changes from 0.4 mm to 2 mm, which means that the strip width only slightly influences the radiation in comparison with the lengths. When the strip dimensions are chosen as 4 mm for length and 0.8 mm for width, the radiation efficiency can reach about 42.81%. This is sufficient to generate that most of the power is radiated with an array of six elements.

Based on the analysis, we proposed a six-metal-element periodic leaky wave antenna array as shown in Fig. 5.7. The metal strips are placed on top of the guiding channel. The design parameters are optimized in CST and listed below the figure. A conventional LWA is terminated with a matching load to absorb the rest of the input power [5-19]. However, in higher frequency bands, this load will increase the cost. In our design, we can omit the terminating load since most of the power is radiated when six elements are used. The residual power is very small. Meanwhile, the influence of the backward wave can also be neglected.

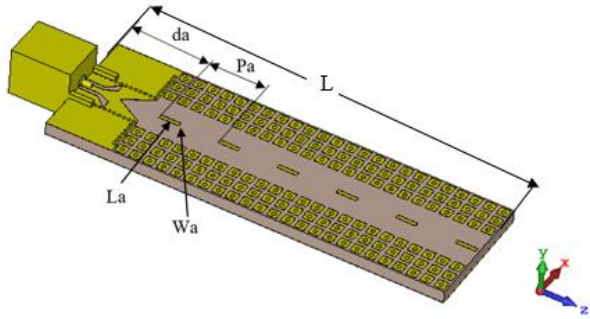

Fig. 5.7 Configuration of the proposed Ku-band periodic leaky wave antenna array,

The length of the structure L = 71.2 mm. (La = 4, Wa = 0.8, Pa = 12, da = 13.4, unit: mm)

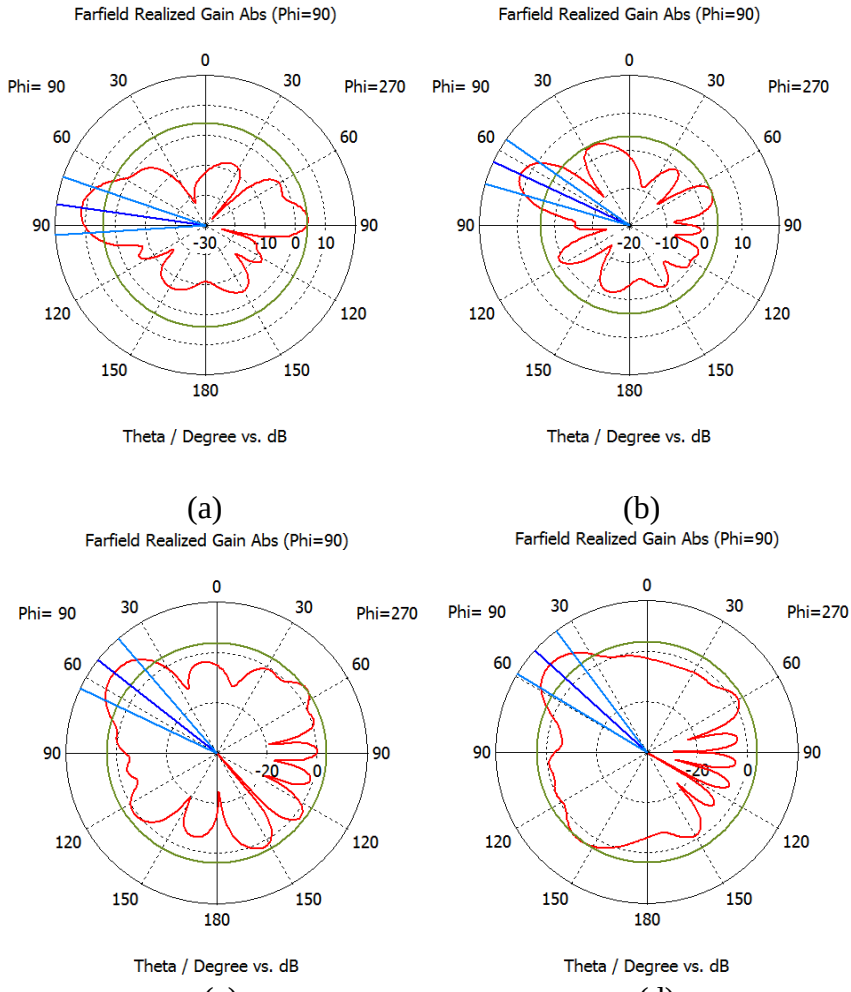

Fig. 5.8 Beam direction at different frequency points, (a) 12.0 GHz, (b) 12.5 GHz, (c) 12.8 GHz, (d) 13.0 GHz

The beam direction of a leaky wave antenna array usually changes with frequency. In Fig. 5.8, the beam directions are plotted at 12.0 GHz, 12.5 GHz, 12.8 GHz and 13.0 GHz, with 82°, 65°, 52° and 48°. The main lobe magnitudes are changed with 11.5 dB, 12.0 dB, 11.8 dB and 11.9 dB. So the main beam can scan from about 82.0° to 48.0° in the forward quadrant.

5.3 Experimental results

The fabricated prototype is shown in Fig. 5.9. The measurement setup in the anechoic chamber is depicted in Fig. 5.10. The return loss is measured with a network analyzer and agrees well with simulations (Fig. 5.11). The reflection coefficient is lower than -10 dB in the frequency range 12.0 - 12.8 GHz. Also, the simulation yields that at 12.5 GHz about 79.9% of the total energy is radiated.

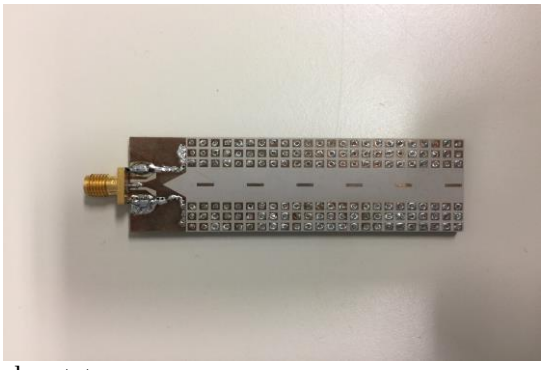

Fig. 5.9 Fabricated prototype

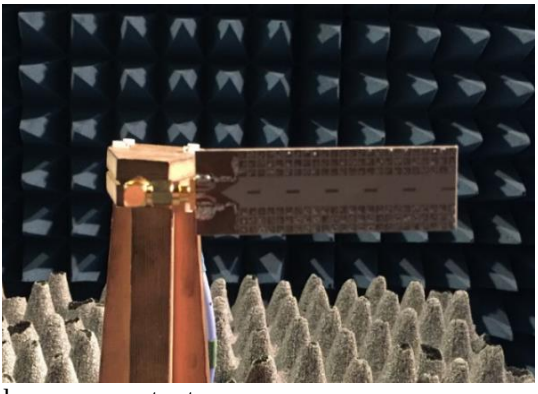

Fig. 5.10 Far field measurement setup

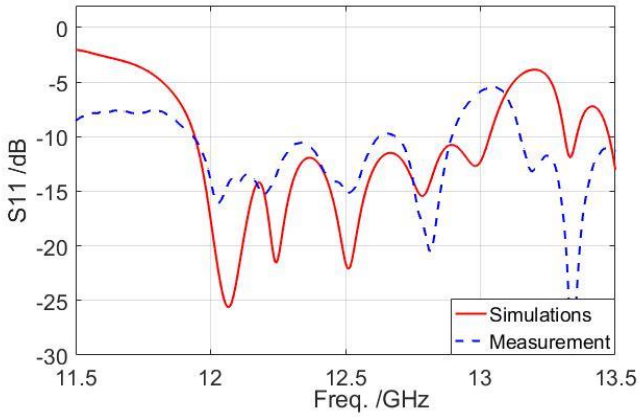

Fig. 5.11 Comparison of the simulated and measured *S* parameters

In Fig. 5.12 and 13, the far field patterns at 12.0 GHz in E and H plane are plotted, both co- and cross-polarization components, respectively. In H plane, the agreement between simulations and measurements is remarkably good over the whole 360 degrees. In E-plane, the discrepancy is larger, especially further away from the main beam. This is due to the mounting situation of the antenna, see Fig. 5.10. The mounting structure and feeding cable are seen in this E plane. The measured cross-polarization component is below -20 dB in both planes. Since the main beam directs to about 82° in E plane, the maximal value in H plane stays close to that in E plane.

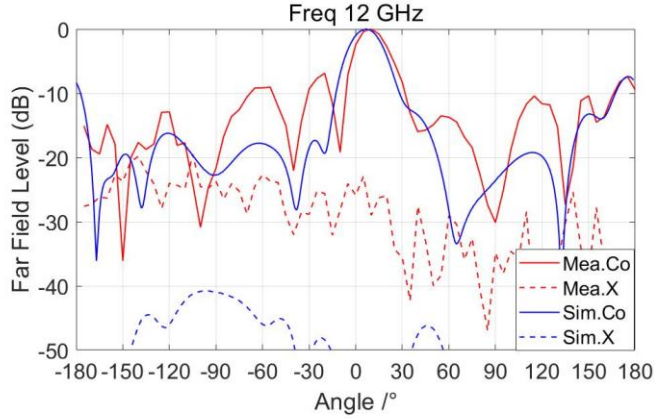

Fig. 5.12 Radiation pattern at E plane (yoz) in 12 GHz

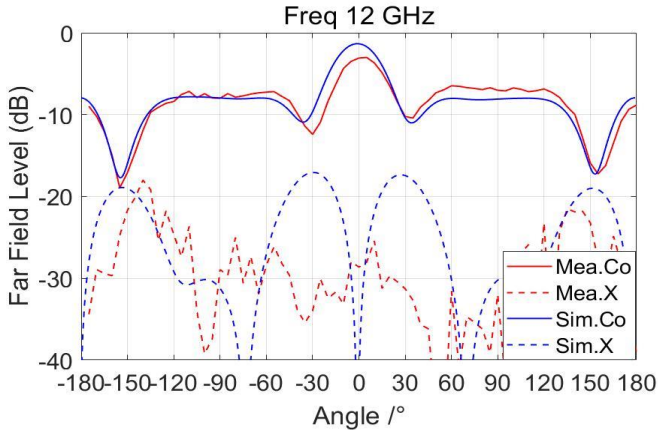

Fig. 5.13 Radiation pattern at H plane (xoy) in 12 GHz

Table 5.2 Realized gain

Freq. [GHz]	12.0	12.5	12.8
Simu. dBi	11.36	11.97	11.71
Meas. dBi	10.0	9.93	10.4

The maximum realized gain is presented in Table 5.2. Both in the simulations and measurements, this gain is almost constant over the band considered. The maximum variations are about 0.5 dB. Also, the measured gain is about 1.5-2 dB lower than the simulated one. This is partially due to the conductor losses in the many solderings, which are hard to take into account in the simulations

5.4 Conclusion

In this chapter, an EBG-based dielectric image guide is proposed and employed as the substrate feeder for a Ku-band leaky wave antenna array. The aligned EBG units are essential to achieve a high transmission efficiency and coupling effect with the printed antenna elements. Results show that the designed antenna array satisfies the requirements for radiation efficiency and gain performance. The planar topology also makes that this antenna has great potential to be integrated with current PCB technology.

Reference

[5-1] D. R. Jackson, C. Caloz and T. Itoh, "Leaky wave antennas," *Proc. Of the IEEE*, Vol. 100, iss. 7, Mar. 2012, pp: 2194-2206.

[5-2] M. Garcia-Vigueras, M. Esquius-Morote, J. P. Carrier, J. R. Mosig, "Dual-beam radiation from 1D leay-wave antennas," *EuCAP 2014*, Hague, Netherland.

[5-3] J. D. Preez and S. Sinha, Leaky Wave Antennas, Chapter of Millimeter-Wave Antennas: Configurations and Applications, Springer International Publish, 2016, pp: 19-38.

[5-4] X. Bai, S. W. Qu, C. H. Chan and K. B. Ng, "Millimeter-wave leaky-wave antenna based on dielectric filled metal groove waveguide," *IEEE 4th Asia-Pacific Conf. Antennas and Propagat.*, Jul. 2015, Kuta, Indonesia.

[5-5] H. Oraizi and M. T. Noghani, "Design and optimization of linear and planar slot arrays on rectangular waveguides," *38th EuMC*, Oct. 2008, Amsterdam, Netherlands.

[5-6] J. Liu, D. R. Jackson and Y. Long, "Substrate integrated waveguide (SIW) leaky-wave antenna with transverse slots," *IEEE Trans. Antennas and Propagat.*, Vol. 60, no. 1, Jan. 2012, pp: 20-29.

[5-7] Y. J. Chen and Y. X. Guo, "60-GHz substrate integrated imaging guide leaky-wave antenna on LTCC," *IEEE Antennas and Propagat. Society Intern. Sympos.*, Jul. 2013, Orlando, USAL, pp: 2141-2142.

[5-8] C. Caloz, T. Itoh and A. Rennings, "CRLH metamaterial leaky-wave and resonant antennas," IEEE Antennas and Propagat. Magaz., Vol. 50, iss. 5, 2008, pp: 25-39.

[5-9] Y. S. Abdo, M. R. Chahamir, J. Shaker and Y. M. Antar, "Broadside radiation by excitation of EBG leaky mode," *IEEE Antennas and Wireless Propagat. Lett.*, Vol. 11, Jul. 2012, pp: 861-864.

[5-10] S. F. Mahmoud and Y. M. M. Antar, "Leaky wave antennas: theory and design," *30th national radio science conf.*, Apr. 2013, Egypt, pp: 1-8.

[5-11] J. L. G. Tornero, A. A. Melcon and F. Mesa et al., "Analysis and design of controllable leaky –wave antennas inspired by Prof. Arthur Oliner," *EuMC 2014*, Rome, Italy.

[5-12] V. Jandieri, P. Baccarelli, G. Valerio and S. Ceccuzzi et al., "Efficient and rigorous analysis of leaky modes in 2-D EBG guiding structures," *Int. Conf. on Electromagnet*. in Advanced Applications," Sep. 2017, Verona, Italy.

[5-13] A. Angulo adn W. Chang. “The launching of surface waves by a parallel plate waveguide,” *IRE Trans. on Antennas and Propagat*., Vol. 7, iss. 4, Oct. 1959, pp: 359-368.

[5-14] Z. Xu, X. Zhang, S. Li, H. Zhao and X. Yin, “Leaky-wave radiation from periodically modulated spoof surface plasmon polaritons,” *6th Asia-Pacific Conf. on Antennas and Propagat.*, Oct. 2017, Xi’an, China.

[5-15] T. Itoh, “Periodic structures for microwave engineering,” Nov. 2004.

[5-16] M. Guglielmi and D. R. Jackson, “Broadside radiation from periodic leaky-wave antennas,” *IEEE Trans. Antennas and Propagat*., Vol. 41, no. 1, Feb. 1993, pp: 31-37.

[5-17] R. Henry and M. Okoniewski, “A broadside scanning substrate integrated waveguide periodic phase reversal leaky-wave antenna,” *IEEE Antennas and Wireless Propagat. Lett.*, Vol. 15, Jul. 2015, pp: 602-605.

[5-18] Y. Asci, M. Pehlivan and K. Yegin, “Dual cavity Ku-band antenna for SatCom applications,” in *Proc. Telecommunication Forum*, Belgrade, Serbia, Nov. 2017.

[5-19] Y. Mohtashami and J. R. Mohassel, “A butterfly substrate integrated waveguide leaky-wave antenna,” *IEEE Trans. Antennas and Propagat.*, Vol. 62, no. 6, Jun. 2014, pp: 3384-3388.

CHAPTER 6 CONCLUSIONS AND OUTLOOK

In this chapter, we conclude the doctoral work and summarize the results in section 6.1. A discussion on the limitations and research objectives for the future are given in section. 6.2.

6.1 Conclusions

The main target of this thesis was the study of the characteristics of dielectric waveguides and their use in antenna design. The first part of this thesis reviewed the background and development of the different types of dielectric waveguides and antennas based on DWs. With the development of RF systems towards higher frequencies, losses caused by traditional metal feeding networks become more and more significant. Dielectric transmission lines can avoid this problem since they do not rely on metallic strips.

In the second part, we researched the rectangular dielectric waveguide. The approximation method of Marcatili for the transmission mode analysis was given first, in order to be able to have an initial design of all parameters. A feeding structure with a printed dipole and an impedance transition was adopted to launch the dominant E_{11}^{x} mode inside the RDW. After that, the coupling and scattering effect between the travelling wave and a metal patch were validated by simulations and measurements in X band. The results showed that a single radiating element is not sufficient to generate a directive radiation beam in the far field.

In order to improve the radiation performance, we extended the work into a four elements array. The 4 antenna elements were designed with a non-uniform topology to avoid the well known stop-band effect occurring in periodic structures. The travelling power was extracted and radiated by these elements. A bi-directional radiation pattern was achieved in X band for in-house radar and localization applications.

After that, to further improve the directivity and gain performance of this antenna, a metal ground was added at a distance of a quarter wavelength from the antenna. The influence of the ground size was analyzed. After an optimization of the structure, the final fabricated prototype produced a directive radiation with a mean beam in the broadside direction and with sufficient gain.

In Chapter 4, a new type of transmission line was proposed, combining a dielectric image guide with EBG units. Different methods for the eigenmode analysis of the EBG unit were given first. Further, a mushroom-like EBG unit was analyzed by employing the eigenmode solver within CST. The optimized structure satisfied our expectations with a stop band covering the targeted frequency range. To excite the fundamental E_{11}^{y} mode inside the dielectric image guide, a grounded CPW to SIW transition structure was proposed for a smooth and efficient mode conversion. In the simulation results of the complete structure a high transmission efficiency was achieved in the required frequency band.

In Chapter 5 of the thesis, on the basis of the proposed EBG-based waveguide, we designed a six-element periodic leaky wave antenna for Ku-band applications. A discussion on the working mechanism and the radiation characteristics of LWAs was given at the beginning of the chapter. Both simulation and experiment results show a high radiation efficiency and gain performance of the fabricated prototype. Within the designed frequency range, the main beam of this antenna can be scanned over more than 30 degrees at the front side.

6.2 Outlook

This thesis presented the analysis and design of dielectric transmission lines and employed them in the design of antennas for different applications. Research in this field also owns many other potential applications which are worthy of further study.

1. Since dielectric waveguides are a kind of open or semi-open structure, the boundary conditions are much more complex than for metal waveguides. Due to this complexity, the theoretical study of the propagation characteristics is still not fully finished. Also, the traditional PCB process suffers from some challenges including fabrication tolerance and reliability of the process. In contrast, the low temperature cofired (LTCC) process is getting increasing attention due to the flexibility in realizing multiple layers, cross-layer vias and embedded cavities, which can be explored for the design of multi-layer structures and improvement of antenna performance at high frequencies.

2. As dielectric waveguide antennas are fed by the substrate, the antenna topology is determined by the substrate, which offers this type of antenna a great advantage in the design of conformal antennas. Dielectric waveguide antennas can be integrated in cylindrically or spherically conformal structures.

3. New 5G communication systems will require the design of massive antenna arrays for beamforming and massive MIMO applications. The mutual coupling effect among different antenna elements will not only decrease the channel isolation, but also influence the radiation efficiency of the whole system. Metamaterials offer a great flexibility in antenna design. The EBG structures proposed in Chapters 4 and 5 could be further explored to see how they can eliminate the coupling effect in arrays.

ACKNOWLEDGEMENT

How time flies. Now I have come to the final phase of my PhD and am going to say goodbye to the wonderful people and this fascinating city of Leuven. Four years of PhD is an import part of my life with contributions from many people. I would like to give my best appreciation to my supervisors, colleagues, friends and my family.

First of all, I would like to thank my supervisor Prof. Guy A. E. Vandenbosch for his guidance and advice that he has given throughout my PhD. I would also like to thank my co-supervisor Prof. Sen Yan. After a terrible experience worked with Xuezhi Zheng in the first two years, I had almost lost all confidence to continue my PhD career. Sen Yan offered me the help and encouragement to pass through that difficult moment. Furthermore, I would like to give my great thanks to the examination committee members, Prof. Dominique Schreurs, Prof. Dirk Van Troyen, Dr. Vladimir Volski and Dr. Ulf Johannsen for their valuable comments and suggestions.

I am grateful that during my PhD I had the opportunity to work with many excellent people. I enjoyed the discussions with them on different ideas, and appreciated their fruitful comments and feedback. I would like to thank Dr. Xu Hantao, Dr. Liu Song, Prof. Huang Binke, Cheng-ming Chen, Jiahao Zhang, Xiaomu Hu, Jiachen Wang, Juncheng Bao and Yang Zhang. Great thanks to our group secretary Natalie Buyckx. She always gave us a lot help patiently and kindly. I would also like to thank all other Telemic colleagues, Tom Vermulen, Bertold Vandenberge, Adriy Serebryannikov, Mario Kupresak, Jona Beysens, Simin, Rachel, Rudy etc.

Besides, I also want to express my special thanks to my Chinese friends in Leuven, Yang Bohan, Jia Xu, Chen Xuanli, Zhang Ren, Pan Ning, Wang Qing, Bao Xiu’e, Liu Hao, Zhang Meng, Ban You, Chen Zhengshen, Zheng Qi, Huang Xiaolin, Liu Zhe, Hang Hanyuan, Li

Zhe, Wang Husen, Xi Xiangming, Guo Kaizhe, Lyv Yifan, Cao Yuhe, Li Yinan, Gai Yuzhu, Xiao Xingzhi, Liu Quanying, Wang Lulu, Li Chao, Guo Cheng, Liao Yuhe, Yuan Shushan, Li Meixia, Wang Yixin, Sheng Shurong, Sun Chanjun, Zhang Jie, Li Xin, Shi Hui, Liu Maoxuan, Zhang Xuan, Luo Xinlong, Jiao Fuchao, Feng Chi, Hou Tianfeng etc., for their company and help in the past four years, and the Chinese badminton team for those energetic weekends we spent together.

I would also like to acknowledge the China Scholarship Council (CSC) for providing me with the financial support for my study in Belgium.

Last but not least, I devote my greatest gratitude to my family. My parents always give me their unconditional love, understanding and support. They are always standing by me and encourage me whenever I am facing difficulties. Thanks to my brother and sister, they are also giving me a lot of support and always make me feel warm in my heart.

PUBLICATIONS

(1) Linghui Kong, Sen Yan, Vladimir Volski, Guy. A. E. Vandenbosch, "Planar nonuniform antenna array fed by a dielectric waveguide," Microwave and Optical Technology Lett. Vol. 60, iss. 4, pp: 849 – 854, Apr. 2018.

(2) Linghui Kong, Sen Yan, Guy A. E. Vandenbosch, "Directive antenna array fed by dielectric waveguide for WiFi applications," Microwave and Optical Technology Lett., Vol. 60, iss. 8, pp: 1963 -1967, Jun. 2018.

(3) Linghui Kong, Xuezhi Zheng, Guy A. E. Vandenbosch, "Deisgn of a dielectric waveguide antenna at microwave frequencies," EuCAP 2017, Paris, France.

(4) Linghui Kong, Sen Yan, Valdimir Volski, Binke Huang and Guy. A. E. Vandenbosch, "Leaky wave array in full planar substrate with EBG based wave guiding channel," IET Microwaves, Antennas and Propagations. Under review.

(5) Linghui Kong, Sen Yan, Vladimir Volski and Guy A. E. Vandenbosch, "A new design of EBG-based dielectric image guide for 5G applications," manuscript in preparation.

(6) Sen Yan, Xiaomu Hu, Jiahao Zhang, Linghui Kong and Guy A. E. Vandenbosch, "Design of a dual-band wearable planar inverted F antenna based on characteristic mode theory," EuCAP 2018, London, UK.